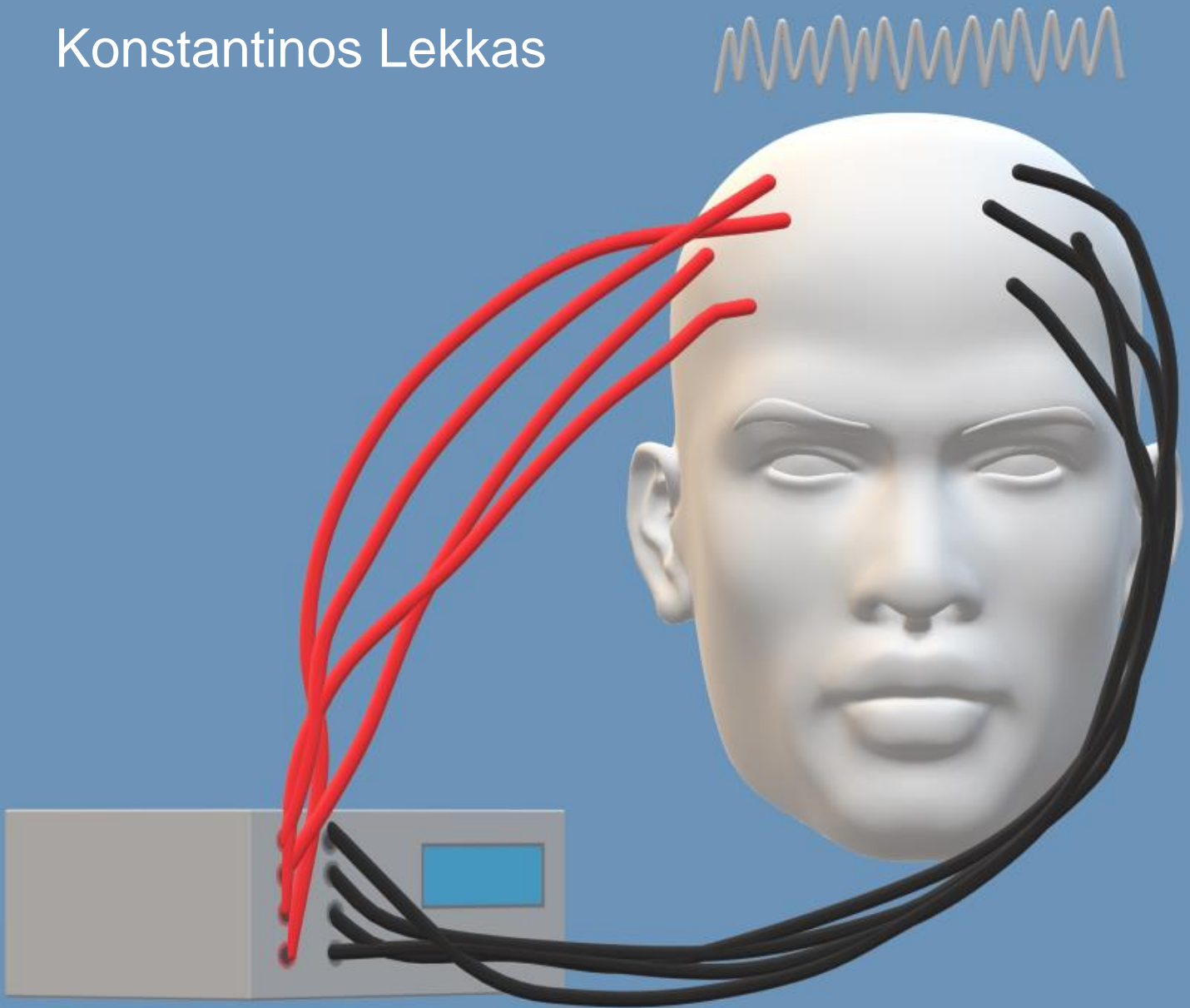


Konstantinos Lekkas



A Power Efficient Multichannel
Neurostimulator Based on the Ultra
High Frequency Technique for
Transcranial Direct Current Stimulation
Applications

A Power Efficient Multichannel Neurostimulator Based on the Ultra High Frequency Technique for Transcranial Direct Current Stimulation Applications

By

Konstantinos Lekkas

in partial fulfilment of the requirements for the degree of

Master of Science
in Biomedical Engineering

at the Delft University of Technology,
to be defended publicly on Wednesday September 18, 2019 at 03:30 PM.

Supervisor:	Prof. dr. ir. W. A. Serdijn	
Thesis committee:	Prof. dr. ir. W. A. Serdijn	TU Delft
	Dr. V. Giagka,	TU Delft
	Prof. dr. P. J. French,	TU Delft
	Prof. dr. J. Dankelman,	TU Delft
	Ir. J. Peuscher,	TMSi BV

This thesis is confidential and cannot be made public until 18/09/2020.

An electronic version of this thesis is available at <http://repository.tudelft.nl/>.



Abstract

Transcranial direct current stimulation (tDCS) is a noninvasive technique, allowing for the reversible modulation of activity in particular brain regions. TDCS has obtained much scientific interest and it promises many potential benefits to the patients.

However, tDCS that is performed today is almost the same with the method that was used 20 years ago (applying 2 mA current, during a 20 min session, using two large surface sponge electrodes). The tDCS module of the future must be characterized by increased portability, battery life and focality.

Many commercially available devices have very low power efficiency, leaving space for the design of low power consumption tDCS devices. Power efficient tDCS modules will also need lower battery capacity and thus lighter batteries, increasing the portability of the system. Regarding focality, there is increased interest from the researchers and physicians for multichannel devices that use small diameter electrodes. These devices can increase the focality and the accuracy of the delivered currents offering more targeted therapies.

In this thesis, the realization of a novel, low power, multichannel stimulation module, made with discrete components, which uses the ultra high frequency (UHF) technique for tDCS applications is implemented. With this approach, the technological benefits of the UHF stimulation technique, regarding increased multichannel power efficiency, are derived, combined with a cost effective, low scale production method. Moreover, contrary to previous integrated circuit (IC) realizations, current control feedback is added to the system.

In this thesis, three prototypes are fabricated, with the last one being an eight channel module that can be supplied from a 3.5 V battery and has a very linear relationship between the selected DAC's codes and the output delivered current and, at the same time, being able to stimulate a wide range of loads (0.148 - 10.11 k Ω) up to 2 mA. Furthermore, the employed novel boost technique shows 40.57% maximum improvement of the power efficiency, compared to the use of a conventional buck-boost converter. Moreover, the feedback system shows significant robustness, achieving only 7.6% output current divergence for 6731% change of the output load's impedance. The module has 4 μ A resolution, which is translated to 0.2% of the maximum delivered current. Except from the high resolution, the system also has a fast transient response, which is less than 2.1 ms. Additionally, when one channel is active, the stimulator shows 43.84% maximum power efficiency. The aforementioned power efficiency is 23.49% higher than the maximum efficiency of state of the art adaptive voltage current source implementations. Additionally, the multichannel system was tested in real life scenarios and its efficiency was compared to a fixed voltage current source module. The system achieved 37.57%, 45.47% and 11.59% power efficiency improvements for two, four and eight channels respectively.

Hence, a novel, multichannel module, with current feedback, is created that offers both high accuracy and improved multichannel power efficiency. The proposed system offers significant benefits compared to the existing solutions. Therefore, the system can be used for future implementations of power efficient multichannel tDCS devices.

Acknowledgements

This thesis might have one author, but there are many people that helped for its completion.

I would like to wholeheartedly thank Prof. dr. ir. W. A. Serdijn for his trust and his support. He is a great teacher and a really nice person. I feel very lucky that I had him as supervisor of my thesis and he inspired me to give my best effort.

I would also like to thank the people of TMSi, where I spent 3 fruitful months, completing my first prototype. Except from their expertise in their field, they offered a very pleasant environment to start doing research. All the people were always willing to help and they showed real interest about my project and my progress.

Furthermore, I would like to thank the people from the Bioelectronics group for their daily positive attitude and their friendly behavior, making my last year at TU Delft a very pleasant experience.

Moreover, I would like to thank A. Kaichouhi and A. Urso for their technical support and M. de Vlieger for helping me to order the project related supplies that I needed.

Last but not least, I would like to thank my family for their support and their unconditional love.

Contents

1. Introduction	17
2. Theoretical background	21
2.1. Introduction.....	21
2.2 Transcranial direct current stimulation.....	22
2.2.1. Introduction.....	22
2.2.2. Basic principles	22
2.2.3. Cellular mechanisms.....	23
2.2.4. Dose	24
2.2.5. Safety.....	25
2.2.6. Efficacy.....	26
2.2.7. Current tDCS devices	27
2.2.8. Electrodes	28
2.2.9. Electrode tissue interphase impedance	30
2.2.10. Applications	31
2.2.11. Home based tDCS	32
2.2.12. Future directions	32
2.3. Discrete components neurostimulators.....	33
2.3.1. Literature search	33
2.3.2. Systems overview	34
2.3.3. Systems comparison.....	35
2.4. Power efficient neurostimulators	37
2.4.1. Introduction.....	37
2.4.2. Systems overview	38
2.4.3. Systems comparison.....	39
2.5. Conclusions.....	40
3. System design.....	43
3.1. Introduction.....	43
3.2. Requirements specifications	43
3.3. Design of the systems.....	46
3.3.1. Morphological boxes	46
3.3.2. Electrode tissue model	51
3.3.3. Introduction to asynchronous DC/DC converters	54
3.3.4. Operating modes.....	56

3.3.5. Choosing the DC/DC converter's inductance and switching frequency.....	57
3.3.6. Transient response	59
3.3.7. Theoretical values.....	63
3.3.8. Simulation results	64
4. Systems fabrication	75
5. MCU programming	81
6. Circuits measurements.....	83
7. Conclusions and recommendations for future work.....	95
Appendix.....	107
A. Matlab code	107
B. Components' List.....	110
C. MCU Code.....	113

Figures

Figure 1: a) Adaptive voltage current source stimulator block diagram b) Minimization of the required voltage for driving the current sources by the use of an adaptive voltage supply $V_{adapt\pm}$ (V_{dd} , V_{ss} are the constant voltages of a current source) for a biphasic pulse [10]. ... 17

Figure 2: a) Current controlled stimulator with adaptive voltage supply and b) the proposed UHF stimulation module [11]. 18

Figure 3: Example of the UHF stimulation for two channel operation [10]. 18

Figure 4: a) Anodal stimulation setup and neuron response, b) Cathodal stimulation setup and neuron response [46], [47]. 23

Figure 5: Waveforms of anodal and cathodal stimulation during tDCS (not to scale) [34]. ... 24

Figure 6: Maximum average current density for different applications and different electrode sizes (recommended values) [57]. 26

Figure 7: a) A 9 channel tDCS module by Soterix Medical [66], b) A 32 channel tDCS module by Neuroelectronics [65]. 28

Figure 8: a) Conductive rubber electrodes with sponge cover and metallic pin, b) Sintered Ag/AgCl pellet electrodes [57]. 28

Figure 9: Impedances of (A) a sham tDCS group, (B) an active tDCS group that used sponge electrodes soaked into tap water, (C) an active tDCS group that used sponge electrodes soaked into 0.9% NaCl solution and (D) an active tDCS group that used conductive rubber electrodes with conductive cream as interface [75]. 30

Figure 10: Stroke rehabilitation through a) excitation of the damaged hemisphere, b) inhibition of the healthy hemisphere [90]. 31

Figure 11: Selection procedure for the studied discrete components devices. 33

Figure 12: a) VSC, b) CCS and c) SCC techniques 37

Figure 13: Comparison between fixed voltage and adaptive voltage supply current source. The adaptive voltage supply current source has the ability to adapt its voltage compliance (red) in order to be close to the required voltage (green) that is needed from the load, so as to be stimulated with the desired current. On the contrary, fixed voltage supply current source has constant voltage compliance, which is independent from the load's needs, leading to higher losses. 44

Figure 14: Comparison between adaptive voltage supply current source and UHF unfiltered power supply for three channels. Using an adaptive voltage supply current source, the voltage compliance must be enough in order its current source to be able to deliver the

desired current to the load. Furthermore, when it delivers current to multiple channels, the voltage must comply with the voltage needs of the most power demanding load, leading to high losses for the less power demanding loads. The aforementioned problems do not occur when an UHF unfiltered power supply is used..... 45

Figure 15: High level block diagram of the proposed neurostimulator. 46

Figure 16: Low level block diagram of the first prototype. 47

Figure 17: Control system of the first prototype. 47

Figure 18: Low level block diagram of the second prototype. 48

Figure 19: a) Charging phase for a conventional boost converter (during this phase the voltage across the load cannot be lower than V_1 minus the voltage across L_1 , D_1 , S_2 and S_3 , b) Discharging phase for a conventional boost converter and the proposed system, c) Charging phase for the proposed system (during this phase the S_2 is open and the load is isolated from the source, letting it to have lower voltage than V_1 , discharging through S_3) and d) The implementation of the PSM technique. 49

Figure 20: a) The PWM and b) the PSM techniques 49

Figure 21: a) Pull-down resistor and b) capacitive coupled level shifting drivers for the high side p type mosfets of the H-bridge [111]. 50

Figure 22: Low level block diagram of the third prototype..... 51

Figure 23: a) Real part and b) Imaginary part of the electrode skin impedance [114]. 51

Figure 24: Electrode tissue's equivalent circuit. 52

Figure 25: Solution space for the $R_f || C_{dl}$ of the RC model. 53

Figure 26: a) Imaginary and b) real part of the measured impedance (orange), compared with the model's impedance (cyan). 53

Figure 27: a) The boost and b) the buck-boost topologies [125]..... 54

Figure 28: An ideal noninverting buck-boost converter with a parallel RC load. 55

Figure 29: Inductor's current at a) boundary of CCM and b) DCM [125]..... 56

Figure 30: Charging (a) and discharging phase (b) for a noninverting buck-boost converter that delivers current to RC load. 59

Figure 31: Schematic diagram of the first prototype..... 69

Figure 32: Schematic diagram of the second prototype (1/2). 73

Figure 33: Schematic diagram of the second prototype (2/2). 74

Figure 34: The fabricated first prototype..... 75

Figure 35: The fabricated second prototype..... 76

Figure 36: The digital part of the third prototype..... 77

Figure 37: Attachment of the analog and the digital PCBs.	77
Figure 38: The analog part of the third prototype.	78
Figure 39: The eight channel testing circuit	78
Figure 40: Measurements and testing setup of the eight channel neurostimulator (without enclosure).	79
Figure 41: Measurements and testing setup of the eight channel neurostimulator (with enclosure).	79
Figure 42: Measured a) inductor's voltage (U_3 's side, 25 % duty cycle), b) inductor's voltage (U_3 's side, 50 % duty cycle), c) load's voltage (25 % duty cycle), d) load's voltage (50 % duty cycle).....	83
Figure 43: First prototype's power efficiency (blue line) and the output currents (yellow line) for 50% duty cycle of PWM and for different resistance values.	84
Figure 44: Relationship between the MCU's DAC's output voltages and the output current of the stimulator for different loads.....	85
Figure 45: The power efficiency of the whole system with the use of a boost converter for different output loads.	85
Figure 46: The relationship between the DAC's codes (1024 values) and the output current of the stimulator, using a boost converter, for different loads.	86
Figure 47: The power efficiency of the system, for one active channel (using boost converter) and different output loads.	87
Figure 48: Comparison between the use of the proposed boost module and a conventional buck-boost converter for two different loads.....	88
Figure 49: Power efficiency of a two channel system for two different scenarios.....	88
Figure 50: Power efficiency of a four channel system for two different scenarios.	89
Figure 51: Power efficiency of an eight channel system for two different scenarios.....	89
Figure 52: Comparison between the proposed system and a fixed voltage current source stimulator.	90
Figure 53: Transient response of the system without overshoot.	91
Figure 54: Transient response of the system with overshoot.	91

Tables

Table 1: Recommended stimulation parameters according to [57].	25
Table 2: Technical specifications of the analyzed commercial tDCS devices.	29
Table 3: Neurostimulators made with discrete components (comparison table).	36
Table 4: Power efficient neurostimulators (comparison table).	41
Table 5: Specifications of the proposed final stimulator.	43
Table 6: Neper frequency for different RC networks.	60
Table 7: Natural frequency for different C and L=175 μ H.	60
Table 8: Natural frequency for different C and L=17.5 μ H.	60
Table 9: Damping factor for different RC networks and L=175 μ H.	60
Table 10: Damping factor for different RC networks and L=17.5 μ H.	61
Table 11: The damped frequency of the system for different RC values and L=175 μ H.	61
Table 12: The damped frequency of the system for different RC values and L=17.5 μ H.	61
Table 13: Inductor's discharging time for different RC combinations and L=175 μ H.	62
Table 14: Inductor's discharging time for different RC combinations and L=17.5 μ H.	62
Table 15: Maximum capacitor that meets the maximum discharging time requirement for different resistance values.	62
Table 16: Average output current for different combinations of output resistance and number of channels (theoretical values, 50 % duty cycle).	64
Table 17: Average output current for different combinations of output resistance and number of channels (C = 50 nF) with the addition of $R_s = 150 \Omega$ in series.	65
Table 18: Percentage difference between the maximum current for the parallel RC network and the series resistor network.	65
Table 19: Average output current for different combinations of output resistance and number of channels (C = 50 nF) with the addition of a series $R_s = 150 \Omega$ resistor and a parallel to the load C = 47 nF capacitor.	66
Table 20: Percentage difference between the maximum current for the parallel RC network and the series resistor network with the addition of a 47 nF parallel capacitor.	66
Table 21: Percentage difference between the initial resistor and the equivalent series resistor with the addition of R_s .	67
Table 22: Average output current for different combinations of output resistance and number of channels (off the shelf components, C = 50 nF) with the addition of a series $R_s = 150 \Omega$ resistor and a parallel to the load C = 47 nF capacitor.	70

Table 23: Average 10 kΩ resistor’s current for different combinations of output resistance and number of channels (off the shelf components, C = 50 nF) with the addition of a series $R_s = 150 \Omega$ resistor and a parallel to the load C = 47 nF capacitor	70
Table 24: Average 10 kΩ resistor’s current for different combinations of output resistance and number of channels (off the shelf components, C = 50 nF) as percentage of the load’s average current.	71
Table 25: Components’ power dissipation for different R_{load} ($R_f = 1 \text{ k}\Omega$, 5 kΩ, 10 kΩ and $R_s = 125 \Omega$).	72
Table 26: Transient and output ripple characteristics for different loads, output currents and converter types.	93

1. Introduction

Neuromodulation has been used as effective treatment method for a plethora of diseases (Parkinson [1], epilepsy [2], chronic pain [3], etc.), as well as for restoring various sensory and motor functions (hearing [4] and vision [5] loss, motor dysfunction due to spinal cord injuries [6], etc.). Neuromodulation is achieved applying electric charge, which creates activation or deactivation of excitable tissue, leading to improved outcome for the patient.

A neurostimulator must have some specific characteristics in order to be used by the patient. The neurostimulator must be:

- small, in order to be easily worn or implanted
- safe, providing the right amount of charge, in order for irreversible hazardous effects not to occur [7]
- power efficient, due to the explantation surgery risks [8], the risk of not providing treatment when the battery is depleted, as also in order the system to be small

There are many techniques for applying electricity to neural tissue. However, in clinical practice, there is strong preference for current controlled stimulators, because of their direct control over the charge that is injected into the stimulated tissue, increasing the controllability and the safety of the device. Many techniques have been proposed in order to improve the efficiency of the implantable current controlled neurostimulators. One commonly used technique is the implementation of adaptive voltage supply, in order to minimize the power dissipation inside the current source, as shown in Figure 1 [9].

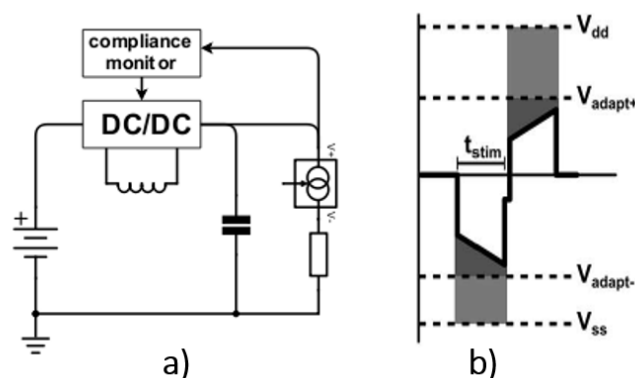


Figure 1: a) Adaptive voltage current source stimulator block diagram b) Minimization of the required voltage for driving the current sources by the use of an adaptive voltage supply $V_{adapt+/-}$ (V_{dd} , V_{ss} are the constant voltages of a current source) for a biphasic pulse [10].

Even though this technique offers better power efficiency than a standard current source, it does not scale up well for multichannel stimulation. This situation occurs, because the DC voltage supply must be designed so that it can drive the most power consuming stimulation site, degrading the energy performance for the other, less energy demanding, sites. In case

that optimal power efficiency is demanded for all channels, the number of power sources must be increased so as to meet the number of stimulation sites.

In [10], the authors proposed a novel integrated neurostimulator that offers high efficiency during multichannel operation. As has been proven in [11], high frequency switched mode monophasic stimulation can have the same effect on the tissue as constant current monophasic stimulation. The authors used the aforementioned method, in order to create a power efficient ultra high frequency (UHF) multichannel neurostimulator. The proposed system was implemented using an adaptive power supply, which delivers charge via an inductor to the stimulation sites, in the form of current pulses. The inductor can provide multichannel operation by delivering current pulses in an alternating way, to more than one stimulation sites semi simultaneously. Since each current pulse is independent from the others and can have its own amplitude, selecting different duty cycles, the waveforms that can be generated for each channel are independent. The difference between the adaptive voltage current controlled stimulator and the proposed current controlled stimulator is shown in Figure 2. An example for two channel operation of the proposed system is shown in Figure 3.

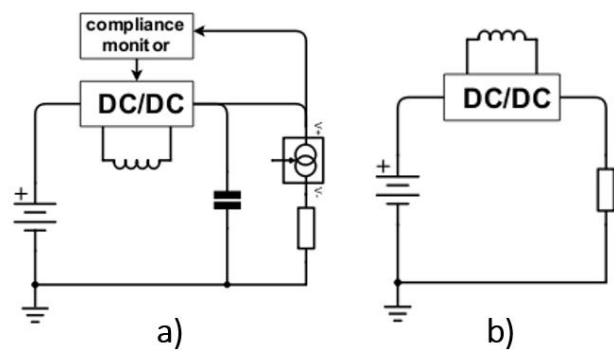


Figure 2: a) Current controlled stimulator with adaptive voltage supply and b) the proposed UHF stimulation module [11].

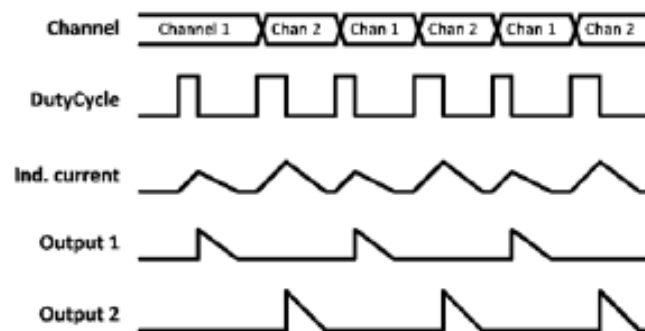


Figure 3: Example of the UHF stimulation for two channel operation [10].

The main application that the aforementioned technique is considered for in this thesis, is for transcranial direct current stimulation (tDCS). According to [12]: “tDCS is a noninvasive method, allowing for the reversible modulation of activity in particular brain regions”. Furthermore, among many benefits that have been published for tDCS, this technique has been shown to be a promising for working memory enhancement [13], depression treatment

[14], as also for stroke rehabilitation [15]. The stimulation's duration is usually less than 40 minutes and the current that is delivered to the patient is equal to or lower than 2 mA for therapeutic purposes and 4 mA for research purposes [16]. The safety aspects of tDCS have been extensively studied, showing that the aforementioned thresholds do not evoke irreversible damage to the patient [16].

In this thesis, a low power stimulation module was designed. The stimulator is the first time discrete component realization of an UHF stimulator for tDCS applications. With this approach, the technological benefits of the UHF stimulation technique were achieved, combined with a cost effective, low scale production method. Moreover, contrary to previous integrated circuit (IC) realizations, current control feedback is added to the system. In order to validate the concept, three prototypes were designed, fabricated and tested.

The thesis is structured in the following way. In Chapter 2, an introduction to tDCS, the current commercially available devices and the future trends is made. Furthermore, discrete components and power efficient stimulation modules are presented, discussed and compared. In Chapter 3, the design of the systems is described. In Chapter 4, the fabrication procedure of the three prototypes is discussed. In Chapter 5, the programming of the systems' MCU is explained. In Chapter 6, the prototypes are measured and tested. In Chapter 7, conclusions and recommendations for future work are made.

2. Theoretical background

2.1. Introduction

Nowadays, there is worldwide strong dependence on drug medication. Drug related treatment has offered cure for many diseases and has alleviated human suffering to a great extent. Nevertheless, the economic costs, as also the side effects of this dependence are shocking. In raw numbers, 70000 individuals die per year, due to drug overdose in the United States [17]. Furthermore, 333.4 billion USD per year are spent on drug prescribed medication [18]. Additionally, the development cost for a drug, in order to reach the market is estimated to be approximately 2.6 billion [19], making the invention of new drugs extremely risky and cost inefficient. Considering also that each drug that is available on the market has on average 70 and up to 500 side effects [20], with many people suffering from diseases for which there is no effective drug related treatment and with the total global yearly spending on healthcare to be estimated to reach 1.5 trillion USD in 2021 [21], alternative, safe and cost effective treatment solutions must be found and offered. One alternative approach that has been shown to be beneficial for the treatment of several diseases is the use of electroceuticals, smart electronic devices that deliver localized, targeted electrical stimulation to the body [22].

This thesis focuses on devices that offer transcranial direct current stimulation (tDCS), which is a promising technique for treatment of many diseases, as also for enhancement of human capabilities. These devices must be safe, reliable and easy to use. Furthermore, there is demand for multichannel modules, which will help neuroscientists and physicians to deliver more targeted currents and therapies to their participants or patients [23]. However, as the number of channels increases, the complexity and the power consumption of these devices also go higher, decreasing their battery life and increasing their size.

Therefore, this chapter aims to:

- Make a short introduction to the reader about the current status of the tDCS technique and its applications.
- Present and compare state of the art tDCS devices that are available to this moment.
- Give an insight in the future trends regarding these devices and the unmet needs of the users.
- Inform about the stimulator types that exist in the literature.
- Elaborate on state of the art methods for efficient multichannel stimulators.
- Conclude how the tDCS stimulation mode of the future will be able to meet the users' needs using knowledge from the literature.

2.2 Transcranial direct current stimulation

2.2.1. Introduction

tDCS is the most investigated therapeutic technology in neuropsychiatry [24], with thousands of publications (according to google scholar [25]) and hundreds of ongoing clinical trials [26]. But what is the definition of this technique? tDCS is a non invasive technique, in which low intensity (4 mA maximum) direct current (DC) is applied via electrodes to the patient's head, in order for his brain to be stimulated and to eventually undergo plasticity [23]. tDCS is used as treatment or side treatment for numerous disorders, such as depression [14], neuropathic pain [27], Parkinson's disease [28], addiction [29], as well as for enhancement of cognitive functions [30]. tDCS devices are very popular, because they offer many benefits compared to alternative stimulation devices.

One advantage of the tDCS modules, is their portability, giving the freedom to be worn even during other therapies (e.g., during transcranial magnetic stimulation (TMS)) or imaging procedures (e.g., during magnetic resonance imaging (MRI)) [31]. Another advantage of these devices is that they have low cost (100 - 1000\$ for commercially available devices) and their use does not need advanced training by the user (physician, researcher, or technician) [32]. From the aforementioned advantages, it is evident that tDCS has the potential to be used as replacement therapy, instead of expensive drug related or other medical device related treatments. Additionally, it has been shown that tDCS has the potential of enhancing the efficacy of existing therapies [33] leading to less costs and less suffering for the patient.

2.2.2. Basic principles

As discussed in the previous paragraph, tDCS delivers low intensity current for a prolonged period, via two electrodes, through the skull. The electrode, which distributes current into skull, is named anode and the electrode, from which current exits the skull, is named cathode. During this procedure, electric fields are created throughout the brain, polarizing the neurons that are exposed to them. The depolarization that is created via these fields is small (approximately 0.3 V/m maximum per 1 mA applied DC current [34]). Despite their small intensity, these fields have been observed to make neurons more susceptible to plasticity. It is important to be mentioned that the fields that are created from a tDCS device have not enough intensity to create action potentials to the neurons by themselves. Hence, the most popular theory states that tDCS fields work as a modulator, which improves the ability of the brain to experience plasticity. From the aforementioned theory, it is evident that tDCS can be used in combination with another stimulus as a booster [35]. Therefore, tDCS can create functional targeting, in which only populations of neurons that are already active due to a sensory or electric stimulus will be affected by the delivered DC current. There exist numerous animal data that confirm this hypothesis [36]. However, tDCS has also been used as monotherapy [37].

2.2.3. Cellular mechanisms

There are several underlined mechanisms that have been investigated, in order to fully understand the effects of tDCS, such as the modification of the synaptic microenvironment (long term potentiation effects [38]), prolonged neurochemical changes [39], complex interactions with neurotransmitter systems [40], connectivity driven remote effects [41] and potential effects on nonneuronal structures (e.g. the vesicular tone [42]). A popular approach is the association of a brain region with an observed symptom and the study of this region during hyperactivity or hypoactivity. At single neuron level, depolarization of the soma and hyperpolarization of the apical dendrite of the neuron leads to its depolarization, which can be achieved placing the electrodes' anode closer to the neuron's dendrite. This setup is called anodal stimulation and it has been shown that it increases the plasticity/excitability of the brain. The opposite setup, placing the anode closer to the soma, which leads to its hyperpolarization and depolarization of the apical dendrite, creates hyperpolarization of the neuron. This setup is called cathodal stimulation and it has been observed that it inhibits the plasticity/excitability of the brain [23]. The two aforementioned stimulation types are shown in Figure 4.

The electric field that is created due to tDCS inside the brain region is less than 1V/m [43]. The soma of most sensitive cells is expected to be polarized with 0.1 mV, when 0.3V/m electric field is applied due to 1mA delivered current. When 2 mA of current is delivered to the skull, the most sensitive neuron will be polarized by 0.2 mV [44]. However, TMS and electroconvulsive therapy (ECT) produce electric fields with magnitudes of 100 V/m [35] that can create action potentials in the neurons [45].

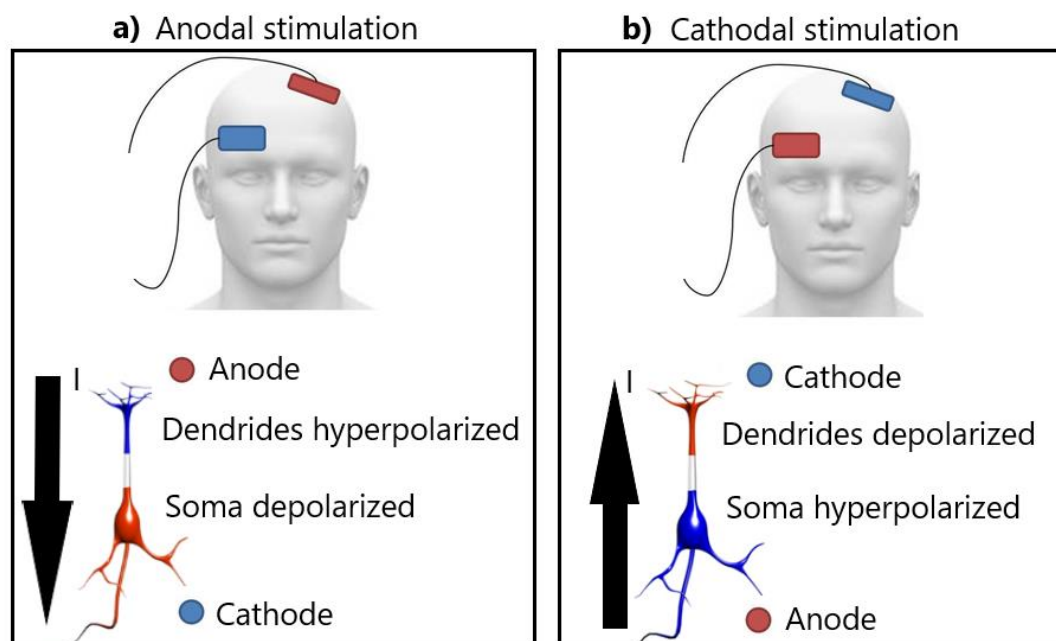


Figure 4: a) Anodal stimulation setup and neuron response, b) Cathodal stimulation setup and neuron response [46], [47].

A valid question is how the interaction of tDCS with the neurons can be assessed, since its amplitude cannot create active potential by itself. A method that is used as golden standard

for evaluating the role of tDCS is the change of the TMS response, when tDCS is applied. It has been shown that the sensitivity of the evoked response due to TMS changes with the use of tDCS [48]. Another method that has been used is application of excitatory postsynaptic potentials (EPSP) to the neuron. EPSP can work as a metric of cellular synaptic efficacy. Measuring it in presence and absence of tDCS, has been observed that when applying anodal tDCS, EPSP is increased. The opposite effect occurs when performing cathodal stimulation [35].

2.2.4. Dose

For tDCS, 1 - 2 mA of DC current is the most commonly applied dose [35]. However, in some studies doses reach the maximum of 4 mA [49]. The therapies can occur in multiple sessions, which typically last from 1 to 30 minutes, with the ramping up and down of the waveform to usually last 10 seconds [35]. A representation of the created waveforms during anodal and cathodal stimulation can be shown in Figure 5.

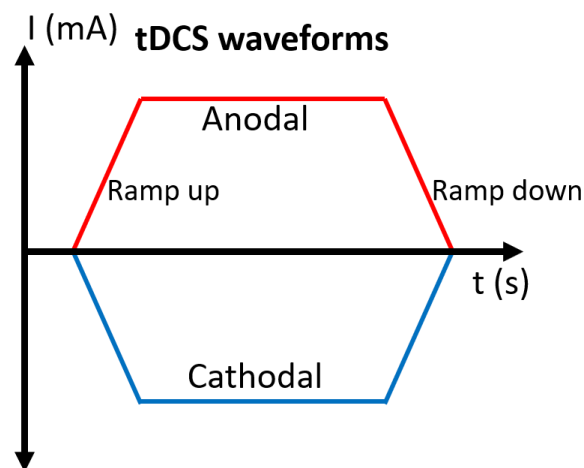


Figure 5: Waveforms of anodal and cathodal stimulation during tDCS (not to scale) [34].

Stimulating rat hippocampal slices *in vitro*, it has been shown that with the increase of the delivered current, the intensity of the electric field will also increase in a linear fashion. Hence, there is a linear relationship between the neurons' membrane polarization and applied electric field intensity [50]. However, modelling the propagation of the electric waves through the human skull and into the brain, it has been observed that current follows very different pathways in different heads, even with the application of same montage and dose. This situation occurs due to variation of anatomical characteristics of each individual's head [51]. Furthermore, the stimulation intensity does not have linear relationship with the desired results [52].

2.2.5. Safety

Nowadays, many tDCS devices are available on the market, giving access to individuals for home use. Moreover, the fabrication of a tDCS device is simple and straightforward even for a person with low technical expertise in the field of electronics, since a tDCS device in its most simple form can be created by a 9 V battery, a current source and two electrodes (the author by no means recommends the fabrication and use of DIY tDCS devices, due to safety concerns [53]).

The tDCS technique has been characterized as “low risk” for the users [54], [55]. Compared to animal clinical trials, it has been shown that the total charge that is needed for a lesion to be created to the brain of a rodent is two orders of magnitude higher than the charge injected for a 20 min, 1 - 2 mA tDCS therapy using 25–35 cm² wet sponges (52400 C/m² and 343–960 C/m², respectively [56]). Furthermore, in a recent review, it has been shown that in a population of over 1000 subjects, with over 33200 tDCS sessions, no serious adverse effect or irreversible injury was observed (40 min, 4 mA and 7.2 C maximum stimulation parameters) [16]. The recommended maximum stimulation values that one of the tDCS device vendors recommends are shown in Table 1. Furthermore, a graph showing a conservative recommendation regarding the maximum average current density that can be used in different applications for different electrode sizes is shown in Figure 6. Average current densities must also be kept far from 14.3 mA/cm², which is the threshold for tissue damage due to tDCS [57].

Table 1: Recommended stimulation parameters according to [57].

Stimulation Parameters	Maximum recommended values
Contact impedance (k Ω)	20
Current per channel (mA)	2
Total current (mA)	4
Voltage compliance (V)	30
Session duration (min)	40
<i>Average current density (mA/cm²)</i>	
(Clinical use)	0.06
(Advanced clinical use)	0.08
(Research use)	0.64

Non serious adverse effects have been observed to occur during tDCS sessions, such as tingling, itching, skin irritation [16], burning sensation and middle pain [58]. These side effects are possibly to be created due to poor electrode skin interface [16]. As interface medium (buffer) electrolytes and gels are used, in order to lower the impedance between the electrode and the skin. In this way the voltage compliance limits of the stimulation device are met, as also non desirable electrochemical effects that could be created are prevented [59]. These effects could occur if the electrode was directly attached to skin, because of the monophasic nature of the tDCS technique that does not implement charge balancing. From the previous discussion, it is evident that safety considerations must be taken and individuals, who are interested to undergo tDCS, should select a safe device from a reliable vendor. Furthermore, they should be advised by an experienced physician about how to deliver the therapy. In order to avoid undesirable effects or malfunction of the tDCS device, the LOTES

guideline has been created [60], which describes the minimum technical criteria (standards) that the commercially available tDCS devices should meet in order to have certain efficacy and safety for the consumers. LOTES has also been advocated by some key player companies in the tDCS device market.

Regarding the availability of tDCS modules, one drawback, especially for the medical devices that are intended to be used in the US, is that they cannot be directly offered to consumers, because they have only been exempted from FDA for investigational use. However, there is a plethora of tDCS devices available in the market that do not have any form of clearance, because they are declared as wellness products and they do not claim medical benefits. Nevertheless, consumers and researchers have the option to purchase them and unofficially use them for medical and investigational purposes [61]. Fortunately, more and more countries have started to allow tDCS as off label treatment for specific diseases [62] and this situation will open the window for the consumers to have access to more reliable devices. Nevertheless, more clinical trials must be still performed in order for the efficacy of tDCS therapy to become unanimously unambiguous and its long term safety to be defined with certainty.

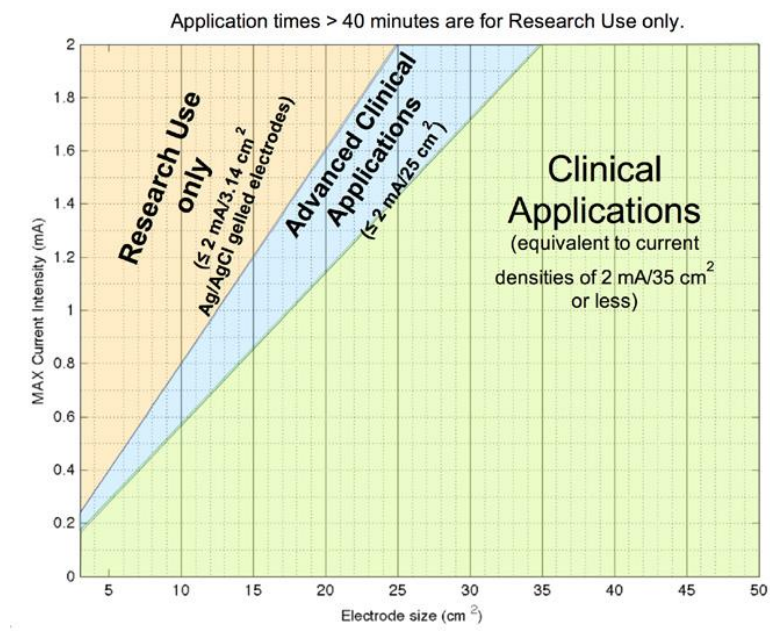


Figure 6: Maximum average current density for different applications and different electrode sizes (recommended values) [57].

2.2.6. Efficacy

Reproducibility of the scientific results between clinical trials is a big issue for the tDCS technique. A tDCS experiment in different centers with different population groups, different applied stimuli, number of sessions, magnitude of applied current, electrode setup and placement method is inevitable to create different effects to the participants and therefore, the results will deviate. Another criticism about tDCS is that it has been tested almost only under laboratory conditions [63]. Therefore, its efficacy in a real life task has not been completely validated, yet. As prof. V. Walsh argues: “Based on the best available studies, from reputable laboratories, we don’t really know where to put the electrodes, we don’t know how

robust the idea is that the effects are excitatory or inhibitory, we don't know what other behaviors are affected, we haven't tested the methods with real world tasks and therefore don't know how they perform outside the lab, and we have no idea in healthy people if they continue to work after more than 2-3 repeated applications." [63]. Nevertheless, there is vast number of papers that support the efficacy of tDCS for treating diseases, as also for increasing the performance of the participants in various tasks.

2.2.7. Current tDCS devices

TDCS devices in general have very simple circuitry. The easiest way of creating a DIY tDCS module is the use of a current source (e.g. a LM134/ 3 terminal current source [64]), one variable resistor for adjusting the current to the desired value, enough batteries, connected in series, for supplying the current source with enough voltage, so as to be able to meet the voltage compliance that the load needs, and two electrodes. Instead of many batteries in series, or a high voltage battery, a low voltage battery could be used with a boost converter stepping up the output voltage to the level that is needed. However, the DIY fabrication and use of a "medical device" may be dangerous and by no means is advised or recommended [53].

There are plenty of companies that create tDCS devices, which certainly meet more safety standards than something created by hobbyists. Regarding the former devices there is wide variety of options. The majority of them weight less than a kilogram. The dimensions vary from completely portable to benchtop devices. The majority of them have one channel, but there are multiple channel options reaching to 32 channels per device [65], with options for going even higher using more than one device simultaneously [66]. Two examples of multichannel devices are shown in Figure 7.

All devices can deliver at least 2 mA of DC current at their output with equal or less than 10% accuracy. Furthermore, their resolution is equal or higher than 50 μ A. Regarding the output voltage compliance, the majority of them tend to be around 30 V, making them able of delivering 2 mA current to loads for up to 15 k Ω resistance. The majority of the devices use Li-Ion batteries, which last for a few hundreds of minutes. All the used batteries have nominal voltage lower than the voltage compliance level. Hence, it is certain that a step up converter exists in their circuit. Regarding their power efficiency, there are not enough technical specifications provided by most vendors, in order to be calculated. Nevertheless, in some devices power efficiency was able to be extracted delivering the maximum output current for their nominal voltage compliance. The maximum power efficiency was 12.8% for single channel modules and 1.88% for multichannel modules. Table 2 displays all the relevant technical specifications for the analyzed commercial tDCS devices.



Figure 7: a) A 9 channel tDCS module by Soterix Medical [66], b) A 32 channel tDCS module by Neuroelectrics [65].

2.2.8. Electrodes

Various types of electrodes have been used for tDCS. The most commonly used electrodes are made of conductive rubber, or metal (typically rectangular 5×5 cm or 5×7 cm). Additionally, saline soaked sponges, or gels are used as electrode skin interphases [67]. Furthermore, there are electrodes available for single or multiple uses. The minimum distance between the electrode and the skin is defined by the thickness of the interphase medium [34]. The use of an interphase medium is crucial, as discussed in previous paragraphs, for avoidance of minor injuries, such as skin irritations. The positioning of the electrodes follows the 10/10 or 10/20 systems used in electroencephalography (EEG). The electrodes are commonly integrated to headgear, which has the form of a cap or a rubber band [23].

There is currently a trend of using electrodes with smaller surfaces that are called high definition (HD) electrodes. HD electrodes are Ag/AgCl electrodes. They typically have small diameter (around 1 cm) and gel is used as interface. The use of HD electrodes is beneficial because it increases focality of the applied current and there is also the option for multi electrode setup that allow spatially precise current steering. The most commonly used HD setup is the 4x1 implementation, in which 1 electrode is used in the center of the targeted area and it is surrounded by 4 electrodes, which have the opposite polarity [68]. The lifespan of Ag/AgCl electrodes is less than the other electrode types, because chloride dissolves through the electrolyte during use [57]. Different electrode types are displayed in Figure 8.



Figure 8: a) Conductive rubber electrodes with sponge cover and metallic pin, b) Sintered Ag/AgCl pellet electrodes [57].

Table 2: Technical specifications of the analyzed commercial tDCS devices.

Parameters	TDCS modules							
Name	Halo sport [69]	DC stimulator mobile [70]	DC stimulator Plus [71]	DC stimulator MC [72]	Starstim 20/32 [65]	Starstim 8 [73]	Model 1300A [74]	Model 9002 [66]
Manufacturer	Halo neuro.	Neuroconn	Neuroconn	Neuroconn	Neuroelectrics	Neuroelectrics	Soterix Medical	Soterix Medical
Enclosure	Headset	Box	Box	Box	Box	Box	Box	Box
Weight (g)	340	112	800	4200	-	85	544	3175
Dimensions (mm)	-	71 X 133 X 15	135 X 225 X 55	420 x 395 x 170	-	87 x 61 x 24.8	201 x 150 x 72	345 x 259 x 152
Channels (#)	1	1	1	8	20/32	8	1	9
Electrodes (#)	3	2	2	16	20/32	8	2	-
I_{max} per channel (mA)	2.2	±2	±4.5	±4	±2	±2	±2	±2.5
Accuracy error (%)	10	2	1	1	1	10	1	1
I_{resolution} (µA)	50	10	-	50	1	1	-	-
V_{compliance} (V)	36	16	20	30	30	30	40	30
R_{max} at 2 mA (kΩ)	18	8	10	15	15	15	20	15
V_{bat} (V)	3.7	-	-	-	3.7	3.7	18	4.8
Battery type	Li-Ion (LiPo)	-	-	-	Li-Ion	Li-Ion	Li-Ion	Ni-MH
Battery life (min)	160	90	360	-	240	716	360	720
Battery capacity (mAh)	-	-	-	-	-	-	600	10000
P_{max} (mW)	-	250	-	-	-	-	-	-
η_{max} (%)	-	12.8	-	-	-	-	4.44	1.88

2.2.9. Electrode tissue interphase impedance

Regarding the electrode tissue interphase resistance, in [75], 15 participants, who were separated into four groups (a sham tDCS group, an active tDCS group that used sponge electrodes soaked into tap water, an active tDCS group that used sponge electrodes soaked into 0.9% NaCl solution and an active tDCS group that used conductive rubber electrodes with conductive cream as interface) had a 20 min, 2 mA session of bifrontal tDCS and their electrode tissue impedance was measured. The results show that the electrode tissue resistance was high in the start of the stimulation (around 20 k Ω) for all groups, but after 30 s the resistance dropped to around 5 k Ω and remained close to this value for the active tDCS groups, as shown in Figure 9. The resistance for the sham tDCS group was low as much as the stimulation lasted and then it almost returned to its initial value.

In [76], different types of HD electrodes and interface mediums were tested at eight participants. During a session, 2mA DC current was delivered for 22 min. For this study five electrode types (Ag pellet, Ag/AgCl pellet, rubber pellet, Ag/AgCl ring and Ag/AgCl disc) and seven gel types (Signa, Spectra, Tensive, Redux, BioGel, Lectron and CCNY-4) were tested. The Ag/AgCl ring electrodes showed optimal comfort among participants feeling no difference between anodal and cathodal stimulation. Regarding the electrode impedance, only the Ag/AgCl ring and Ag/AgCl disc showed low resistance, which was equal or less than 2.5 k Ω for all the gel mediums. For other electrode types, high resistance levels were observed, for which the required stimulation voltage exceeded the compliance level, leading to the termination of the session.

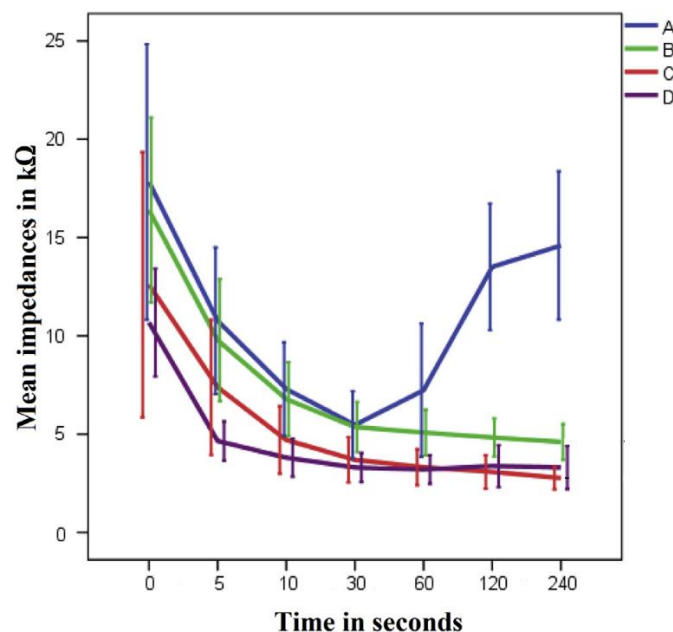


Figure 9: Impedances of (A) a sham tDCS group, (B) an active tDCS group that used sponge electrodes soaked into tap water, (C) an active tDCS group that used sponge electrodes soaked into 0.9% NaCl solution and (D) an active tDCS group that used conductive rubber electrodes with conductive cream as interface [75].

2.2.10. Applications

There are many application areas for which tDCS has the potential to be beneficial. Some of them are disease related (e.g., poststroke rehabilitation [77], pain management [27], depression [14], addictions [29], schizophrenia [78] and dementia treatment [79]) and others are related to the enhancement of human capabilities, (e.g. cognitive enhancement [30]). In the next paragraphs stroke rehabilitation and cognitive enhancement will be further discussed.

Regarding poststroke rehabilitation, there exists extensive literature, specialized for the treatment of visuospatial neglect [80], paresis [81] and aphasia [82]. The existing theories support that inside a healthy brain, many interhemispheric interactions occur. In this case, when one hemisphere has a lesion, the other changes its interaction with the damaged one. Through the literature, many stimulation approaches have been investigated. One approach supports that the damaged hemisphere must be excited and a second approach supports that the healthy hemisphere must be inhibited [83]. The aforementioned two approaches are illustrated in Figure 10. There also has been shown that tDCS influences the excitability of the motor cortex. Moreover, the motor cortex's excitability is polarity and setup dependent. Furthermore, excitability's after effects depend on the duration and the polarity of the applied field and they can last at least some minutes after the current delivery [84].

Regarding the cognitive enhancement, several studies have shown that tDCS can help individuals to perform one task better [85] or enhance their memory [13]. In [85], it has been shown that careful implementation of tDCS and execution of a specific task can double the rate of learning. Another study [86] showed that tDCS had better efficacy than taking caffeine for the sleep deprived participants, in order to sustain their vigilance, with less side effects for them. Furthermore, using tDCS, language [87], learning & memory [88], and executive functions [89] have been shown to be improved.

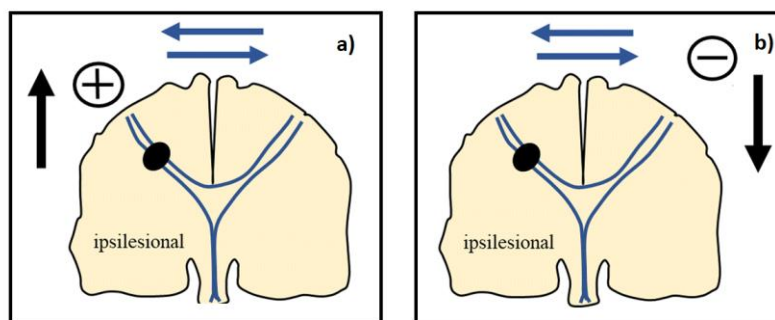


Figure 10: Stroke rehabilitation through a) excitation of the damaged hemisphere, b) inhibition of the healthy hemisphere [90].

2.2.11. Home based tDCS

Regarding tDCS, a current trend is the effort of creating home based tDCS treatments and clinical tests. It could be argued that people have already the possibility of performing tDCS at their house, using neither FDA approved nor CE marked devices that they can easily buy from the market. However, the use of these devices, in an unsupervised environment, might create side effects to the users. Hence, a correctly implemented home-based tDCS therapy should be defined as the use of FDA approved, or CE marked tDCS devices, at home, with the supervision of technical experts and/or physicians. The users/patients/participants must have access to the information that they need regarding the use of these devices. Furthermore, extra attention is needed for the management of potential accidents or side effects that might occur [91].

This approach will have many benefits for the patients/participants, as also for the physicians and the researchers. First of all, the costs associated with travelling to the clinic, the preparation of the patients/patients by the personnel and the use of the clinical settings will be diminished. Furthermore, patients/participants that are not able to travel (due to severe illness, or disability) will have the possibility to perform their therapy/test at home. Last but not least, this would be an opportunity for studying more easily the long lasting effects of tDCS, since the multiple visits to the clinical settings for multi session treatments might be difficult for the patients/participants [91].

2.2.12. Future directions

TDCS that is performed today is almost the same as the method that was used 20 years ago (applying 2 mA current, during a 20 min session, using two large surface sponge electrodes [23]). The tDCS module of the future must have increased portability, increased battery life, focality and sensing capabilities. Regarding portability, there are available commercial devices that have small size [70]. However, size could be further decreased, if the devices were power efficient enough to use batteries with smaller profile. Furthermore, as was found in Section 2.7, many existing devices have very low power efficiency. This situation urges the design of low power tDCS devices. Power efficient tDCS modules will also smaller capacity batteries benefiting the portability of the system.

Moreover, there is an increased interest from the researchers and physicians for multichannel devices that use small diameter electrodes. These devices can increase the focality and the accuracy of the delivered currents, offering more targeted therapies [92], and they could also be used in closed loop tasks [93]. For example, if the participant's eyes do not pay attention to a task, by means of closed loop tDCS, the participant can be made aware again. Combination of electroencephalogram (EEG) with tDCS using the same electrodes would be really beneficial for implementing the closed loop algorithm, in which EEG signal will be recorded and stimulation will be adapted in real time. This technique will use elements of the reciprocity theory, in which the recorded potentials at the surface of the skull can be inverted, in order to return to the same regions that created them, forming the same fields through the brain, without the need for localization of the original sources. Additionally, the integration of EEG sensors, heart rate monitors, galvanic skin response meters, etc., will provide extra biomarkers for the system. However, with more stimulation channels, the power dissipation,

the complexity and the size of the modules will become higher. Hence, it is evident that research towards power efficient multichannel tDCS devices is of utmost importance for the future of the field.

2.3. Discrete components neurostimulators

2.3.1. Literature search

In the literature, there is only one single channel tDCS implementation that uses integrated circuits (ICs) [94]. Furthermore, all the commercially available tDCS devices have been made with discrete components. Therefore, it would be beneficial for companies, as also for researchers (since discrete components prototyping is more time and cost efficient) power efficient designs to be implemented for the next generation of PCB based tDCS modules. In the next paragraphs, literature research is presented for the PCB based stimulation devices that exist up to now.

The search was made via the Scopus database [95], on 09/08/2019, using the keywords:

Stimulator, low cost, cost efficient, cost effective, PCB, discrete, off the shelf, portable, wearable, tDCS, direct current (DC), transcranial electrical stimulation (TES)

and combinations of them. The search was constrained to devices from 2010 to 2019, leading to 89 relevant results. From these results, devices that did not have application to the central nervous system (CNS), as also devices that were not fabricated (only simulated) were excluded. Furthermore, because of the importance of extracting some power efficiency information of the device, due to the nature of this thesis, literature that did not provide enough information for this topic was also excluded, leading to 5 devices. The selection procedure is also illustrated in Figure 11. An overview of the selected devices is presented in the next paragraphs. Additionally, Table 3 is provided for faster comparison between the most important characteristics of the discussed devices.

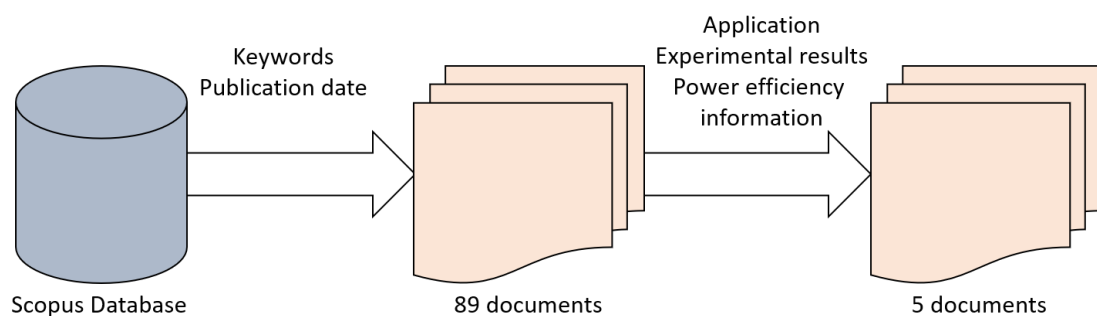


Figure 11: Selection procedure for the studied discrete components devices.

2.3.2. Systems overview

In 2010, Vidal and Ghovanloo created a 4 channel, charge based neurostimulator, using discrete components, for deep brain stimulation (DBS) applications [96]. The charge based or switched capacitor based stimulator (SCS) uses 1 μF capacitor banks (charged positively for anodic and negatively for cathodic stimulation) that are discharged to the stimulated tissue. For the charging of the capacitors a flyback DC/DC converter is used that can be supplied with a 2.5 V battery and the charging sequence is controlled by a MSP430 microcontroller. For the change of the output current mosfets are used, controlled by digital potentiometers. The system performs charge balanced biphasic stimulation. Hence, for charge balancing, a floating current sensor is used. The device was designed for 0.3 - 3 μF / 1.1 - 2.5 k Ω series load and it can deliver up to 5 mA current, having ± 11.4 V voltage compliance. The device showed 58.8% maximum power efficiency for one stimulated channel.

In 2013, Ewing et al. created a wearable two channel current controlled stimulator (CCS) for DBS applications in rodents [97]. The voltage supply of the system is a 3.7 V LiPo battery. The size of the system is 33 \times 20 \times 8 mm and weights 11.5 g. The voltage compliance of the device is 20 V and it is provided by a charge pump. The current sources were transistor based and they were adjusted using digital potentiometers. Furthermore, switching of current sources was made using mosfets. The system performs charge balanced biphasic stimulation. Hence, charge balancing was made by a negative phase pulse with equal area to that during the anodic pulse. After the end of the biphasic pulse, the stimulated tissue is shorted. The device is designed for 12 k Ω loads and it is able to deliver 1 mA current (13 μA resolution). The maximum power consumption of the device for stimulation of 12 k Ω load with 100 μA current is estimated to be less than 6.67% using two channels.

In 2014, Samani et al. designed a two channel, wireless controlled backpack neurostimulator for CNS applications in rodents [98]. The system delivers up to 2 mA current (1 μA resolution) and has 6V voltage compliance. The dimensions of the system are 15 \times 20 \times 40 mm and weights 13.5 g. The system uses a voltage controlled current pump (Howland pump) that is controlled via a DAC, which is programmed from a low power PIC microcontroller. The voltage supply is a 3.7 V battery. The system is designed for 0.5 - 1.5 k Ω load resistances and has 0.7% accuracy. The system dissipates 5 mW quiescent power.

In 2015, Acosta et al. created a small profile neurostimulator, made from discrete components, for DBS applications in rodents [99]. The stimulator's size is 8 \times 7 mm² and weights 2.3 g. The system consists of a low power MCU (supplied by a 3V linear regulator) that uses its internal 5 bit DAC to vary the output current that is delivered by a transconductance amplifier. The amplifier is supplied by a DC/DC converter, that has 5.6V input supply, provided by Zinc Air cells. The voltage compliance of the device is 12 V and the delivered current can be 100, 200, 300 or 400 μA . The system was designed for loads in the order of 3 k Ω . The system has an rms error of 7.3% and has a power efficiency of 4.43% for delivering the maximum current to a 3 k Ω load.

In 2018, Olafsdottir et al. designed an implantable spinal cord stimulator for rodents [100]. The whole device is supplied by a 6 V battery. In the PCB there is an embedded MCU, which is programmed via a PC. The MCU calculates the maximum voltage that is needed for the load measuring a testing pulse with its inbuilt ADC. Moreover, it controls a step up converter to adapt its output voltage 1.75 V higher than the voltage needed for the stimulation of the

tissue. For the delivery of the current, a power efficient current source topology is used, which is controlled by a 6 bit DAC that is programmed via the MCU. The size of the device is 13.5 cm³. Furthermore, the device has 28 V voltage compliance and can deliver up to 1 mA (10 μ A resolution) current to 25 k Ω loads, with 97.48% accuracy. The device has a 35.5 % maximum power efficiency.

2.3.3. Systems comparison

From the overview, it can be seen that the majority of the discrete components systems have been designed to have small size and weight, in order to be able to be implanted in rodents. In [97], [98] and [99] CCS devices were used. These devices have current sources that are fed from a fixed voltage supply. Therefore, they will have low power efficiency, when they will need to deliver low currents to light loads. In [100], the implemented device, having an adaptive voltage compliance, offers significantly higher power efficiency at low power loads compared to the previous modules. Moreover, the SCS module in [96] has the best maximum power efficiency, which was expected because it doesn't dissipate power due to the proper biasing of the current sources that all the CCS must have. However, it has lower voltage compliance compared to [100] and [97], minimizing the range of applications that it can be used for.

Table 3: Neurostimulators made with discrete components (comparison table).

Parameters	TDCS devices				
Reference	[96]	[97]	[98]	[99]	[100]
Authors	Vidal & Ghovanloo	Ewing et al.	Samani et al.	Acosta et al.	Olafsdottir et al.
Year	2010	2013	2014	2015	2018
Application	DBS	DBS	CNS stimulation	DBS	ESCS
Stimulation type	SCS	CCS	CCS	CCS	Adaptive CCS
Channels (#)	4	2	2	1	1
V_{Input supply} (V)	2.5	3.6	3.7	5.6	6
V_{compliance} (V)	10	20	6	12	28
I_{max} (mA)	5	1	2	0.4	1
I_{resolution} (μA)	-	13	1	-	10
Accuracy error (%)	-	-	0.7	7.3	2.5
R_{typical} (kΩ)	1.1 - 2.5	12	0.5 - 1.5	3	10 - 25
η_{max} (%)	58.8	6.7	48.4	3.48	35.5
Dimensions	-	31.5 x 17 x 5.7 mm	15 x 20 x 40 mm	8 x 7 mm	13.5 cm ³
Weight (g)	-	11.2	13.5	2.3	-

2.4. Power efficient neurostimulators

2.4.1. Introduction

In the literature, three basic types of neurostimulation techniques can be observed, depending on the way that the output source stimulates the tissue. These techniques are:

- Voltage controlled stimulation (VCS)
- Current controlled stimulation (CCS)
- Switched capacitor based stimulation (SCS)

In VCS, a desired voltage is applied at the ends of the electrodes, in CCS a desired current is delivered through the electrodes and in SCS a capacitor bank is charged with a specific charge and in a two step procedure the charge is delivered to the selected tissues through the electrodes. The aforementioned techniques are shown in Figure 12.

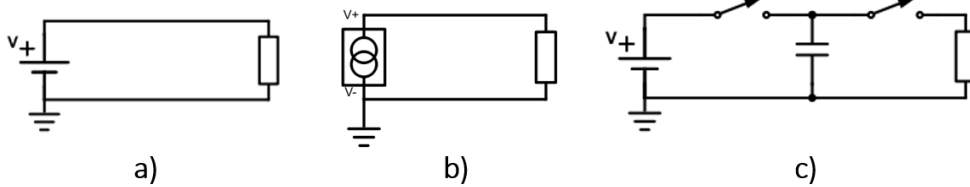


Figure 12: a) VCS, b) CCS and c) SCC techniques

In [101], an experimental study was made about the efficiency between the aforementioned basic stimulator types. The setup was consisted by two platinum circular electrodes, with 2.3 mm² diameter, put into saline solution and a PCB that consisted of a VCS, a CCS and a SCS. The electrode electrolyte resistance and capacitance were 962 Ω and 810 nF respectively. The average power efficiency was calculated from the average value of ten stimulation cycles. The power efficiency's equation is:

$$\eta = \frac{P_{av,out}}{P_{av,in}} \quad (1)$$

Where $P_{av,out}$ is the average power that the load consumes and $P_{av,in}$ is the average power that is supplied at the input of the system from the power supply. The efficiencies were 92%, 65% and 77% for the VCS, CCS and SCS technique, respectively. Therefore, we observe that the VCS is the most power efficient. However, because the electrode tissue interface has dynamic characteristics there is no direct control of the delivered charge to the tissue [102], leading to safety concerns, since overcharge can lead to safety hazards [103]. This phenome happens, because the resistance of the tissue has dynamic properties [104]. Therefore, if we apply a constant voltage to the tissue the current that will pass through the tissue will not be constant. The excitability of the tissue depends on the time current strength equation [105]:

$$I_{th} = \frac{I_R}{1 - e^{-Kt}} \quad (2)$$

where I_{th} is the threshold current that is needed to be applied for a duration t , in order action potentials to be created, I_R is called the rheobase current and it is the minimum current that can stimulate the tissue, when it is applied for infinite time duration, and K is an experimentally derived constant that depends on the electrode/tissue characteristics [105]. Consequently, a constant voltage cannot specify neither the exact excitation time nor the exact excitation strength. Therefore, there is strong preference for current controlled stimulators in clinical practice, even though they are the least power efficient.

In SCSs, for better power efficiency, the capacitance and the number of the discharging capacitors should be increased leading to bigger and bulkier devices. Furthermore, the power efficiency drops even lower, as much as the supply voltage deviates from the desired output voltage. Additionally, activating multiple channels simultaneously, the number of switches as well as the power dissipation of the system due to switching is increased. Therefore, for multielectrode implementations, SCS does not scale up well.

In the next section, an overview will be made of various neurostimulation modules with improved power efficiency. Additionally, Table 4 is provided for faster comparison between the most important characteristics of the discussed devices. All the systems were implemented as ICs. Systems that were only simulated and not fabricated were excluded. From the overview, systems that have wireless power supply were also excluded. The reason for this is that the system that will be implemented for the thesis will use a battery. Therefore, power efficiency improvements regarding AC/DC converters will not be applicable.

2.4.2. Systems overview

In 2012, Afrin & Sarpeshkar implemented a VCS using dynamic power supply [106]. In this implementation the output voltage was adapted to the minimum voltage compliance that is needed from the system to stimulate the tissue with the desired current. Current feedback is provided by a shunt current sensor. In this implementation also energy recycling is achieved via a forward buck/reverse boost converter, which charges back the power supply during the second charge balancing phase. Furthermore, since the system does not have current sources, the power dissipation that would be needed for driving its transistors is avoided. The system has up to 300 % less power dissipation compared to a fixed voltage supply conventional current source.

In 2013, Williams & Constandinou created a fully integrated 8 channel neurostimulator that uses CCS [9]. This stimulator uses dynamic voltage scaling (DVS). In this implementation there is a DC/DC converter that uses switched capacitors. In the capacitor network, each capacitor has a different voltage level. The voltage level is controlled by feedback in order to comply with the minimum voltage required for the current source and the H-bridge that exist at each output. Nevertheless, the current source requires some voltage compliance in order to work properly, thereby increasing the losses. Furthermore, the increased number of switches that are needed for the switching capacitor network as also the finite number of implemented voltages reduce the efficiency and the precision of the system respectively. The stimulator offers 50% less power dissipation compared to a conventional current source.

In 2013, Lin et al. designed an implantable neurostimulator for epilepsy applications [107]. The stimulator, via its current source, is able to deliver up to 40 μ A currents to 10 – 300 k Ω

loads. The system consists of a high voltage generator that was created with a 4 stage charge pump, implemented with 15 pF capacitors, working at 25 MHz. The generator has a voltage compliance of 14 V and it is adapted to the load's resistance via a feedback network. The feedback network consists of a current mirror and a comparator. The whole system is supplied by 3.3V and it has 1.1 - 1.4 mW power consumption.

In 2016, van Dongen & Serdijn designed an 8 channel neurostimulator using an ultra high frequency unfiltered dynamic supply [10]. The system uses a buck-boost converter, which operates in discontinuous conduction mode (DCM) and delivers high frequency (1 MHz) current pulses to its loads. At the output there is no current source or output filter capacitance, because the loads are directly charged by the converter's current pulses. This happens due to the capacitive properties of the electrode tissue interface. Hence, the load builds the desired stimulation voltage by itself. The system works with an input voltage of 3.5 V. Furthermore, it can perform biphasic stimulation using an H-bridge for each electrode. Except from the 3.5 V supply, a 20 V supply is also needed for the driving of the high side switches of the H-bridge. The system can deliver up to 10 mA of current to 1 k Ω loads, having a voltage compliance of 10 V. During the stimulation of multiple channels, the system administers the pulses in alternate form to each channel. Hence the frequency that each channel can receive a pulse is inversely proportional to the number of stimulation channels that are used. The charge balancing of the load takes place using a single comparator for all the channels and inserting counter charge pulses. The efficiency of the system can reach 40% for multichannel operation.

In 2016, Lee et al. created an implantable neurostimulator that was tested for epilepsy treatment [108]. The system uses one DC/DC converter to feed the current sources, via intermediate capacitors, during the anodic phase (forward boost) and takes back energy from the load during the cathodic phase (forward buck). The system uses direct voltage forming (DVF), in order to adapt, in real time, the compliance voltage of each channel to the voltage level that is needed for the load, plus the voltage compliance of the current sources. For the switching of the converter, a pulse skipping PWM quasi PID (D-PS-PWMQPID) technique is used. Furthermore, the converter uses active diodes via a dead time detector (DTD). The system is supplied from a 6V single supply and can deliver up to 1.23 mA current with 10 V voltage compliance and has maximum power efficiency of 75% (for the DC/DC converter only).

In 2019, Urso et al. [109], improved the system proposed in [10]. The system now has active diodes for the buck-boost converter implementing a zero current detection technique, instead of freewheel diodes that consume more power, due to their forward voltage. Furthermore, drivers were implemented for the high side switches of the H-bridge and they were fabricated using thin gate oxide transistors. With this addition the whole system can be supplied by a single 3.6 V battery. The new power efficiency of the system reaches 68%, when all channels are used.

2.4.3. Systems comparison

In the systems described in [106] and [108], energy recycling is implemented during the opposite phase of the stimulation. However, because in tDCS monophasic direct currents are delivered, these techniques are not applicable. Furthermore, [9], [107], [108] have current sources that dissipate power in order to meet their voltage compliance. In [108] the voltage

on the capacitors that are used for delivering the charge to the current source, must be really close to the voltage supply for the charge transfer to be efficient. Moreover, in [106], [9] and [107] the use of adaptive voltage compliance is possible for one channel, but in case of multiple channels the voltage complies with the most demanding load making the lighter loads to be power inefficient.

[10] and [109] do not have current sources to dissipate power and the voltage supply can be adapted for each channel individually and semi simultaneously, opening the way for efficient multichannel implementations. However, there are considerations regarding the efficacy of the ultra high frequency (UHF) stimulation technique. In [11] the authors made simulations delivering 100 kHz square pulses to myelinated and unmyelinated axons. Furthermore, they tested these pulses, in vitro, to Purkinje cells. The results were promising, showing that the cells were activated with the same way as using classic stimulation waveforms. Nevertheless, the effect of UHF stimulation for long periods has not yet been tested.

2.5. Conclusions

The aim of this chapter was to shape the specifications for the tDCS device of the future. The most important indications by the market, as also by researchers was the devices to have increased portability and a high number of channels. However, we observed that some of the commercially available devices and especially those with multiple channels are bulky and they have poor power efficiency. Furthermore, the increase of the number of the existing channels would lead to even poorer performance. After searching the literature for discrete components stimulation modules, we concluded that they are portable but they do not use techniques for multichannel power efficiency. Nevertheless, designers of stimulation ICs have invented techniques for increasing the number of channels without sacrificing power efficiency. Therefore, the stimulator that is designed for this thesis should use these techniques, in order to be smaller and more power efficient, leaving the opportunity for integration of a high number of channels.

Table 4: Power efficient neurostimulators (comparison table).

Parameters	Power efficient neurostimulators					
Reference	[106]	[9]	[107]	[10]	[108]	[109]
Authors	Afrin & Sarpeshkar	Williams & Constandinou	Lin et al.	van Dongen & Serdijn	Lee et al.	Urso et al.
Year	2012	2013	2013	2016	2016	2019
Stimulation type	CCS	CCS	CCS	Unfiltered dyn.supply	CCS	Unfiltered dyn.supply
Channels (#)	1	8	1	8	4	8
V_{Input supply} (V)	3.3	6	3.3	3.5	6	3.5
V_{compliance} (V)	-	11.5	14	10	10	10
I_{max} (mA)	0.45	0.5	0.04	10	10	10
R_{typical} (kΩ)	0.5 - 2	6.8	10 - 300	0.1 - 1	0.3 - 1	0.1 - 1
η_{max} (%)	84 (only the dynamic power supply)	80 (only the DC/DC converter)	-	40	75 (only the DC/DC converter)	68
Multichannel efficiency	No	Yes	No	Yes	Yes	Yes

3. System design

3.1. Introduction

For this thesis, three different designs were created. The first design is a single channel module that uses the UHF stimulation technique. In the second design, significant improvements were made, regarding the power consumption of the system, implementing capacitive coupled high side drivers for the pmosfets of the H-bridges and a novel boost converting technique. For the third design, an eight channel version of the second design was made that has better current accuracy than its predecessor. In the next sections there will be a detailed presentation about the three implemented designs.

3.2. Requirements specifications

As presented in Chapter 2, extensive research has been made on the current state of neurostimulators that have been used as commercial products for tDCS applications, the neurostimulation modules (fabricated with discrete components) that have been proposed in the literature, as well as power efficient multichannel stimulation techniques. From the research findings and from extensive discussions with professionals in the field, Table 5 was created, which includes the target specifications for the final system of this thesis. These values correspond to a competitive commercial system, which (if it has high enough power efficiency) will be able to meet the needs of the users.

Table 5: Specifications of the proposed final stimulator.

Parameters	Values
Type	Unfiltered dynamic supply
Channels (#)	8
Electrodes (#)	16
Power supply type	Battery
$I_{\text{output, max}}$ (mA)	2
$I_{\text{output, min}}$ (μA)	50
$I_{\text{output, resolution}}$ (μA)	10
$V_{\text{input, supply}}$ (V)	3.5
$V_{\text{compliance}}$ (V)	22
R_{max} (k Ω)	10
η_{max}	As much as possible
Charge balancing	Passive

As we can see from Table 5, the stimulators use an unfiltered dynamic supply. This power supply has many benefits compared to an adaptive voltage current based source, which is the state of the art regarding its power efficiency [100]. The stimulators that use an adaptive voltage supply might offer significantly less power consumption (compared to fixed voltage current source stimulators as shown in Figure 13), when they stimulate one channel.

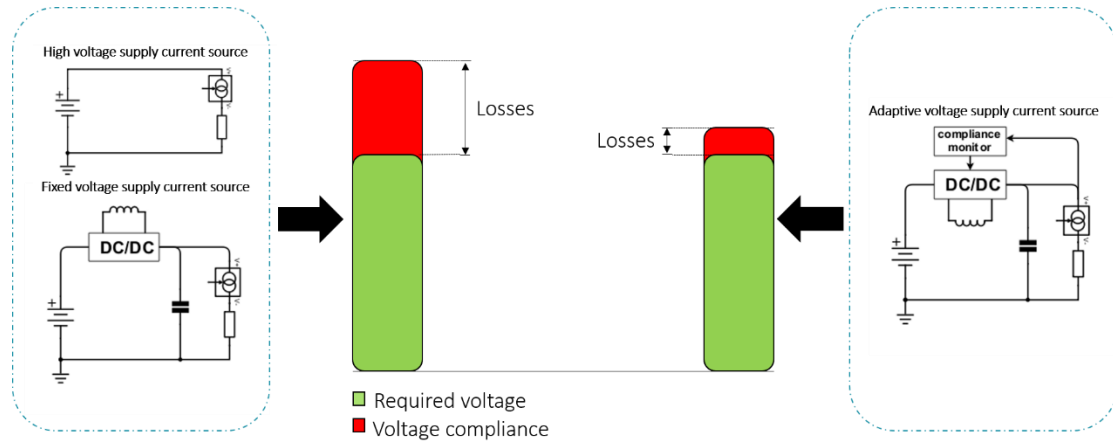


Figure 13: Comparison between fixed voltage and adaptive voltage supply current source. The adaptive voltage supply current source has the ability to adapt its voltage compliance (red) in order to be close to the required voltage (green) that is needed from the load, so as to be stimulated with the desired current. On the contrary, fixed voltage supply current source has constant voltage compliance, which is independent from the load's needs, leading to higher losses.

However, when the stimulation of multiple sites is needed, the power efficiency drops. This situation occurs because the voltage of the current source must be compliant with the most power demanding load. Therefore, the voltage drop at the current sources that deliver current to lighter loads will be higher, increasing the power dissipation of the system. Furthermore, current sources, by default, must have some internal voltage drop, in order to work properly, leading to significant power consumption. The unfiltered dynamic supplies deliver current pulses to different loads without using current sources. Hence, the required voltage that each channel needs for being stimulated properly, is built across the electrode tissue interface. Therefore, it is estimated that this device could serve up to eight channels simultaneously, having less power dissipation than the adaptive voltage supply. The aforementioned comparison is shown in Figure 14.

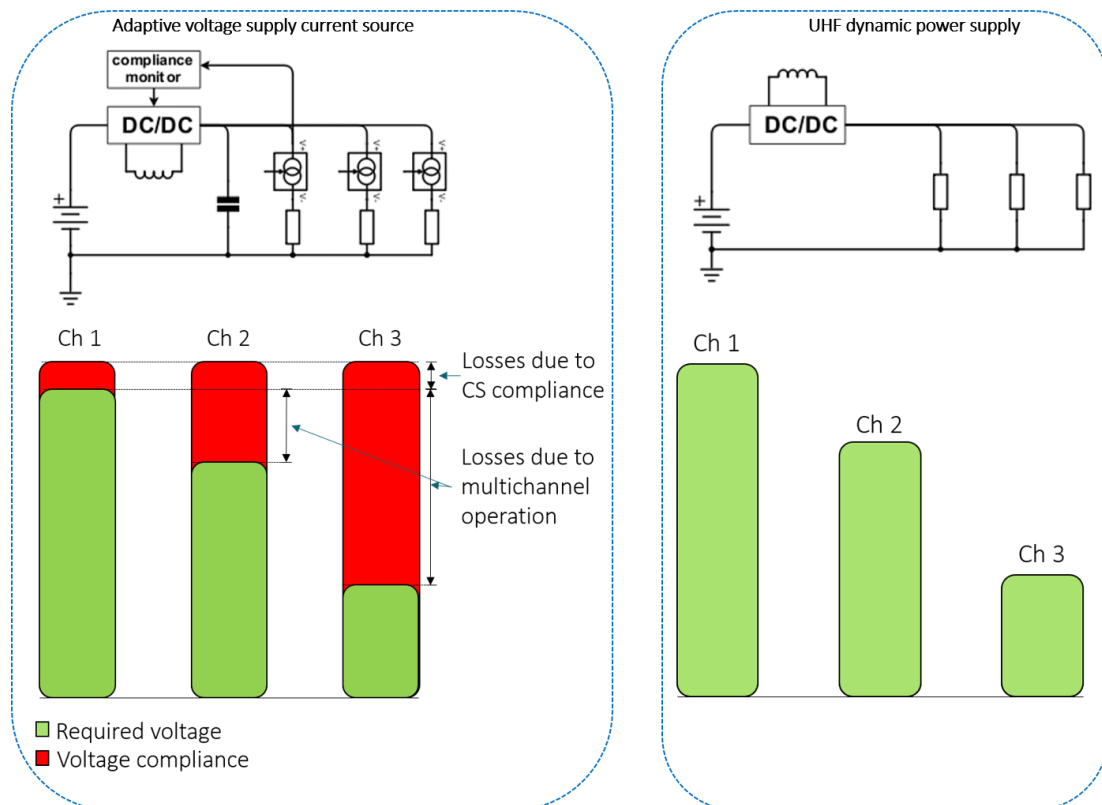


Figure 14: Comparison between adaptive voltage supply current source and UHF unfiltered power supply for three channels. Using an adaptive voltage supply current source, the voltage compliance must be enough in order its current source to be able to deliver the desired current to the load. Furthermore, when it delivers current to multiple channels, the voltage must comply with the voltage needs of the most power demanding load, leading to high losses for the less power demanding loads. The aforementioned problems do not occur when an UHF unfiltered power supply is used.

The only power source of the system will be a 3.5 V battery. As maximum stimulation current, ± 2 mA was chosen, which can be delivered for load impedances up to 10 k Ω , while keeping the compliance voltage at 22 V (2 V higher than the voltage needed for the maximum load). In case the compliance voltage requirement is not met, the device will deliver less current to the tissues. A target for the current's resolution is 10 μ A, with the minimum delivered current to be 50 μ A. Charge balancing was chosen to be passive, implemented by the natural discharge of the tissue after a tDCS therapy, since no severe problems have been reported for the users [16]. Regarding safety, the switching nature of our design (DC/DC converter and H-bridges) minimizes the probability of connecting directly the battery to the load, thereby reducing the probability of single-fault hazardous situations. It also must be noted that the aforementioned values are average stimulation values. The peak values of the current pulses that will be used will be higher, but limited to 100 mA, in order to comply with the electrical equipment standards for medical applications (IEC 60601 - 2 - 10).

3.3. Design of the systems

3.3.1. Morphological boxes

After setting the requirements of the proposed system in Section 3.2, a high level block diagram was implemented, as it is shown in Figure 15. As we can see, the battery voltage is the input for an inductive DC/DC converter. The converter transforms the DC voltage of the input into current pulses. The current pulses can be delivered to multiple loads in an alternate way, charging them semi simultaneously. The half bridges (H-bridges) are able to reverse the polarity of the load. A feedback mechanism updates the parameters of the converter, in order the desired current to be delivered to the tissues, even when electrode tissues' impedances change.

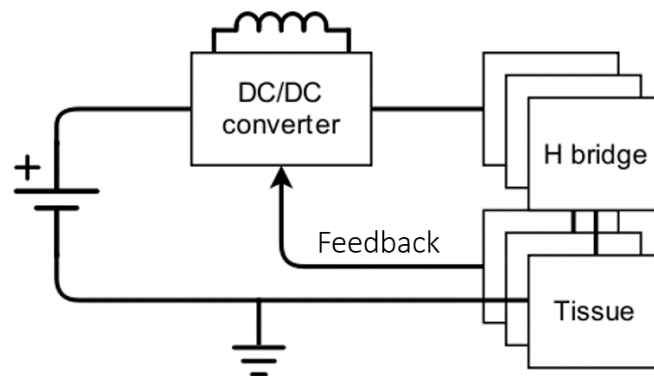


Figure 15: High level block diagram of the proposed neurostimulator.

In Figure 16, a detailed block diagram of the first prototype is depicted. Via a serial peripheral interface (SPI), a digital microcontroller unit (MCU) is programmed by the user. The MCU uses its inbuilt pulse width modulation (PWM) system, which sets the opening and closing time of the switches of an asynchronous buck-boost converter. Moreover, the MCU controls the switches of the H-bridge. The high side of the H-bridge is driven by pull-down resistor drivers and all the other low side mosfets are controlled by off the shelf, low side drivers. Furthermore, the MCU takes as input the measurements from current sensors of the stimulated loads, via its inbuilt analog to digital converter (ADC).

The feedback system works as follows:

1. A current value is selected by the user in order to stimulate the tissue.
2. The microcontroller translates this current into a pulse width and sends the information to the DC/DC converter.
3. The drivers control the switches of the asynchronous buck-boost converter and a current waveform is sent to the tissue.
4. The current sensor measures the current that goes through the tissue and sends it back to the microcontroller.

- The microcontroller receives the current value from its ADC and compares the average sensed current with the selected current, correcting the pulse width of the converter, in order to minimize the error.

A simple diagram of the control system is shown in Figure 17.

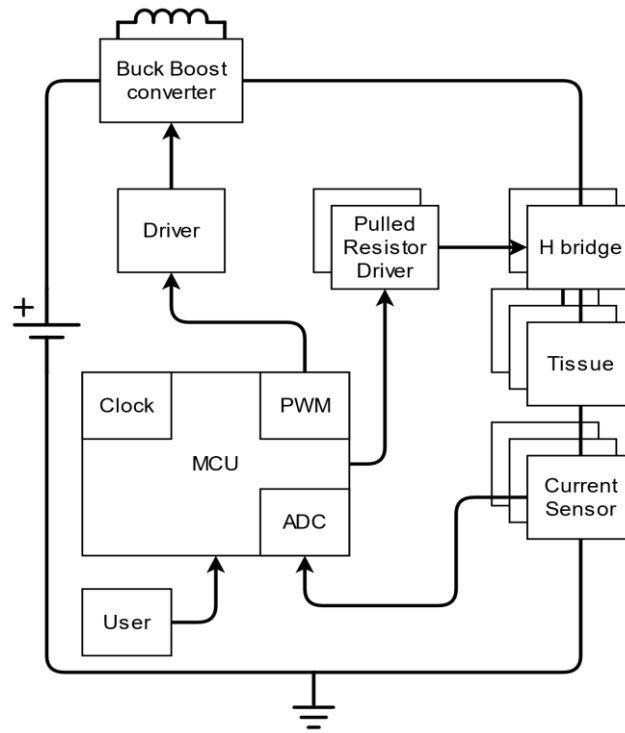


Figure 16: Low level block diagram of the first prototype.

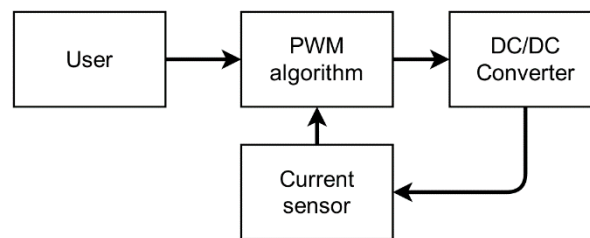


Figure 17: Control system of the first prototype.

In Figure 18 the detailed box diagram of the second prototype is displayed.

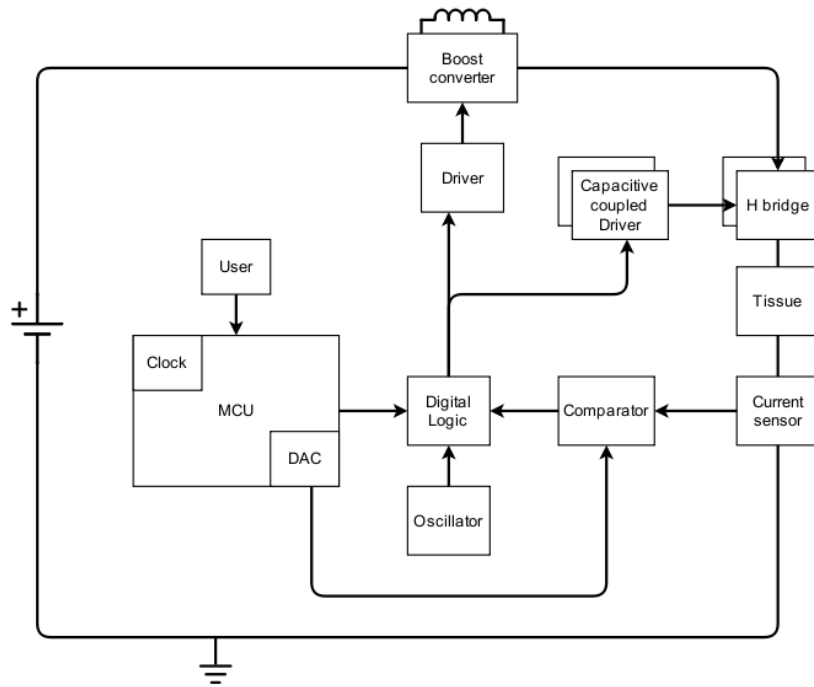


Figure 18: Low level block diagram of the second prototype.

In the second prototype, a boost converter is used as a DC/DC converter instead of a buck-boost converter. Even though the boost converter can only step up the voltage provided by the input supply, using a different pulse modulation technique and isolating the channels from the converter using the high side switches of the H-bridge, output voltages that are lower than the input supply can be achieved. This method increases the power efficiency, due to the lower number of switching components that implement a boost converter, compared to a buck-boost converter. In Figure 19, there is a boost converter that supplies the load through an H-bridge. For this example, it is assumed that, during the initial state, switches S2 and S3 are closed in order to provide monophasic stimulation to the tissue. During the discharging phase of the inductor (in which the current is delivered to the tissue), the proposed system works the same as a conventional boost converter. However, during the charging phase in the proposed system, switch S2 is open, in order to provide isolation between the load and the converter. In this way, the tissue has the possibility to be discharged through S3. In a conventional system, if the voltage across the load is lower than the input voltage supply, diode D1 is forward biased and current would run through the tissue in order to create 3.5 V difference across it. Therefore, the proposed system, in combination with the pulse skipping modulation (PSM) technique, makes the tissue able to be stimulated with currents that need voltages across the load that are lower than the nominal input voltage.

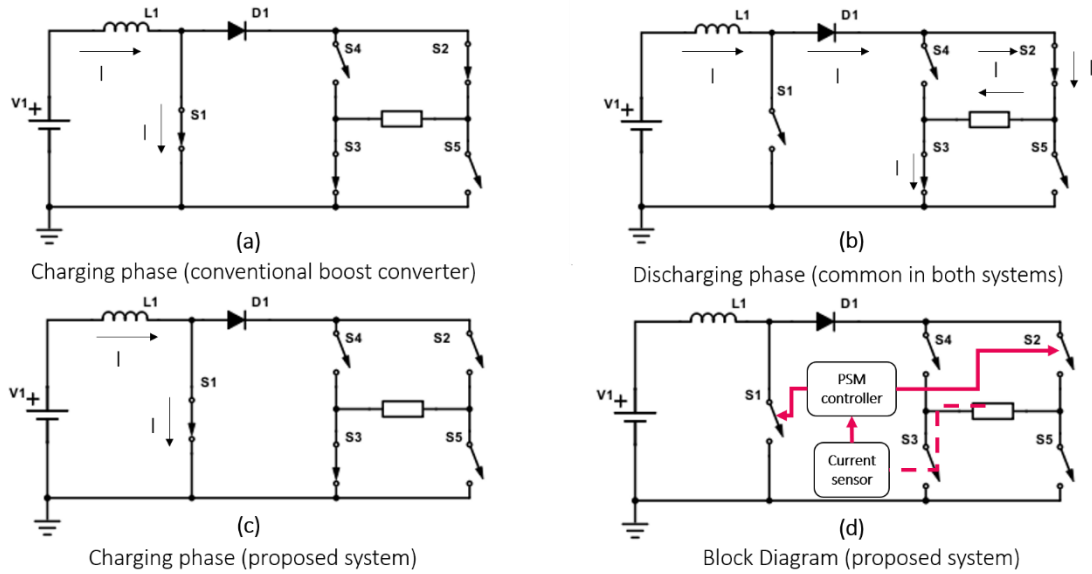


Figure 19: a) Charging phase for a conventional boost converter (during this phase the voltage across the load cannot be lower than V_1 minus the voltage across L_1 , D_1 , S_2 and S_3), b) Discharging phase for a conventional boost converter and the proposed system, c) Charging phase for the proposed system (during this phase the S_2 is open and the load is isolated from the source, letting it to have lower voltage than V_1 , discharging through S_3) and d) The implementation of the PSM technique.

In PWM, pulses are delivered to the switches of a DC/DC converter with a fixed frequency, creating current pulses (when in DCM), which are delivered to the load. In order the amplitude of the aforementioned current pulses to change, the width of each pulse must be adjusted to a specific value. In this way the average current at the output of the converter changes. On the other side, during PSM, the width of the pulses remains constant and in the case that the average current that is needed to be delivered to the load is lower than the measured one, pulses will be skipped until the average current is adjusted to the desired value. In this way, less switching for the used components takes place, leading to a higher power efficiency for light loads [110]. The two techniques are shown in Figure 20.

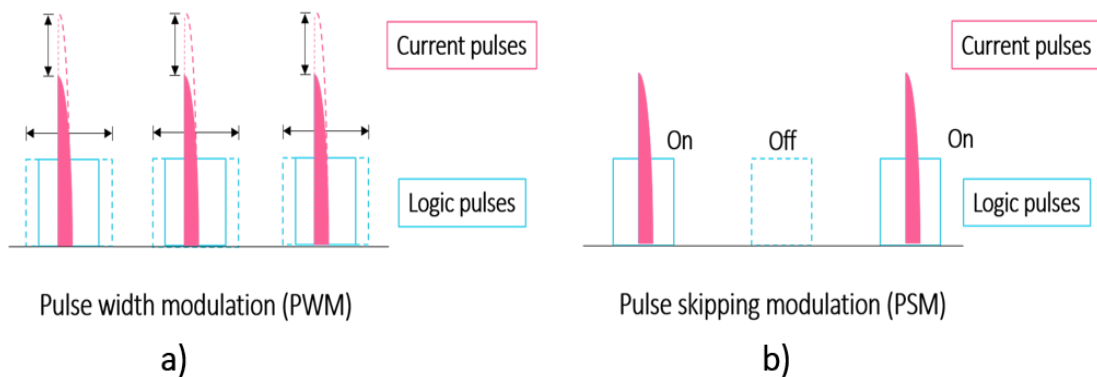


Figure 20: a) The PWM and b) the PSM techniques

Furthermore, instead of the resistive high side drivers that dissipate a lot of quiescent power, drivers that use capacitively coupled level shifting were implemented. In Figure 21, the two

drivers are displayed. Using the resistive high side drivers, when transistor Q_1 is closed, the gate of Q_2 is grounded, creating enough V_{sg} for turning Q_1 on and letting in this way the current to be delivered to the tissue. However, when the load of the tissue is comparable to R_1 , there will be high power dissipation due to R_1 . The capacitive coupled driver uses a level shifter that changes the voltage of capacitors C_1 and C_2 , in order to supply the high side mosfet with $V_{sg} = 3.5$ V when it is desired to be turned on. There is also a charging circuit for charging the capacitors of the level shifter during their transient state, but it stays off during the steady state. Using the capacitive coupled drivers, the power dissipation is minimized due to their low quiescent current [111].

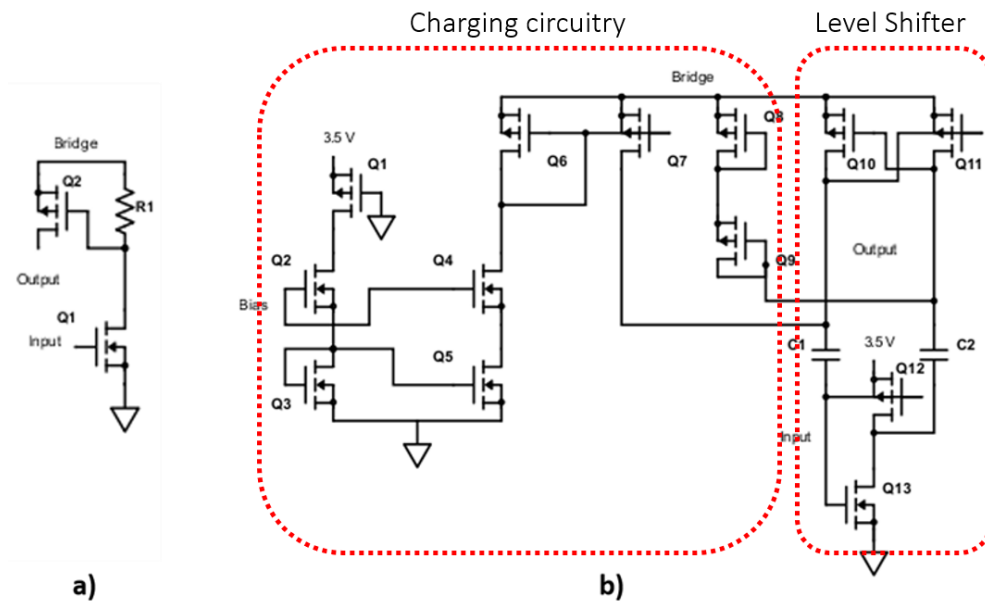


Figure 21: a) Pull-down resistor and b) capacitive coupled level shifting drivers for the high side p type mosfets of the H-bridge [111].

Regarding the feedback system of this prototype, the average current is measured using a low resistance, sensing resistor and a low pass filter. Afterwards, the measured current is compared using an off the shelf analog comparator with the desired current, adjusted by the inbuilt DAC of the MCU. Depending on whether the current is higher or lower than the desired one, a logic circuit decides whether the pulses that are created by the oscillator will reach the converter drivers or whether they will be skipped (PSM algorithm).

In Figure 22, a detailed box diagram of the third prototype is depicted: an eight channel stimulator. The system uses almost the same block diagram that was used for the second prototype. However, only one DC/DC converter is used for the delivery of the current pulses to every channel, using the UHF technique. With this technique each pulse that is created from the converter is sent in an alternate fashion to each channel, building up their voltage semi simultaneously across the load. In this implementation off the shelf DACs are used for better output current range and accuracy and a more complex digital system was created for the expansion of the system from one to eight channels.

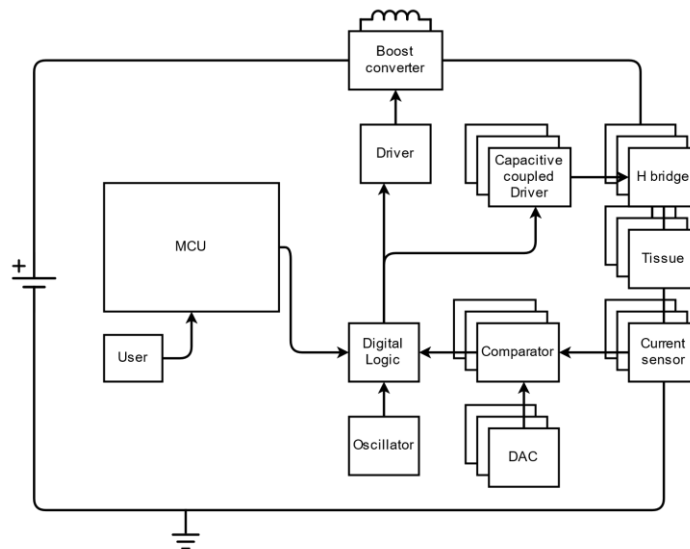


Figure 22: Low level block diagram of the third prototype.

3.3.2. Electrode tissue model

For the design and the test of the proposed systems, an electrode tissue model is needed. Because we need to administer DC current to the tissue, the use of polarizable electrodes is not recommended due to their capacitive behavior, which does not let the current pass to the tissue [112]. Therefore, we will try to derive parameters regarding non-polarizable electrodes, such as Ag / AgCl electrodes. Ag / AgCl electrodes are also commercially available for tDCS applications [113]. In [114], the electrode skin contact impedance on the human head of 47 participants was measured for frequencies ranging from 10 Hz to 1 MHz using Ag / AgCl powder electrodes. The results for the real and the imaginary part of the impedance are shown in Figure 23. From Figure 23, we can observe that both impedance parts (real and imaginary) are dramatically decreasing as frequency is increasing.

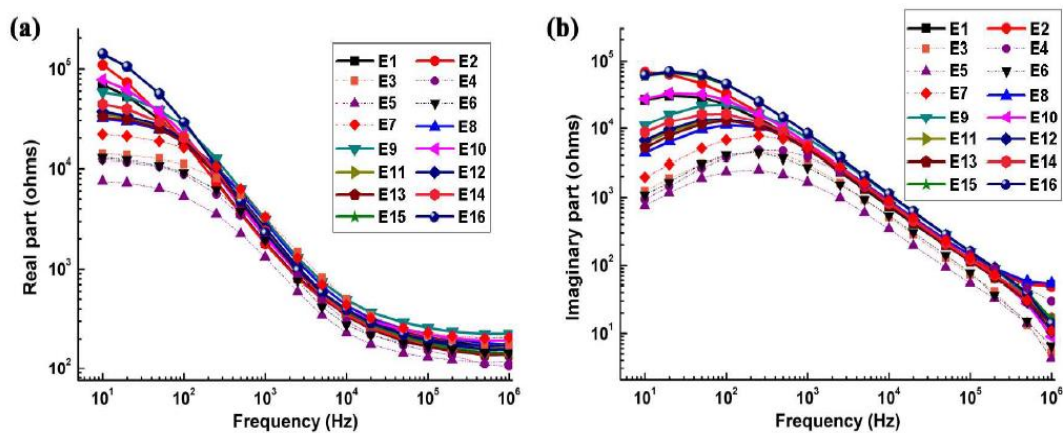


Figure 23: a) Real part and b) Imaginary part of the electrode skin impedance [114].

In order to create an equivalent circuit that matches with the measurements, the method described in [115] was used. The model consists of a parallel RC network (R_f , C_{dl}), which models the electrode tissue's interface, in series with a resistor R_s which models the tissue impedance. The model is shown in Figure 24.

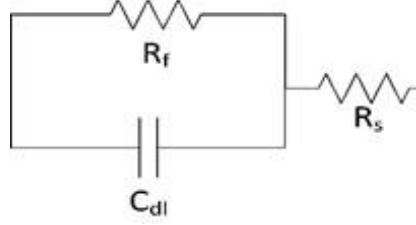


Figure 24: Electrode tissue's equivalent circuit.

The equation of the model's impedance is:

$$Z(\omega) = R_s + \frac{R_f}{1 + j\omega R_f C_{dl}} = R_s + \frac{R_f}{1 + (\omega R_f C_{dl})^2} - j \frac{\omega R_f^2 C_{dl}}{1 + (\omega R_f C_{dl})^2} = Z'(\omega) + jZ''(\omega) \quad (3)$$

where Z' and Z'' are the measured impedances shown in Figure 23.

The R_s can be derived from:

$$R_s = Z(f \rightarrow \infty) = 135 \Omega \quad (4)$$

Other R_s measurements found in the literature are 100Ω for Ag/AgCl electrodes well attached to skin [116], [117] and $< 1 \text{ k}\Omega$ for wet Ag/AgCl electrodes [118].

Furthermore, in the literature, values of the $R_f \parallel C_{dl}$ for well attached Ag/AgCl electrodes are $2 \text{ k}\Omega \parallel 20 \text{ nF}$, $500 \Omega \parallel 100 \text{ nF}$ for two electrodes, when there is imbalance between the electrode electrolyte impedance [116], [119] and $100 \text{ k}\Omega \parallel 10 \text{ nF}$ for wet Ag/AgCl electrodes [118]. In order to find the optimal values for the $R_f \parallel C_{dl}$ combination, we used MATLAB's [120] *lsqnonlin* function [121] (a non linear least square solver) for different initial values of $R_f \in [100 \Omega, 100 \text{ k}\Omega]$, $C_{dl} \in [10 \text{ nF}, 100 \text{ nF}]$ and the same boundaries. The code is given in the Appendix A. The solution space is shown in Figure 25. For $R_f \parallel C_{dl} = 44.51 \text{ k}\Omega \parallel 100 \text{ nF}$ the comparison graphs between the measured and the model values are shown in Figure 26. As we can observe, the model fits well to the measurements.

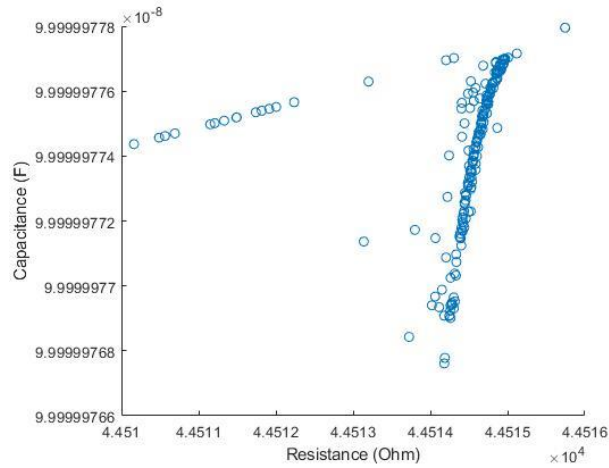


Figure 25: Solution space for the $R_f \parallel C_{dl}$ of the RC model.

In the previous section, a model based on Ag/AgCl electrodes was created. However, using other materials for tDCS electrodes (conductive rubber electrodes, enclosed in a perforated sponge pocket, which is saturated with electrolytes) the contact impedance of healthy subjects that performed tDCS had a mean value of 2.93 ± 1.04 k Ω in [122]. Furthermore, according to [123], there is the possibility of achieving DC impedance (< 5 k Ω) using metal, conductive rubber, or rubber electrodes with conductive gel. Moreover, in [76], where 35 cm² sponge electrodes were used, the electrode tissue impedance was around 20 k Ω in the beginning for all groups, but after 30 s the impedance dropped to around 5 k Ω and remained at this level.

From the previous discussion we can conclude that the electrode tissue capacitance is in the nF range and the resistance can be tens of k Ω , but it has dynamic characteristics and drops to some k Ω when the tissue starts to be stimulated. Therefore, because in this design stage we do not want the type of the electrodes that the system will use to be constrained, we will test our system for the model values: $R_s = 150$ Ω , $R_f \in [0.5$ k Ω , 10 k $\Omega]$ and $C_{dl} \in [1$ nF, 100 nF].

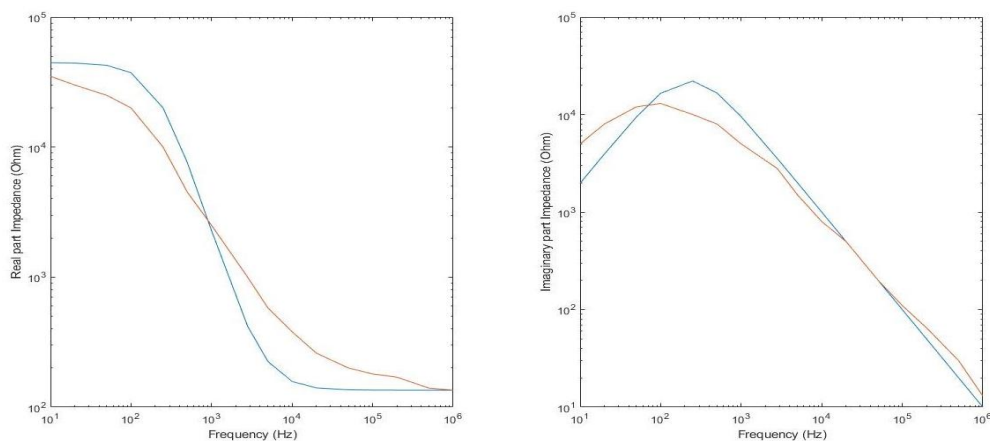


Figure 26: a) Imaginary and b) real part of the measured impedance (orange), compared with the model's impedance (cyan).

3.3.3. Introduction to asynchronous DC/DC converters

An inductive DC/DC converter offers a power efficient method for transferring energy to another DC voltage level, charging and discharging one or more inductors. Inductors have the property of storing energy in the magnetic field that they create. There are three types of DC/DC inductive converters [124]:

- Step down (Buck)
- Step up (Boost)
- Step up/down (Buck-boost)

A buck converter scales down the input voltage, a boost converter scales up the input voltage and a buck-boost converter has both functions [124]. All of them have the same working principle, in which an inductor is charged, storing its energy into the magnetic field and then the energy is transformed again into an electric current that is delivered to the load, achieving the desired voltage. For the scope of the thesis, only the boost and the buck-boost converters will be analyzed further. The analysis is based on [125].

In Figure 27, a circuit diagram of a boost and a buck-boost converter topology are depicted. The converters have two states depending on the position of their switch.

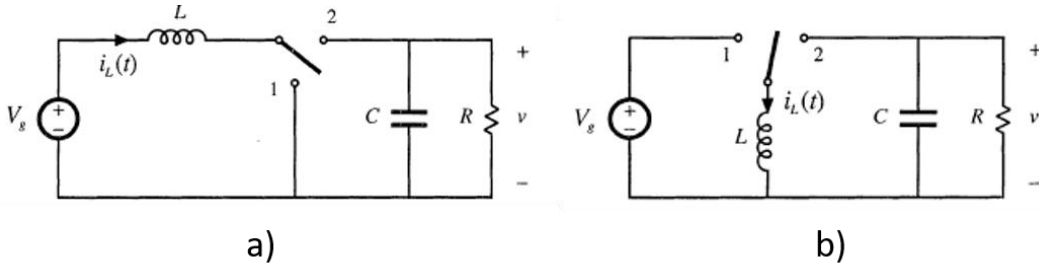


Figure 27: a) The boost and b) the buck-boost topologies [125].

During the period that the switch is in Position 1 (charging state) the voltage source creates a voltage drop across the inductor, which starts to increase its current. The current through the inductor increases continuously with a slope of:

$$\frac{dI_L}{dt} = \frac{V_{in}}{L} \quad (5)$$

where L is the inductance of the inductor.

During this period, the energy of the magnetic field of the inductor increases. We assume that the switch remains in Position 1 for time:

$$t = DT \quad (6)$$

where

$$D \in [0,1] \quad (7)$$

is the duty cycle and T is the period of the converter's switching function.

At time t the inductor current will be:

$$I_{L\ peak} = \frac{V_{in}}{L} DT \quad (8)$$

After $t_1 = DT$, the switch changes to Position 2 (discharging state). The inductor loop now also includes the load resistance, making the inductor decrease its current. However, the inductor opposes to the current change using the energy that was stored in its magnetic field during the charging period. In this way, a voltage is created across the inductor, leading to voltage difference across the load.

In boost converters, the output voltage will be higher than the input voltage for every $D > 0$. In buck-boost converters, if $D > 0.5$, the output voltage is higher (in absolute value) than the source voltage. On the contrary, if $D < 0.5$, the output voltage is lower (in absolute value) than the source voltage. The input/output voltage relationship for the boost converter is:

$$\hat{V}_{out} = \frac{1}{1-D} V_{in} \quad (9)$$

Additionally, the input/output voltage relationship for the buck-boost converter is:

$$\hat{V}_{out} = \frac{-D}{1-D} V_{in} \quad (10)$$

As we observe, the output voltage for the buck-boost converter is inverted. In order to circumvent this phenomenon, we will use a noninverting topology, which uses four switches (two programmable switches and two nonprogrammable switches, implemented with mosfets and diodes respectively) [126]. The noninverting buck-boost converter has exactly the same characteristics as the inverting buck-boost converter, apart from the inversion [124]. The DC/DC converter works as buck-boost converter, when both switches turn on/off simultaneously. An ideal noninverting buck-boost converter is shown in Figure 28. Furthermore, if switch S_1 is closed during the operation of the converter, the system works as a boost converter. With this topology, boost converters were implemented for the second and the third prototype.

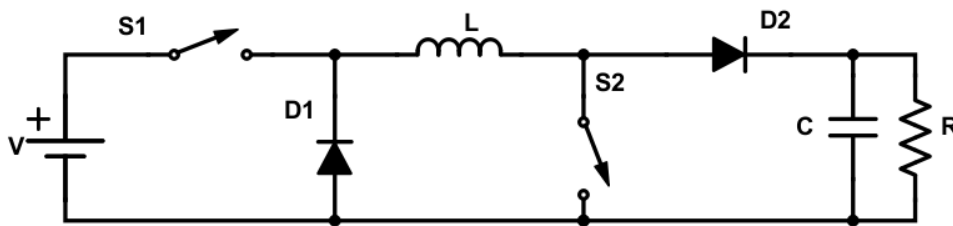


Figure 28: An ideal noninverting buck-boost converter with a parallel RC load.

3.3.4. Operating modes

For the inductive DC/DC converters there are two operation modes:

- Continuous conduction mode (CCM)
- Discontinuous conduction mode (DCM)

These two modes are separated by the lowest value that the inductor current can have. In CCM the inductor never fully discharges and its current value never drops to zero. On the contrary, in DCM the inductor is fully discharged and its current has a zero value during part of the discharging period. Therefore, a new state can be introduced between the discharging period of the inductor and the beginning of the next charging period (dead state). The inductor current for the boundaries of CCM and DCM, as also for DCM are shown at Figure 29.

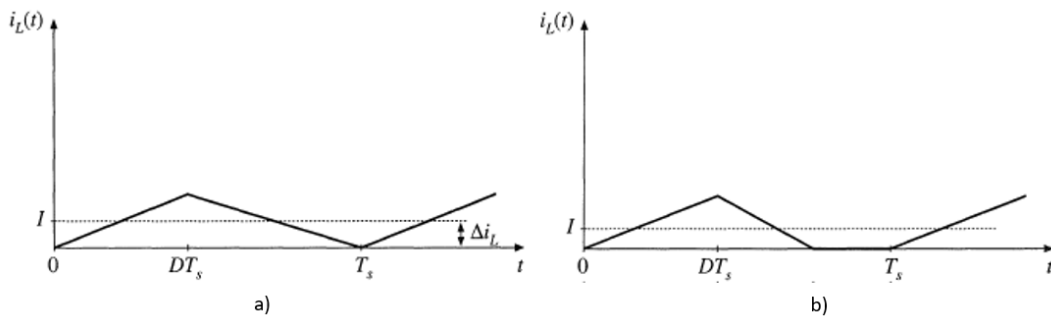


Figure 29: Inductor's current at a) boundary of CCM and DCM and b) DCM [125].

For the DCM, the input/output voltage relationship is changed to:

$$\hat{V}_{out} = \frac{1 + \sqrt{1 + 4D^2/K}}{2} V_{in} \quad (11)$$

for the boost converter and

$$\hat{V}_{out} = \frac{-D}{\sqrt{K}} V_{in} \quad (12)$$

for the buck-boost converter, where

$$K = \frac{2L}{RT} \quad (13)$$

As we can see from (11) – (13), in DCM, the voltage gain, except from the duty cycle, depends also by the load's resistance R, the switching period T and the inductor inductance L.

The condition for the converter to work in DCM is:

$$K < K_{crit} \quad (14)$$

where

$$K_{crit} = D(1 - D)^2 \quad (15)$$

for the boost converter and

$$K_{crit} = (1 - D)^2 \quad (16)$$

for the buck-boost converter.

The DCM working condition can also be expressed including the load resistance:

$$R > R_{crit} \quad (17)$$

where

$$R_{crit} = \frac{2L}{D(1 - D)^2T} \quad (18)$$

for the boost converter and

$$R_{crit} = \frac{2L}{(1 - D)^2T} \quad (19)$$

for the buck-boost converter

The diode DC current, which is also the load current, is:

$$\hat{I}_D = \frac{1}{T} \left(\frac{1}{2} I_{L, peak} D_2 T \right) = \frac{V_{in} D D_2 T}{2L} \quad (20)$$

where

$$D_2 = \frac{K}{D} \frac{1 + \sqrt{1 + 4D^2/K}}{2} \quad (21)$$

is the normalized discharging time for the boost converter and

$$D_2 = \sqrt{K} \quad (22)$$

is the normalized discharging time for the buck-boost converter.

3.3.5. Choosing the DC/DC converter's inductance and switching frequency

In this section, important parameters for the used DC/DC converters are selected. The following analysis and the selection of the parameters was made for the optimization of the buck-boost converter.

The frequency of the pulses must be high enough, in order up to 2 mA DC current to be able to be delivered to the load using UHF stimulation, but it should not be too high, because it

increases the power consumption of the switching components. For the first prototype, the working frequency of the system is:

$$f = 100 \text{ kHz} \quad (23)$$

This frequency was chosen as operating frequency and balances the aforementioned tradeoffs. The exact value is based on Equation (24), which is applicable for buck-boost converters.

$$\frac{\hat{I}_D}{I_{L \text{ peak}}} = \sqrt{\frac{Lf}{2R}} \rightarrow T = \frac{1}{f} = \frac{L}{2R} \left(\frac{I_{L \text{ peak}}}{\hat{I}_D} \right)^2 \quad (24)$$

From (24), we see that the peak to average current ratio, keeping the load resistance constant, depends only on the Lf product. However, from (8) we observe that if we want to have a specific peak current the Lf product must remain constant. Therefore, the only reason to have a higher frequency is to lower the inductance value and consequently the size of the inductor. This technique would be very useful for the design of an implantable device, where the physical dimensions of the inductor are crucial. However, in the design of a wearable device, it appears more important to have lower power consumption due to the lower operating frequency of the switches.

The voltage source will be 3.5V. With this voltage we will be able to feed the buck-boost converter, as well as to give power to all the digital, sensing and driving circuits of the system, keeping the power consumption relatively low. Some of the mosfets must have V_{gs} more than 3.5V in order to switch on/off properly. Hence, drivers will be used that will have 5 V output voltage provided by a regulated, 3.5 to 5 V, charge pump.

In order the system to meet the IEC standards, the peak current must have a limit of:

$$I_{L \text{ peak max}} = I_{D \text{ peak max}} = 100 \text{ mA} \quad (25)$$

Therefore for:

$$D = D_{\text{max}} = 0.5 \quad (26)$$

$$V_{in} = 3.5 \text{ V} \quad (27)$$

$$T = \frac{1}{f} = 10 \text{ } \mu\text{s} \quad (28)$$

$$I_{L \text{ peak}} \leq I_{L \text{ peak max}} \rightarrow \frac{V_{in}}{L} DT \leq I_{L \text{ peak max}} \rightarrow L \geq \frac{V_{in} D_{\text{max}} T}{I_{L \text{ peak max}}} \rightarrow L \geq 175 \text{ } \mu\text{H} \quad (29)$$

Choosing $L = 175 \text{ } \mu\text{H}$, we have to calculate if the converter works in DCM. Using the maximum duty cycle, $D_{\text{max}} = 0.5$ and for minimum resistance $R_{\text{min}} = 500 \text{ } \Omega$, we derive from (14) that the system is in DCM and consequently, this will hold for all the duty cycles and the resistance values that will be used.

Furthermore, in the multichannel modules, current pulses must be delivered from one converter to multiple channels in an alternate fashion. The switching frequency of the

converter cannot be lower than 100 kHz, because choosing $N = 8$ channels, the period, in which all the channels will work for one time, is:

$$T' = NT = 80 \mu s \quad (30)$$

And the frequency will be:

$$f' = \frac{1}{T'} = 12.5 \text{ kHz} \quad (31)$$

Frequency f' is in the range of frequencies that are used for high frequency conduction blocking of the neurons [127]. Frequencies of 100 kHz per channel and above do not belong in this range. Therefore, a switching frequency of 1 MHz was selected for the multichannel implementations, leading to 125 kHz switching frequency per channel. Furthermore, the maximum current must remain the same as the single channel versions. Hence, for frequency of 1 MHz the inductance of the inductor must be 17.5 μH .

However, the aforementioned equations do not include the effect of the load capacitors during the transient responses of the system, a topic that will be discussed in the next section.

3.3.6. Transient response

Ideally, during the transient response, as also in steady state, the current pulse of the inductor must have a duration smaller than T , because, if this statement does not hold, the inductor will not be discharged completely before the next charging step, leading to interference between the channels. In the next paragraphs, the discharging time of the inductor is analyzed. For simplicity, in the calculations, series resistance R_s , from the model depicted in Figure 24, is omitted. The analysis was based on [128], [129].

As it is shown in Figure 30, transition exist from charging phase (a), to discharging phase (b) of the inductor for a noninverting buck-boost converter. During the discharging phase, there exist a parallel RLC network with variable initial capacitor's voltage and fixed initial inductor's current, equal to $I_{L \text{ peak}}$.

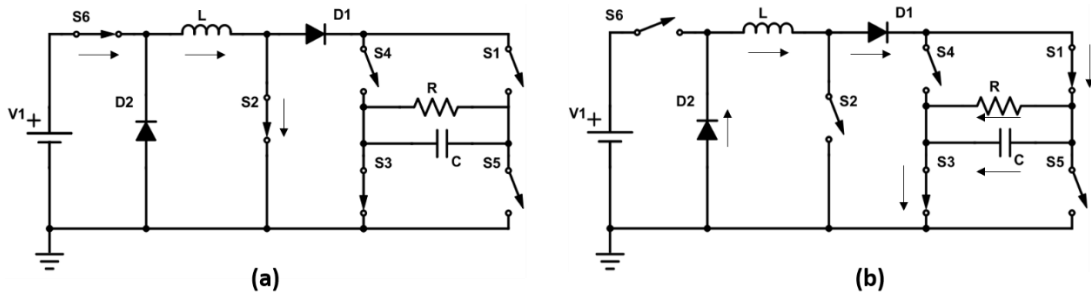


Figure 30: Charging (a) and discharging phase (b) for a noninverting buck-boost converter that delivers current to RC load.

Because during the first discharging period the initial capacitor's voltage is zero, we will analyze the circuit assuming:

$$V_0 = 0 \quad (32)$$

Furthermore, because the RLC network is a second order system, we have to specify the type of its response. The neper and natural frequencies of the system, assuming minimum/maximum resistance of 500 Ω / 10 k Ω and minimum/maximum capacitance of 1 nF / 100 nF, are shown on Tables 6 - 8:

Table 6: Neper frequency for different RC networks.

a (rad/s)	R = 500 Ω	R = 10 k Ω
C = 1 nF	10 ⁶	5 10 ⁴
C = 100 nF	10 ⁴	500

Table 7: Natural frequency for different C and L=175 μ H.

ω_o (rad/s)	L = 175 μ H
C = 1 nF	2.39 10 ⁶
C = 100 nF	2.39 10 ⁵

Table 8: Natural frequency for different C and L=17.5 μ H.

ω_o (rad/s)	L = 17.5 μ H
C = 1 nF	7.56 10 ⁶
C = 100 nF	7.56 10 ⁵

where

$$a = \frac{1}{2RC} \quad (33)$$

and

$$\omega_o = \frac{1}{\sqrt{LC}} \quad (34)$$

are the neper and natural frequencies respectively.

Additionally, the damping factor of the system is shown in Tables 9, 10 and it is given from Equation (35).

$$\zeta = \frac{1}{2R} \sqrt{\frac{L}{C}} \quad (35)$$

Table 9: Damping factor for different RC networks and L=175 μ H.

a (rad/s)	R = 500 Ω	R = 10 k Ω
C = 1 nF	0.42	0.02
C = 100 nF	0.04	0.002

Table 10: Damping factor for different RC networks and L=17.5 μH.

a (rad/s)	R = 500 Ω	R = 10 kΩ
C = 1 nF	0.13	0.007
C = 100 nF	0.01	0.0007

Furthermore, from Tables 6 - 8 and Tables 9, 10, we observe that $a < \omega_o$ and $\zeta < 1$ respectively, for all the boundary conditions. Therefore, the system will have an underdamped response. The capacitor's voltage for an underdamped response can be described by the following equation:

$$v(t) = e^{-at}(B_1 \cos \omega_d t + B_2 \sin \omega_d t) \quad (36)$$

with

$$B_1 = v_c(0^+) \quad (37)$$

and

$$v_c'(0^+) = -aB_1 + \omega_d B_2 = -\frac{i_L(0^+)}{C} - \frac{v_c(0^+)}{RC} \rightarrow B_2 = \frac{aB_1 - \left(\frac{i_L(0^+)}{C} + \frac{v_c(0^+)}{RC}\right)}{\omega_d} \quad (38)$$

where

$$\omega_d = \sqrt{\omega_o^2 - a^2} \quad (39)$$

is the damped frequency of the system. The damped frequency for the RC boundaries of the system is shown in Tables 11 and 12:

Table 11: The damped frequency of the system for different RC values and L=175 μH.

ω_d (rad/s)	R = 500 Ω	R = 10 kΩ
C = 1 nF	$2.17 \cdot 10^6$	$2.39 \cdot 10^6$
C = 100 nF	$2.39 \cdot 10^5$	$2.39 \cdot 10^5$

Table 12: The damped frequency of the system for different RC values and L=17.5 μH.

ω_d (rad/s)	R = 500 Ω	R = 10 kΩ
C = 1 nF	$7.49 \cdot 10^6$	$7.56 \cdot 10^6$
C = 100 nF	$7.56 \cdot 10^5$	$7.56 \cdot 10^5$

Because of (32):

$$B_1 = v_c(0^+) = V_o = 0 \quad (40)$$

and

$$v_c(t) = e^{-at} B_2 \sin(\omega_d t) \quad (41)$$

where

$$B_2 = -\frac{i_L(0^+)}{\omega_d C} \quad (42)$$

The inductor's current is:

$$i_L = \frac{1}{L} \int v_c(t') dt' = -\frac{i_L(0^+)}{LC\omega_d} \frac{e^{-at}}{(a^2 + \omega_d^2)} [-a \sin(\omega_d t) - \omega_d \cos(\omega_d t)] \quad (43)$$

where

$$i_L(0^+) = I_{L \text{ peak max}} = -100 \text{ mA} \quad (44)$$

The time that i_L becomes zero for different RC combinations is shown in Tables 13 and 14:

Table 13: Inductor's discharging time for different RC combinations and L=175 μ H.

t_2 (μ s)	R = 500 Ω	R = 10 k Ω
C = 1 nF	0.9	0.7
C = 100 nF	6.8	6.6

Table 14: Inductor's discharging time for different RC combinations and L=17.5 μ H.

t_2 (μ s)	R = 500 Ω	R = 10 k Ω
C = 1 nF	0.23	0.21
C = 100 nF	2.1	2.08

The maximum allowed discharging time is:

$$t_{max} = (1 - D)T = 5 \mu\text{s} \quad (45)$$

for f=100 kHz

and

$$t_{max} = (1 - D)T' = 500 \text{ ns} \quad (46)$$

for

$$T' = \frac{1}{f'} = \frac{1}{1 \text{ MHz}} = 1 \mu\text{s} \quad (47)$$

The maximum capacitor that can be used, so as the discharging phase of the inductor to be below the t_{max} threshold for f=100kHz and L=175 μ H is shown in Table 15.

Table 15: Maximum capacitor that meets the maximum discharging time requirement for different resistance values.

C (nF)	t = 5 μ s
R = 500 Ω	53.73
R = 10 k Ω	57.70

Hence, capacitors until 50 nF will not disturb the DCM mode, even in transient response. However, for the second and third prototype that have L=17.5uH inductors and switch with frequency f=1MHz, this capacitance would create CCM. Nevertheless, the implemented pulse skipping modulation technique is expected to make these prototypes to work having DCM response even when this load capacitance is selected. The code for finding the maximum capacitance and for plotting the inductor current for different RC values can be found in the Appendix A.

3.3.7. Theoretical values

The average output current can be described by:

$$\widehat{I_{Load}} = \widehat{I_D} = \frac{V_{in} D D_2 T}{2L} \quad (48)$$

where

$$D_2 = \sqrt{K} = \sqrt{\frac{2L}{RT'}} \quad (49)$$

From (48), (49) we derive:

$$\widehat{I_{Load}} = \frac{V_{in} D \sqrt{\frac{2L}{RT'}} T}{2L} = \frac{V_{in} D \sqrt{\frac{2L}{RNT}} T}{2L} = V_{in} D \sqrt{\frac{T}{2LNR}} \quad (50)$$

From (50), we observe that the average current depends on the input voltage, the duty cycle, the Lf product, the load resistance and the number of active channels. Furthermore, the Lf product is constant in the three implemented prototypes.

Because the average current of the capacitor is zero, all the current passes through the load resistors. Table 16 shows the maximum average current that the stimulator can provide to the tissue for resistances from 500 Ω to 10 k Ω and for 1, 2, 4, and 8 channels, based on (50).

Observing Table 16, it is worth mentioning that even though the maximum average current drops significantly with the increase of the output resistance, the current that can be provided with the parallel combination of eight channels is 8.4 mA even for a 10 k Ω resistor, which is far bigger than the maximum current that can be delivered during tDCS.

Table 16: Average output current for different combinations of output resistance and number of channels (theoretical values, 50 % duty cycle).

Maximum current (mA)		Number of channels			
		1	2	4	8
Resistance (k Ω)	0.5	13.23	9.35	6.61	4.68
	1	9.35	6.61	4.68	3.31
	2	6.61	4.68	3.31	2.34
	3	5.40	3.82	2.70	1.91
	4	4.68	3.31	2.34	1.65
	5	4.18	2.96	2.09	1.48
	6	3.82	2.70	1.91	1.35
	7	3.54	2.50	1.77	1.25
	8	3.31	2.34	1.65	1.17
	9	3.12	2.20	1.56	1.10
10	2.96	2.09	1.48	1.05	

3.3.8. Simulation results

When a resistor $R_s = 150 \Omega$ is inserted in series with the RC load the circuit, in order to model the tissue impedance as shown in Section 3.3.2, the behavior of the system changes. During the discharging time, the inductor discharges its current in order to increase the capacitor voltage. However, this time the series R_s resistor creates also its own voltage drop, due to the inductor current decreasing the voltage across the capacitor. When the current goes to zero the capacitor discharges only to its parallel resistance, as during the parallel RC network case. In [130] a study can be found on the transient and steady state response of buck-boost converters operating in DCM. The equations include the inductors parasitic resistance that could be used as the series resistance of the network that we study. Nevertheless, the results give no intuition about the exact role of the R_s resistance to the circuit, except from the fact that increasing the R_s is lowering the steady state output voltage and assuming constant output resistance, also the steady state output current. Table 17 shows simulation results with the addition of the R_s resistor and Table 18 shows the percentage difference between the two aforementioned networks due to the addition of the series resistor.

Table 17: Average output current for different combinations of output resistance and number of channels ($C = 50 \text{ nF}$) with the addition of $R_s = 150 \Omega$ in series.

Maximum current (mA)		Number of channels			
		1	2	4	8
Resistance ($k\Omega$)	0.5	7.03	4.04	2.22	1.15
	1	5.85	3.51	2.02	1.11
	2	4.69	2.93	1.76	1.01
	3	4.06	3.00	1.59	0.93
	4	3.64	2.34	1.46	0.88
	5	3.34	2.17	1.37	0.84
	6	3.10	2.03	1.30	0.79
	7	2.92	1.91	1.23	0.76
	8	2.76	1.82	1.17	0.73
	9	2.63	1.74	1.13	0.71
10	2.52	1.67	1.09	0.68	

Table 18: Percentage difference between the maximum current for the parallel RC network and the series resistor network.

Current percentage (%)		Number of channels			
		1	2	4	8
Resistance ($k\Omega$)	0.5	-46.86	-56.79	-66.41	-75.43
	1	-37.43	-46.90	-56.84	-66.47
	2	-29.05	-37.39	-46.83	-56.84
	3	-24.81	-21.47	-41.11	-51.31
	4	-22.22	-29.31	-37.61	-46.67
	5	-20.10	-26.69	-34.45	-43.24
	6	-18.85	-24.81	-31.94	-41.48
	7	-17.51	-23.60	-30.51	-39.20
	8	-16.62	-22.22	-29.09	-37.61
	9	-15.71	-20.91	-27.56	-35.45
10	-14.86	-20.10	-26.35	-35.24	

The two trends that can be derived from Table 18 are that increasing the active channels and decreasing the parallel resistance, leads to more divergence from the parallel RC model, decreasing more the average maximum current. Furthermore, from the simulations it was found that, the voltage ripple of the output voltage was significantly higher with the addition of R_s .

From the analysis above, we conclude that the series resistance in the output of the system has very undesirable effects. One possible solution would be the addition of a capacitor in parallel with the load. In this way, during the discharging phase of the inductor, no resistance will be in series with the added capacitor and hence its voltage should approximate the output voltage of the parallel RC network. When the inductor current becomes zero the capacitor will feed the series combination of the R_f , R_s resistors, as shown in Figure 24. The simulation results of the network, shown in Figure 24, with a 50 nF capacitor in parallel and the whole network

being supplied by a buck-boost converter are shown in Table 19. The percentage difference between the proposed network and the parallel RC network is shown in Table 20. Because the maximum capacitor value that could be used was a little above 50 nF, the selected capacitor that was placed parallel to the load, was chosen to be 47 nF, which is the closest standard capacitance value below 50 nF.

Table 19: Average output current for different combinations of output resistance and number of channels ($C = 50$ nF) with the addition of a series $R_s = 150$ Ω resistor and a parallel to the load $C = 47$ nF capacitor

Maximum current (mA)		Number of channels			
		1	2	4	8
Resistance (k Ω)	0.5	11.44	7.87	5.25	3.32
	1	8.64	6.01	4.10	2.71
	2	6.33	4.43	3.07	2.09
	3	5.24	3.68	2.56	1.77
	4	4.57	3.21	2.25	1.56
	5	4.10	2.89	2.03	1.41
	6	3.75	2.65	1.86	1.29
	7	3.48	2.45	1.72	1.20
	8	3.26	2.30	1.62	1.13
	9	3.08	2.17	1.53	1.07
10	2.92	2.06	1.45	1.02	

Table 20: Percentage difference between the maximum current for the parallel RC network and the series resistor network with the addition of a 47 nF parallel capacitor.

Current percentage (%)		Number of channels			
		1	2	4	8
Resistance (k Ω)	0.5	-13.53	-15.83	-20.57	-29.06
	1	-7.59	-9.08	-12.39	-18.13
	2	-4.24	-5.34	-7.25	-10.68
	3	-2.96	-3.66	-5.19	-7.33
	4	-2.35	-3.02	-3.85	-5.45
	5	-1.91	-2.36	-2.87	-4.73
	6	-1.83	-1.85	-2.62	-4.44
	7	-1.69	-2.00	-2.82	-4.00
	8	-1.51	-1.71	-1.82	-3.42
	9	-1.28	-1.36	-1.92	-2.73
10	-1.35	-1.44	-2.03	-2.86	

Because the average current that is delivered to the load equals to the DC current that is delivered to load's resistance, assuming all the capacitors as open circuits, introducing the R_s , the resistive load becomes the series combination of R_s and R_f as shown in Figure 24. The percentage change in the resistive load is shown in Table 21.

Table 21: Percentage difference between the initial resistor and the equivalent series resistor with the addition of R_s .

		Resistance percentage change (%)
Resistance (k Ω)	0.5	30.00
	1	15.00
	2	7.50
	3	5.00
	4	3.75
	5	3.00
	6	2.50
	7	2.14
	8	1.88
	9	1.67
	10	1.50

From Tables 19 and 20 we observe that the introduction of the 47 nF parallel capacitor significantly minimized the divergence of the series resistor network from the parallel RC network, increasing the average output current and reducing the output's voltage ripple. Furthermore, the difference between the aforementioned two networks will be even lower taking into consideration the increase of the equivalent resistance with the addition of R_s as shown in Table 21.

The schematic diagram of the first prototype is shown in Figure 31. As we see, two of the four switches of the buck-boost converter have been made with nmos transistors and the other two with diodes. For the diodes, Schottky diodes were selected because of their high switching speed, as well as their small forward voltage. For the nmos transistors, transistors with very low $V_{gs,th}$ were chosen, in order to be compatible with our low supply voltage design. However, in order to be sure that the mosfets will be completely on, a charge pump was used for converting the 3.5 V, supplied by the DC source, into 5 V DC, which will be the high voltage value for the transistors' gates. Furthermore, the selected mosfets have also very low total gate charge Q_g , in order to switch on and off quickly.

Because the logic signals will be delivered by a microcontroller, drivers were used between the microcontroller's outputs and the gates of the transistors, so as to protect the microcontroller from high currents during switching, and also to deliver enough current and the proper V_{gs} to the transistors, so as the transistors to perform fast switching and to be completely turned on.

For the anodic and cathodic stimulation capability of the system, two H-bridges were used. In the H-bridges p-type mosfets were used as high side switches and n-type mosfets as low side switches. For the driving of the pMOS transistors, a combination of a series nMOS transistor and a resistor was used. This combination is able to pull down the pmos gate voltage when the nmos is on, creating enough V_{sg} for turning on the pmos transistor. When the nmos is off, the pmos' gate and source follow the DC/DC converter output voltage keeping the transistor off. For the selection of the resistor, a trade-off was made between being able to provide a high current to the pmosfet's gate for fast switching (low resistance value) and having less power consumption (high resistance value). Finally, 10 k Ω resistors were selected. For sensing the load's DC current, a 12 Ω resistor in series with the load was placed. The voltage across

the resistor was filtered using a 10 μ F capacitor and was amplified using a noninverting, low voltage, opamp. The gain of the opamp is:

$$A = 1 + \frac{R_8}{R_7} = 76 \quad (51)$$

The aforementioned gain was selected, in order up to 4 mA to be able to be measured and converted into 3.65 V. However, because the microcontroller's ADC has an input range of 3.3V, there might be some issues when the opamp's voltage goes above this value. Therefore, for safety reasons, currents above 3.6 mA must be avoided. An ideal choice would be to use a 10 Ω resistor instead of the 12 Ω resistor that the sensor uses. Nevertheless, during the fabrication only 12 Ω resistors were available. For protection of the system from transient responses of the voltage supply, decoupling capacitors were used close to the main voltage supply source and also connected to the voltage supply pads of all the ICs. Additionally, for overvoltage protection of the transistors of the channels and the tissue, a 20 V Zener diode was placed at the output of the buck-boost converter. Furthermore, there are still high amplitude (hundreds of milliamperes), low duration (a few nanoseconds) spikes that pass through the 47 nF parallel capacitor, due to the hard switching of the bridges' mosfets. These spikes may also pass through the tissue, if the tissue model also contains a parallel capacitor without a resistor in series. However, this is not the case in the electrode tissue model that we are using.

Moreover, because the components that will be used are not ideal, parasitic capacitance and resistance will be introduced. Additionally, for some components, their exact values were not found at the suppliers' stock. Therefore, the closest values to the ideal ones were chosen. For example, the inductor will have 180 μ H inductance and not 175 μ H. Furthermore, the diodes are expected to have 0.4 to 1 V forward voltage and not zero voltage as in the ideal case. Moreover, MOSFETs and diodes are far from ideal switches, having limited switching speed, as also limited conductance. Additionally, all the used (passive, active) components have parasitic effects that may change the behavior of the system.

The simulation results of the system, using off the shelf components, are shown in Table 22. Furthermore, the average current that the 10k Ω resistances of the bridge consume is shown in Table 23. The current consumption of the 10k Ω resistance as percentage of the average current consumption of the load is shown in Table 24.

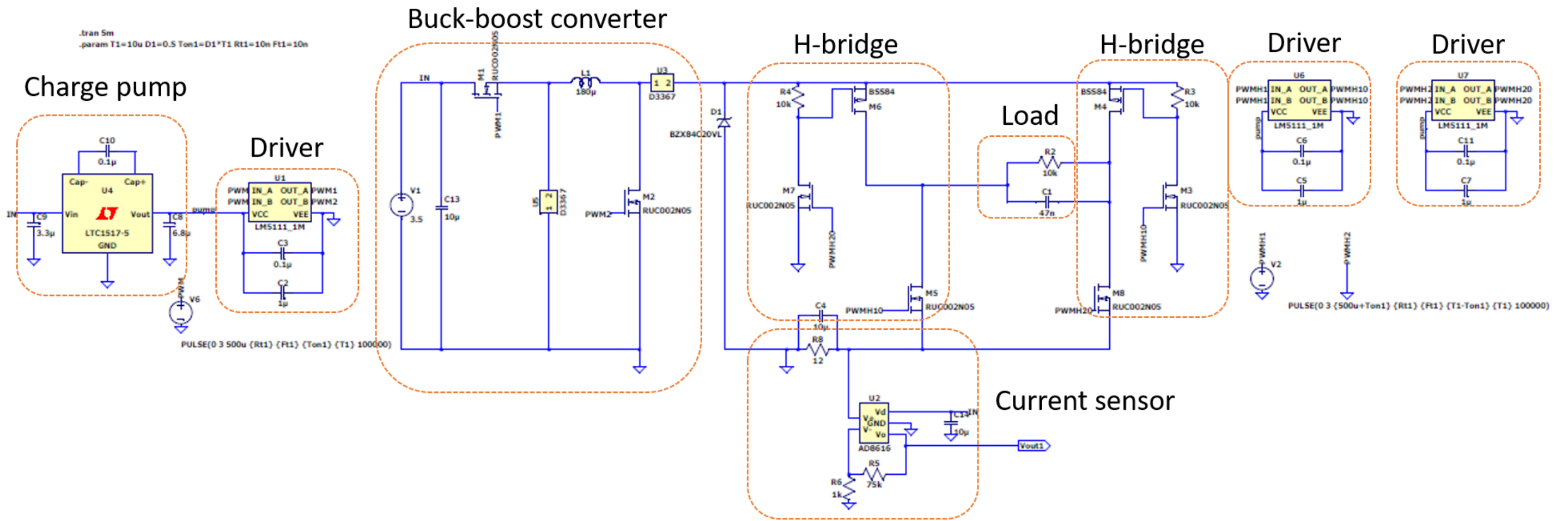


Figure 31: Schematic diagram of the first prototype.

Table 22: Average output current for different combinations of output resistance and number of channels (off the shelf components, C = 50 nF) with the addition of a series $R_s = 150 \Omega$ resistor and a parallel to the load C = 47 nF capacitor

Maximum current (mA)		Number of channels			
		1	2	4	8
Resistance (k Ω)	0.5	6.95	4.26	2.44	1.26
	1	5.58	3.59	2.18	1.23
	2	4.25	2.85	1.82	1.10
	3	3.52	2.43	1.60	1.00
	4	3.05	2.15	1.44	0.92
	5	2.71	1.94	1.32	0.85
	6	2.44	1.78	1.22	0.80
	7	2.23	1.65	1.15	0.76
	8	2.05	1.54	1.08	0.72
	9	1.90	1.44	1.03	0.69
10	1.79	1.36	0.98	0.66	

Table 23: Average 10 k Ω resistor's current for different combinations of output resistance and number of channels (off the shelf components, C = 50 nF) with the addition of a series $R_s = 150 \Omega$ resistor and a parallel to the load C = 47 nF capacitor

Maximum current (mA)		Number of channels			
		1	2	4	8
Resistance (k Ω)	0.5	0.28	0.09	0.04	0.01
	1	0.39	0.14	0.05	0.02
	2	0.54	0.19	0.07	0.02
	3	0.64	0.23	0.08	0.03
	4	0.72	0.27	0.09	0.03
	5	0.80	0.30	0.10	0.04
	6	0.86	0.32	0.12	0.04
	7	0.91	0.34	0.12	0.04
	8	0.96	0.36	0.13	0.05
	9	1.00	0.38	0.14	0.05
10	1.04	0.39	0.15	0.05	

Table 24: Average 10 kΩ resistor’s current for different combinations of output resistance and number of channels (off the shelf components, C = 50 nF) as percentage of the load’s average current.

Current Percentage (%)		Number of channels			
		1	2	4	8
Resistance (kΩ)	0.5	4.03	2.11	1.64	0.79
	1	6.99	3.90	2.29	1.63
	2	12.71	6.67	3.85	1.82
	3	18.18	9.47	5.00	3.00
	4	23.61	12.56	6.25	3.26
	5	29.52	15.46	7.58	4.71
	6	35.25	17.98	9.84	5.00
	7	40.81	20.61	10.43	5.26
	8	46.83	23.38	12.04	6.94
	9	52.63	26.39	13.59	7.25
10	58.10	28.68	15.31	7.58	

From Table 22, we see that for eight channels, even for 10 kΩ R_f , a combined 5.28 mA average current is achievable by the designed system, which is higher than the maximum needed for tDCS.

Table 25 shows the power dissipation for each component of the circuit, for a 50% pulse width, 100 kHz, square waveform, for different resistance values. From Table 25, we observe that the components that dissipate the most power are the nmosfet M_1 , the diode D_2 and the inductor. Furthermore, when the load resistance is comparable with the driving circuit’s resistance R_2 , the current through R_2 rises and so does its power dissipation.

Hence, from Tables 22, 23, 24 and 25, we observe that the pull down 10 kΩ resistor, as well as the components that implement the forward buck-boost converter consume a lot of current. Hence, more power efficient driving circuits and converter topologies should be used in future implementations.

The second prototype was made to address the aforementioned power efficiency issues. For the creation of the high side drivers the same nmosfets and pmosfets that were selected for the first prototype were used. The capacitors of the drivers were chosen to be 10 nF, taking as tradeoff to be fast enough for isolating the load, when it is not stimulated. On the other side they must have enough capacitance so as to deliver the appropriate charge for turning on the driven pmosfets. The frequency of the system is 1 MHz, in order to simulate how the system will behave when it will have eight channels (third prototype). Moreover, a high slew rate opamp was used for the second prototype, because there was an issue with large gain variations in the first prototype due to the selected opamp’s low slew rate. The detailed schematic diagram of the second prototype is shown in Figures 32 and 33.

The third prototype’s schematic diagram because of its size, as also because it has many similarities with the second prototype is not shown. In the third prototype, an off the shelf DAC was used, because the inbuilt DAC of the MCU could not provide voltages lower than 0.55 V, decreasing the range of the available output currents. Furthermore, a voltage reference

was used, in order to provide 2.5 V to the DAC as reference voltage, and the opamp's gain was adjusted from 0 to 2.5 V, for measuring the output's average output current.

Regarding the digital part of the last two prototypes, off the shelf logic gates and edge triggered flip flops were used that can work from a 3.5 V supply. Moreover, attention was given for the inputs and the outputs of the digital components to have less capacitance than their datasheet specifications, in order to be able to transmit and receive signals, using buffers when it was needed.

Next, the circuits were fabricated with real components and tested. The list of the used components is given in the Appendix B.

Table 25: Components' power dissipation for different R_{load} ($R_f = 1 \text{ k}\Omega$, $5 \text{ k}\Omega$, $10 \text{ k}\Omega$ and $R_s = 125 \Omega$).

$R_{load} \text{ (k}\Omega\text{)}$	1.125		5.125		10.125	
$P_{consumed}$	mW	%	mW	%	mW	%
Voltage source	91.90	100.00	85.69	100.00	86.68	100.00
Charge pump	0.34	0.37	0.31	0.36	0.36	0.42
Drivers	0.01	0.01	0.01	0.01	0.01	0.01
Buck-boost converter	45.75	49.78	32.60	38.04	30.19	34.83
Nmosfet M_1	18.15	19.75	11.97	13.97	11.31	13.05
Nmosfet M_2	2.39	2.60	2.68	3.13	2.92	3.37
Inductor	10.58	11.51	9.45	11.03	9.09	10.49
Diode D_1 (Source's side)	2.90	3.16	1.69	1.97	1.38	1.59
Diode D_2 (Load's side)	11.73	12.76	6.81	7.95	5.49	6.33
Zener diode	0.00	0.00	0.00	0.00	0.00	0.00
Active H-bridge	5.32	5.79	13.32	15.54	21.14	24.39
Pmosfet M_6	1.79	1.95	0.98	1.14	0.84	0.97
Nmosfet M_8	0.19	0.21	0.59	0.69	0.97	1.12
R_2	2.70	2.94	11.31	13.20	18.94	21.85
Nmosfet M_3	0.64	0.70	0.44	0.51	0.39	0.45
Inactive H-bridge	0.00	0.00	0.00	0.00	0.00	0.00
Pmosfet M_5	0.00	0.00	0.00	0.00	0.00	0.00
Nmosfet M_7	0.00	0.00	0.00	0.00	0.00	0.00
R_1	0.00	0.00	0.00	0.00	0.00	0.00
Nmosfet M_3	0.00	0.00	0.00	0.00	0.00	0.00
Load	39.72	43.22	40.04	46.73	34.37	39.65
R_3	34.01	37.01	38.66	45.12	33.72	38.90
R_4	5.71	6.21	1.38	1.61	0.65	0.75
Current sensor	3.94	-	5.21	-	5.18	-
R_5	0.41	-	0.09	-	0.04	-
R_8	0.16	-	0.08	-	0.04	-
R_7	0.00	-	0.00	-	0.00	-
Opamp	3.37	-	5.04	-	5.10	-

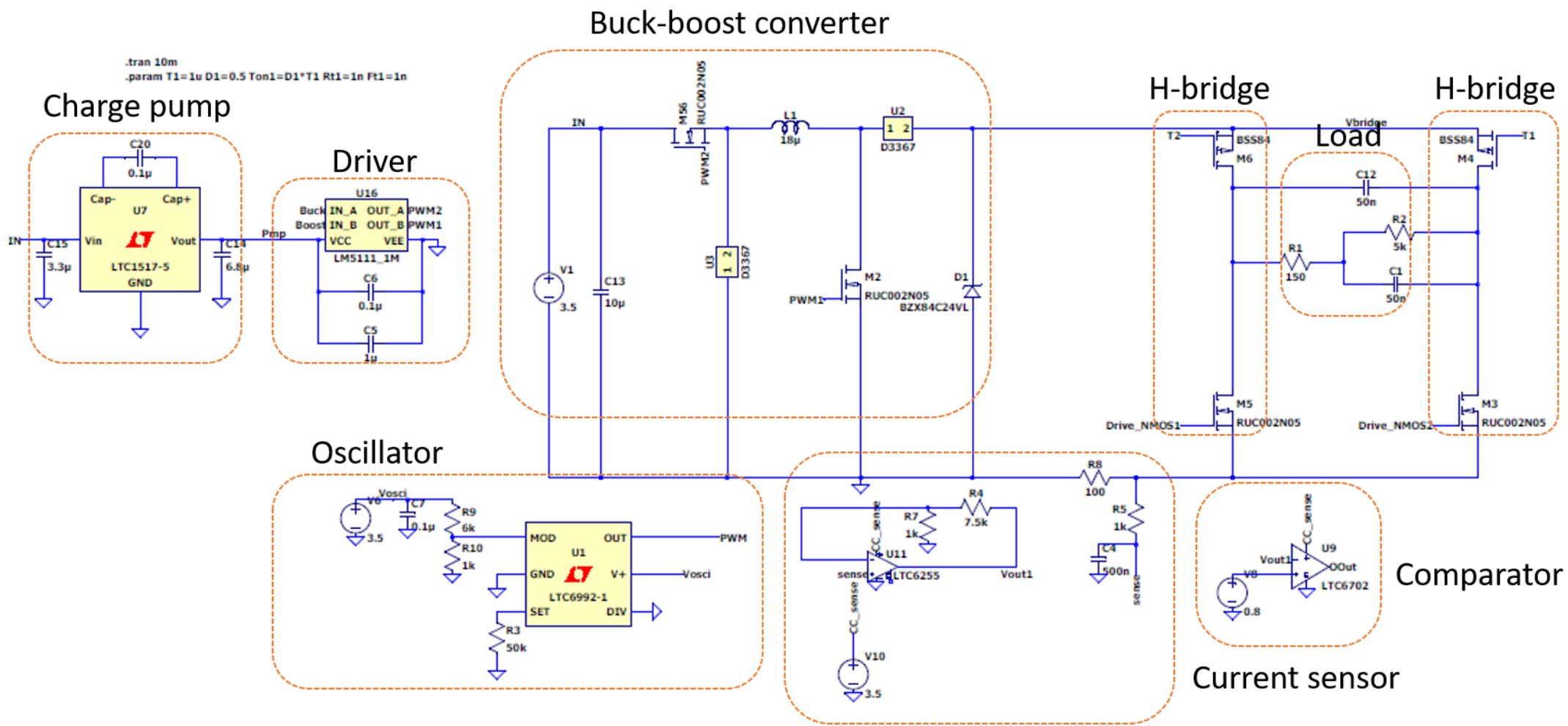


Figure 32: Schematic diagram of the second prototype (1/2).

High side driver

High side driver

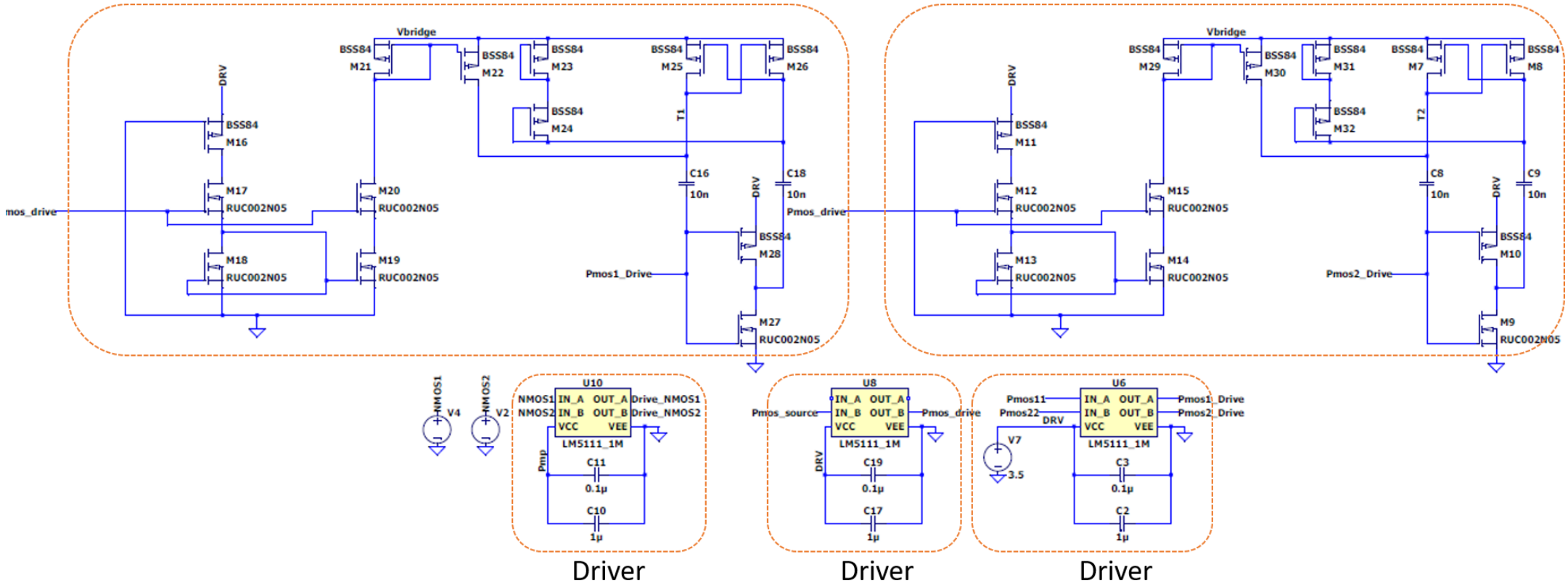


Figure 33: Schematic diagram of the second prototype (2/2).

4. Systems fabrication

The first prototype was made on an epoxy glass composite (1.5 mm, 100 mm x 160 mm) prototyping board, which is ideal for through hole components. The fabricated circuit with the MCU is shown in Figure 34. After the fabrication of the board, first measurements were made using a benchtop voltage supply that delivered 3.5 V to the circuit, instead of using a battery and a benchtop waveform generator that delivered a 50 % pulse width, 100 kHz, waveform, instead of using the MCU. The aforementioned waveform was applied to both the buck-boost converter's nmosfets. The gate of the first H-bridge's mosfets were grounded, so as to the one H-bridge to be completely off during the whole operation, when the second H-bridge's mosfets received 5 V voltage from their driver, so as the second H-bridge to be completely on during the whole operation, providing positive voltage across the load.

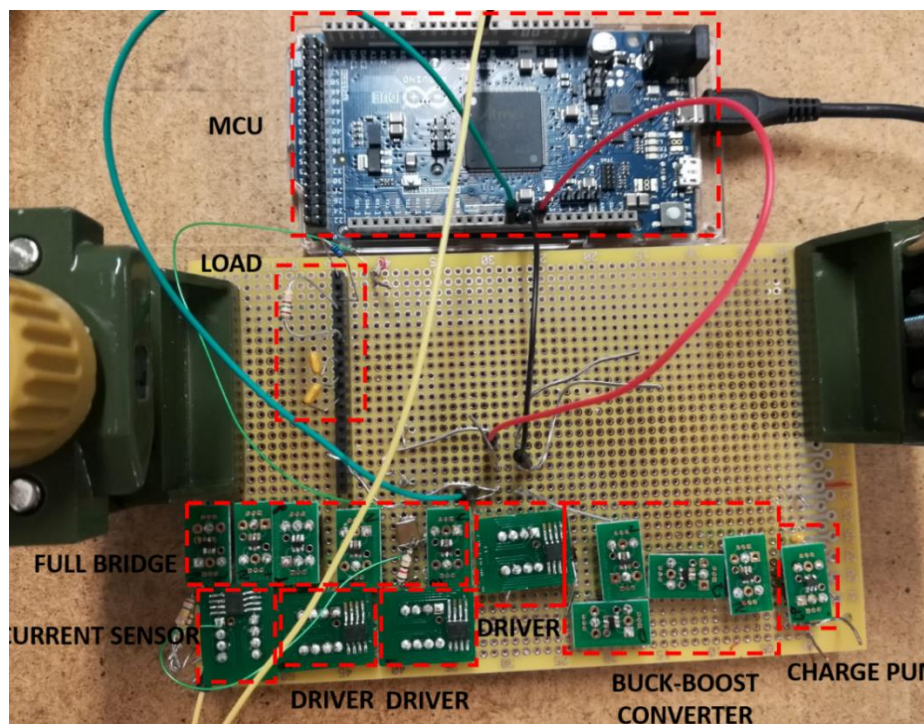


Figure 34: The fabricated first prototype.

For the fabrication of the second prototype, a 4 layer PCB was designed. The top layer was used for connecting most of the components. The second layer was used as ground layer. The third layer was used for supplying the components from the power sources and the bottom layer was used for connections between components for which there was no space at the top layer. The spaces that do not contain components or traces were covered with copper that

was grounded. Moreover, the areas of the switching, digital and sensing components were separated as much as possible. The complete design was made so as to shorten the current paths from the traces to the ground plane, minimizing voltage drops and interference between the traces. Regarding the design rules, the track width was 0.25 mm and the clearance between the tracks was also 0.25 mm. The fabricated second prototype is shown in Figure 35. The prototype was attached to the same MCU that was used for the first prototype. The MCU can be controlled via a PC, via which the stimulator can be programmed. The size of the system is 153 x 106 mm.

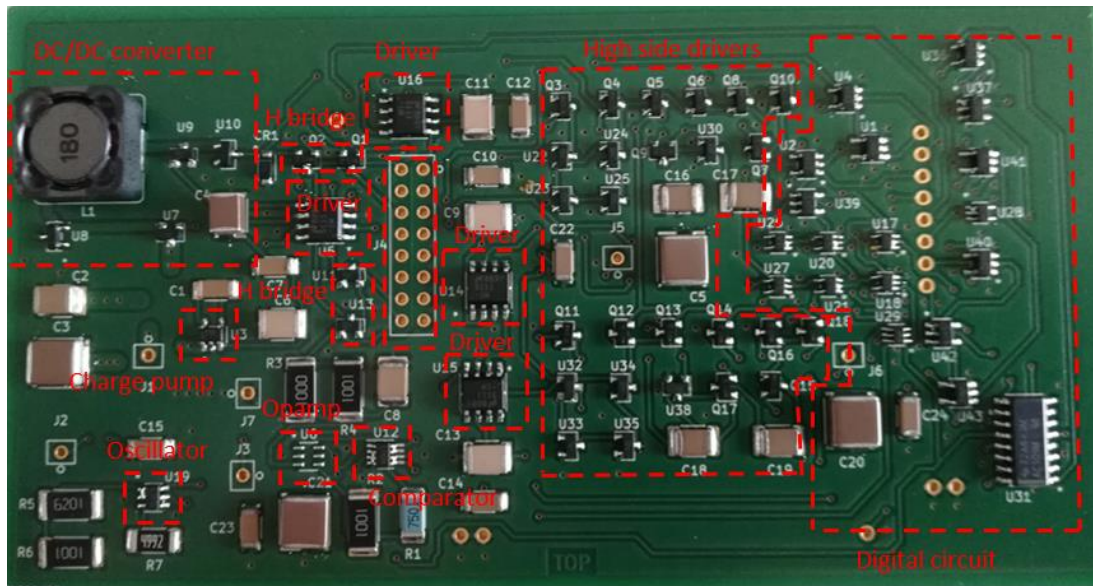


Figure 35: The fabricated second prototype.

The third prototype was fabricated in a similar way as the second prototype. However, the digital part, because of its increased complexity compared to the second prototype, was fabricated on a separate PCB, as shown in Figure 36. Both PCBs have sizes of 303 x 146 mm.

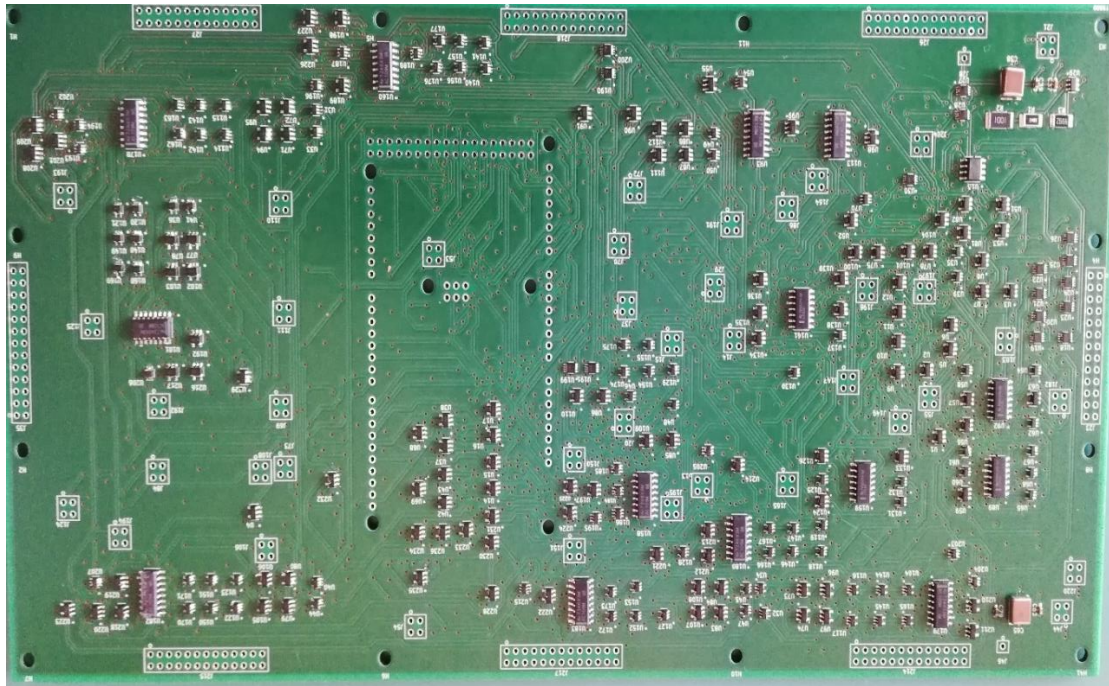


Figure 36: The digital part of the third prototype.

The two PCBs were attached as shown in Figure 37. For the control of the system, the same MCU that was used to the previous prototypes, was attached under the digital part. The analog part is shown in Figure 38.

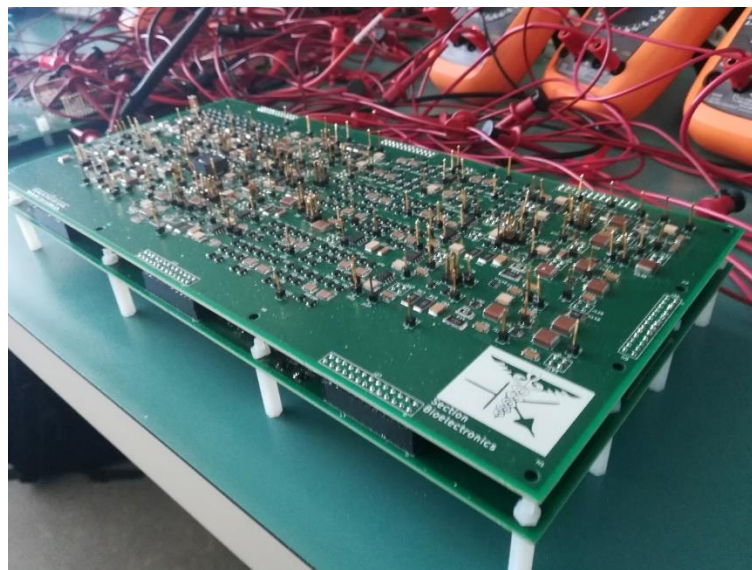


Figure 37: Attachment of the analog and the digital PCBs.

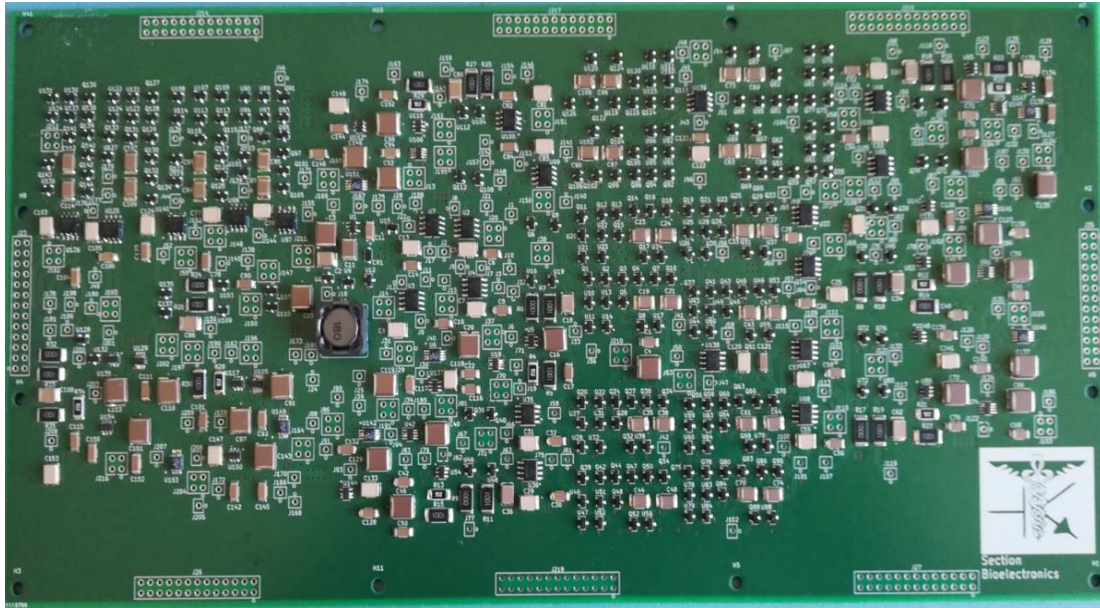


Figure 38: The analog part of the third prototype.

Except from the neurostimulator, a two layer PCB containing eight channels of testing loads was fabricated. Each channel contains seven loads. Each load consists of a 149.6Ω resistor in series with the parallel combination of a $10.12 \text{ k}\Omega$, $7.60 \text{ k}\Omega$, $5.21 \text{ k}\Omega$, $2.53 \text{ k}\Omega$, $1.144 \text{ k}\Omega$ or a 656Ω resistor with a 47 nF capacitor. Parallel to each load there was another 47 nF capacitor and the seventh load consisted only a 149.6Ω resistor in parallel with a 47 nF capacitor. The PCB is depicted in Figure 39.



Figure 39: The eight channel testing circuit

The test and measurement setup for the eight channel neurostimulator is shown in Figure 40 without an enclosure and in Figure 41 with an enclosure, in which the stimulator is programmed via a USB cable from the PC. Different blocks of the circuit (e.g. drivers, digital logic and sensing circuitry) have different power supply pins, in order to be measured separately by the available multimeters and their power consumption to be calculated.



Figure 40: Measurements and testing setup of the eight channel neurostimulator (without enclosure).

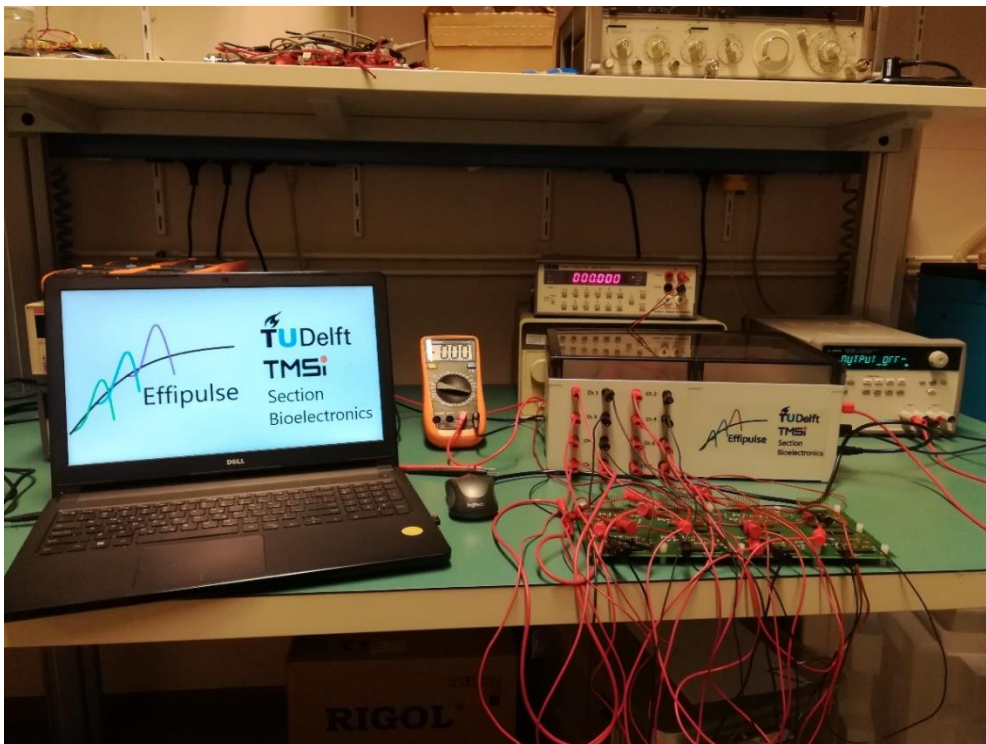


Figure 41: Measurements and testing setup of the eight channel neurostimulator (with enclosure).

5. MCU programming

For the first prototype, an MCU was extensively used for measuring the current, as well as for implementing the PWM algorithm for the DC/DC converter. Therefore, for the control of the mosfets' gates, an Arduino Due, AT91SAM3X8E [131] MCU was used. At first, the user chooses the initial duty cycle for the PWM waveform. After this, the MCU's ADC takes as input the output voltage, derived from the current sensor. The MCU translates the DC voltage that was received to the corresponding current and displays it on the screen. If the user wants to change the delivered current, he/she types at the MCU's terminal the letter "c" followed by the desired current value in mA. Hereafter, the MCU will change the duty cycle of the PWM channel that controls the DC/DC converter, so as the output current that is delivered to the load to be adjusted to the desired value. According to (50), there is linear relationship between the average load's current and the duty cycle. Furthermore, there is also the possibility for the control loop to frequently check whether the current has diverged from the desired value. This phenomenon can happen due to the dynamic behavior of the electrode tissue interface impedance, as well as from human movement. If this is the case, the duty cycle will automatically change, so as the error between the desired and the delivered current to the tissue to be minimized. The code of the MCU programmer is a modified version found in [132] and some video tutorials and is given in the Appendix C. The microcontroller was tested separately from the stimulator, with success, running the aforementioned algorithm. However, the integration of the two boards was not made, due to a malfunction that occurred to the current sensor after the first series of measurements.

For the second prototype, instead of using the MCU's inbuilt ADC, a discrete components feedback circuit was implemented for the PSM technique. With the MCU the polarity of stimulation can be controlled, as also if a boost or buck-boost converter will be used. Furthermore, the MCU can send commands to the system to charge the high side drivers. Moreover, the inbuilt 12 bit DAC of the MCU was used for controlling the output current through the feedback network. However, the used DAC could not deliver low value voltages (minimum of 0.55 V), leading to inefficiency for selecting low value output currents.

In the third prototype, eight 10 bit DACs were used (one for each channel), which made the system able to stimulate the loads with low value currents. Furthermore, in the last prototype, the MCU was able to program the DACs via its SPI interface. Additionally, with the use of the MCU, selection among 1, 2, 4 and 8 channels is possible. The MCU is also able to perform all the functions that can be performed with the second prototype.

6. Circuits measurements

For the first prototype, the output voltage of the load's high side and the inductor (from the side of U_3 as it is depicted in Figure 31) are shown in Figure 42. As was expected using the PWM technique, the output current pulse from the inductor can be adjusted depending on the pulse width of the control pulses (yellow waveform). More specifically, in Figure 42, it is shown that doubling the pulse width leads to the doubling of the output voltage and hence, the output current.

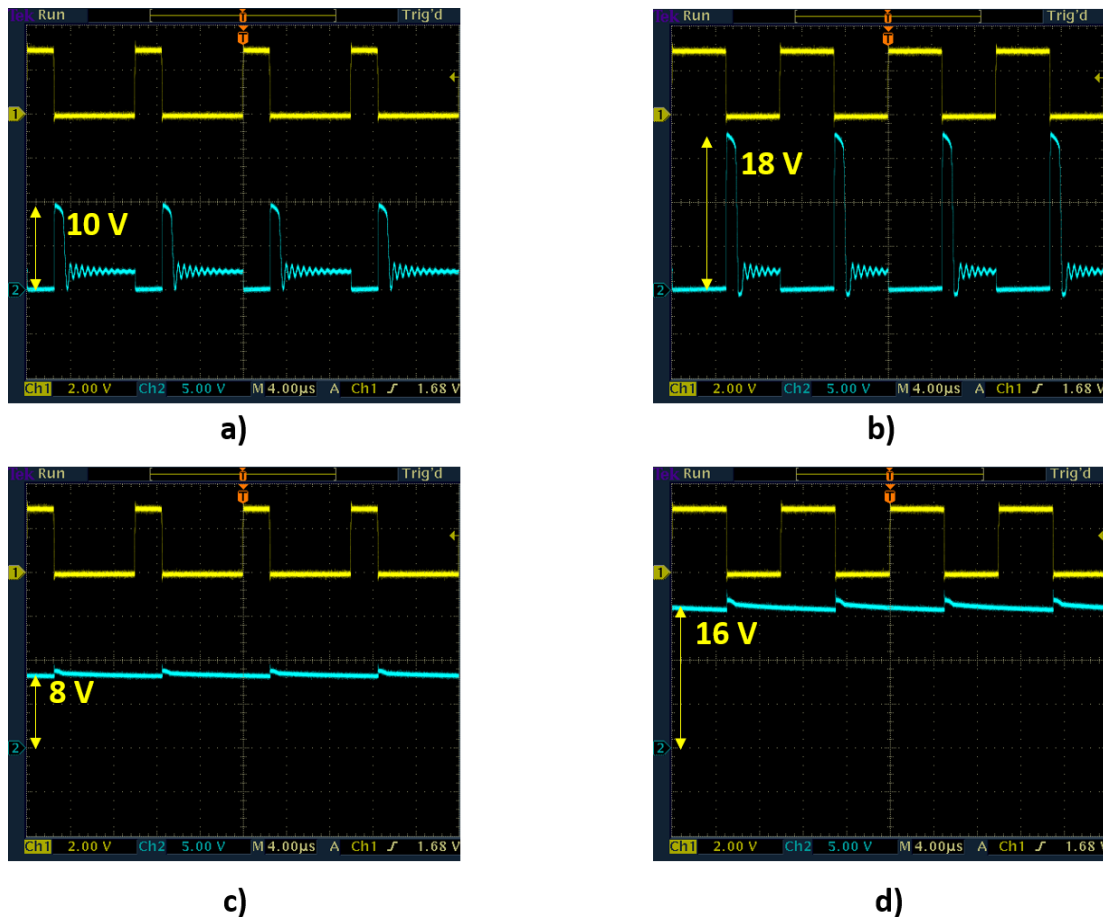


Figure 42: Measured a) inductor's voltage (U_3 's side, 25 % duty cycle), b) inductor's voltage (U_3 's side, 50 % duty cycle), c) load's voltage (25 % duty cycle), d) load's voltage (50 % duty cycle).

In the second and the third prototype, the control pulses have fixed width (50%). In order the output that can be made with the 25% pulse width from the first prototype to be created, some control pulses are skipped, leading to a lower frequency signal that creates the same steady state current as the PWM technique.

For the first prototype, because the feedback network started to malfunction (probably due to poor connection between the components) during system testing, not many measurements were taken. However, in Figure 43 that the power efficiency and the output currents for 50% duty cycle of PWM and for different resistance values are shown we can see

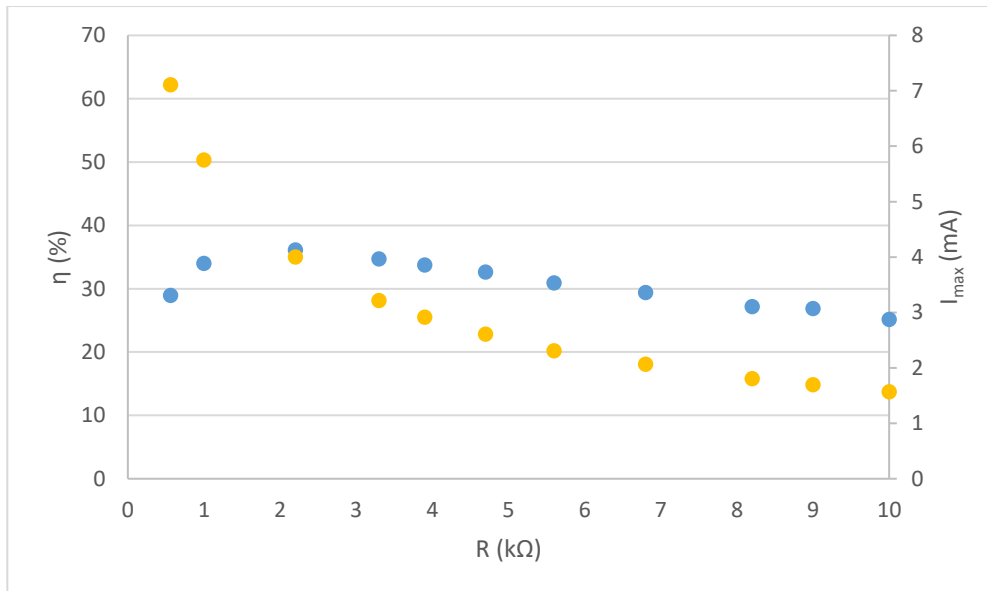


Figure 43: First prototype's power efficiency (blue line) and the output currents (yellow line) for 50% duty cycle of PWM and for different resistance values.

that the system can provide enough current for tDCS to loads until 6.8 kΩ. Furthermore, the power efficiency is below 30% for currents that are in the tDCS range.

For the second prototype, the relationship between the MCU's DAC's output voltages and the output current of the stimulator, for different loads, is shown in Figure 44. As can be observed, the system is very linear, with 2.8% output current divergence for 300% change in resistance. However, the MCU's DAC does not provide low output voltages (0.55 V minimum), leading to 661 μA minimum load current, which does not fulfill the specifications.

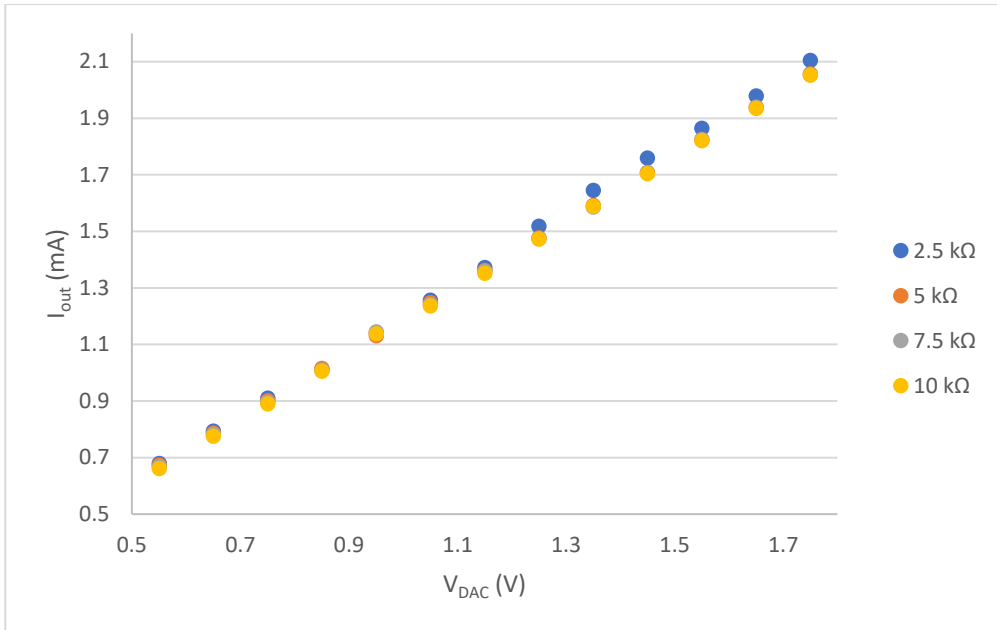


Figure 44: Relationship between the MCU's DAC's output voltages and the output current of the stimulator for different loads.

The power efficiency of the whole system with the use of a boost converter, for different output loads, is shown in Figure 45. The maximum power efficiency that is achieved by the system is 42.24%.

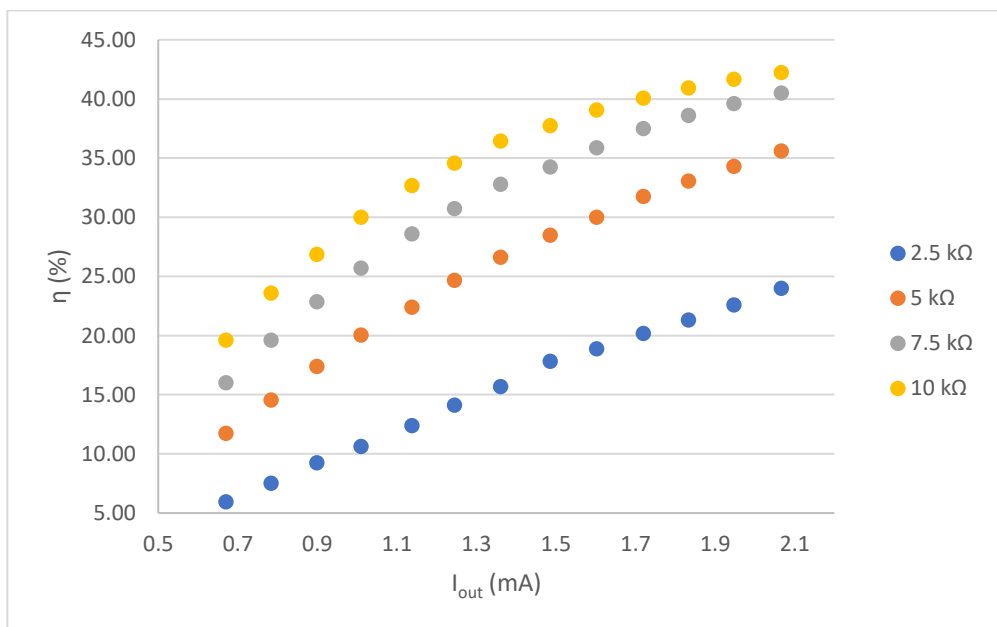


Figure 45: The power efficiency of the whole system with the use of a boost converter for different output loads.

For the third prototype, the relationship between the DAC's codes (1024 values) and the output current of the stimulator, using a boost converter, for different loads, is shown in Figure 46. As it can be observed the system is very linear, with 7.6% output current divergence for 6731% change in resistance. Hence, the system can work reliably for vast changes in outputs loads. Furthermore, the minimum output current that can be delivered is 35 μ A and the current's resolution is 4 μ A, which are 1.75% and 0.2% of the possible maximum current for tDCS applications (2 mA).

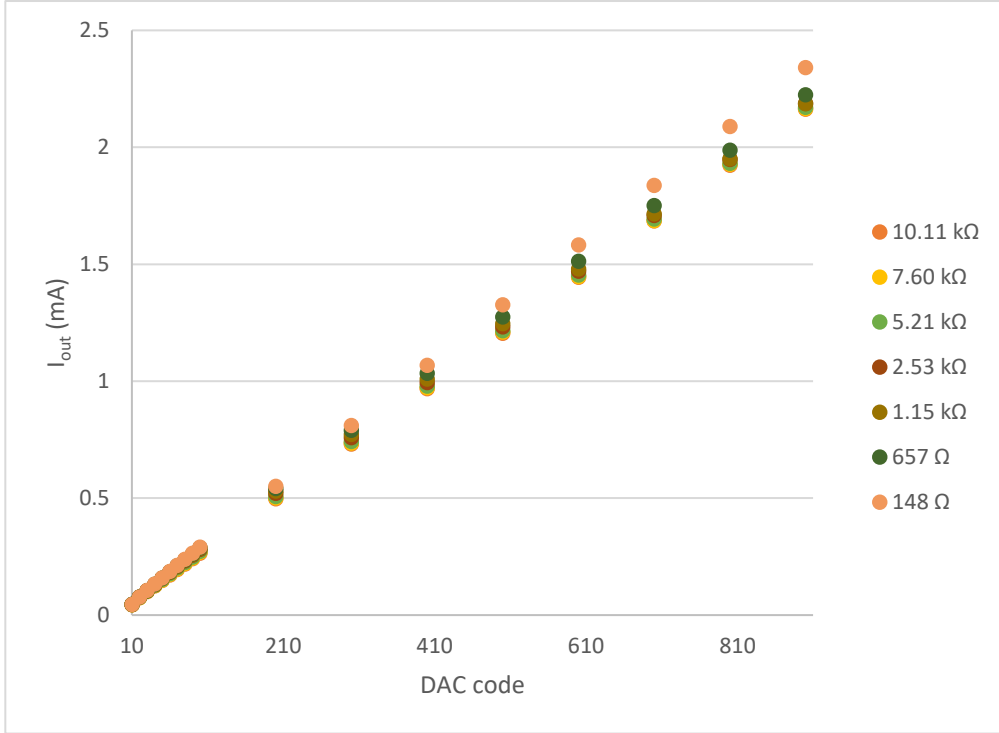


Figure 46: The relationship between the DAC's codes (1024 values) and the output current of the stimulator, using a boost converter, for different loads.

The power efficiency of the system is displayed in Figure 47 for a single channel implementation (using a boost converter) and different output loads. The power efficiency is calculated by the equation:

$$\eta = 100 \frac{V_{out} I_{out}}{V_{in} \left(I_{core} - \frac{N'}{N} I_{core,quiescent} + I_{sense} - \frac{N'}{N} I_{sense,quiescent} + I_{drivers} - \frac{N'}{N} I_{drivers,quiescent} \right)} \% \quad (52)$$

where I_{core} is the current consumed by the DC/DC converter, the charge pump and the low side drivers that the current pump supplies, I_{sense} is the current consumed by the measuring circuit and the DACs, $I_{drivers}$ is the current consumed by the low side drivers that are not supplied by the charge pump and the high side drivers, N is the number of the systems channels and

$$N' = N - N_{used} \quad (53)$$

where N_{used} is the number of active channels. The maximum power efficiency that the system can achieve is 43.84%, which is 23.49% higher than the state of the art adaptive voltage current source stimulator, presented in [100].

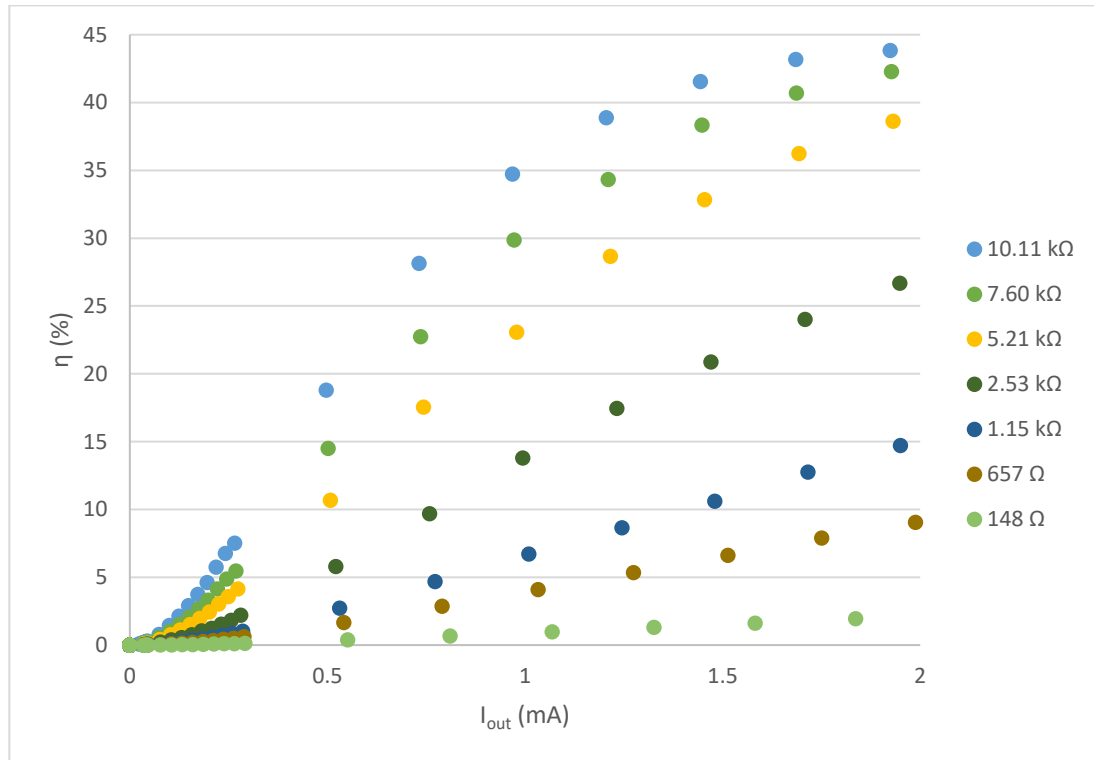


Figure 47: The power efficiency of the system, for one active channel (using boost converter) and different output loads.

The power efficiency comparison between the use of the proposed boost module and a conventional buck-boost converter, is shown in Figure 48 for two different loads. As expected the proposed technique is more power efficient than the conventional one, reaching to 40.57% improvement.

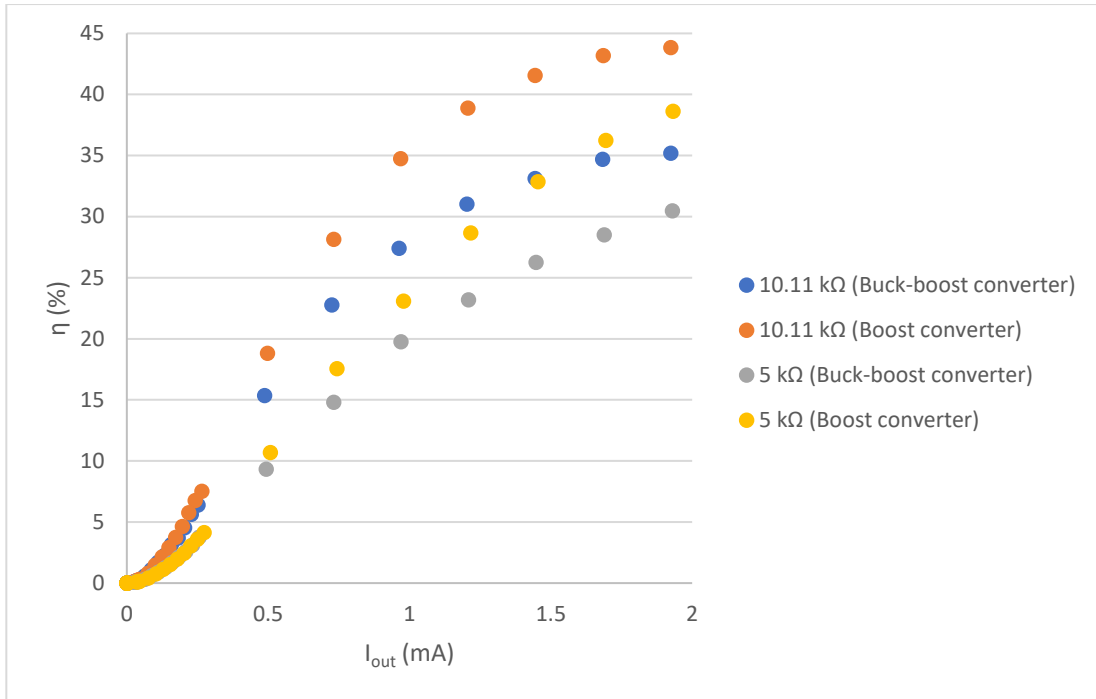


Figure 48: Comparison between the use of the proposed boost module and a conventional buck-boost converter for two different loads.

For multichannel testing, two scenarios were implemented. The first scenario assumes that the first channel's load has 10 k Ω resistance and the other channels 5 k Ω resistance. The second scenario assumes that the first channel's load has 10 k Ω resistance and the other channels 2.5 k Ω resistance. The power efficiency for both scenarios for two, four and eight channels are shown in Figure 49, 50 and 51 respectively.

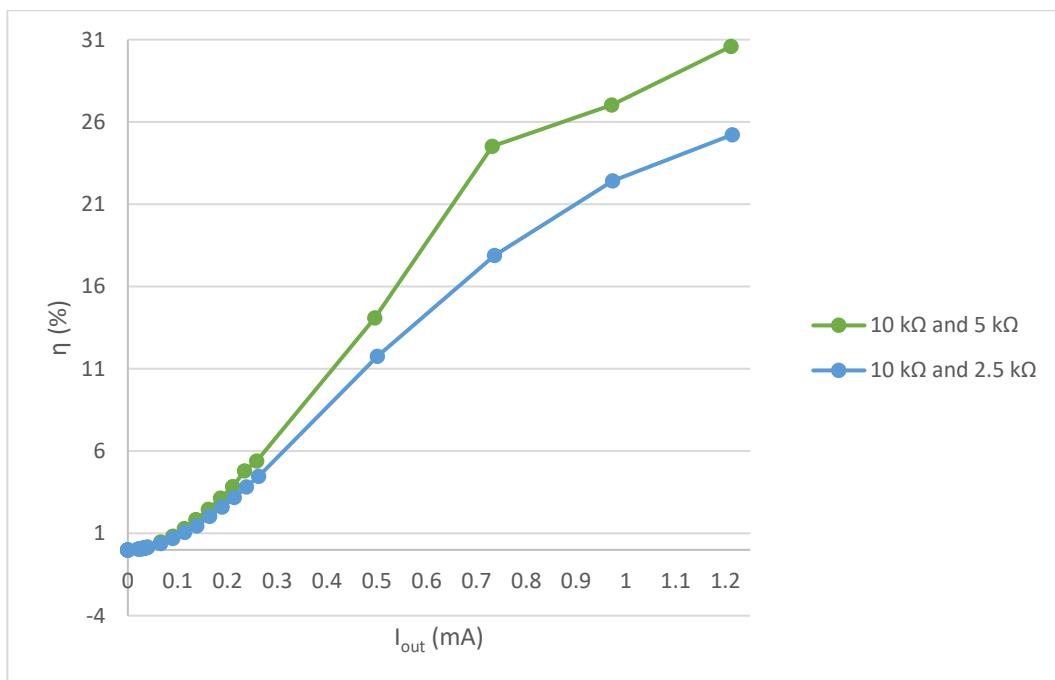


Figure 49: Power efficiency of a two channel system for two different scenarios.

The system has been designed, in order each channel to be able to deliver to its load $2/N_{\text{active}}$ mA.

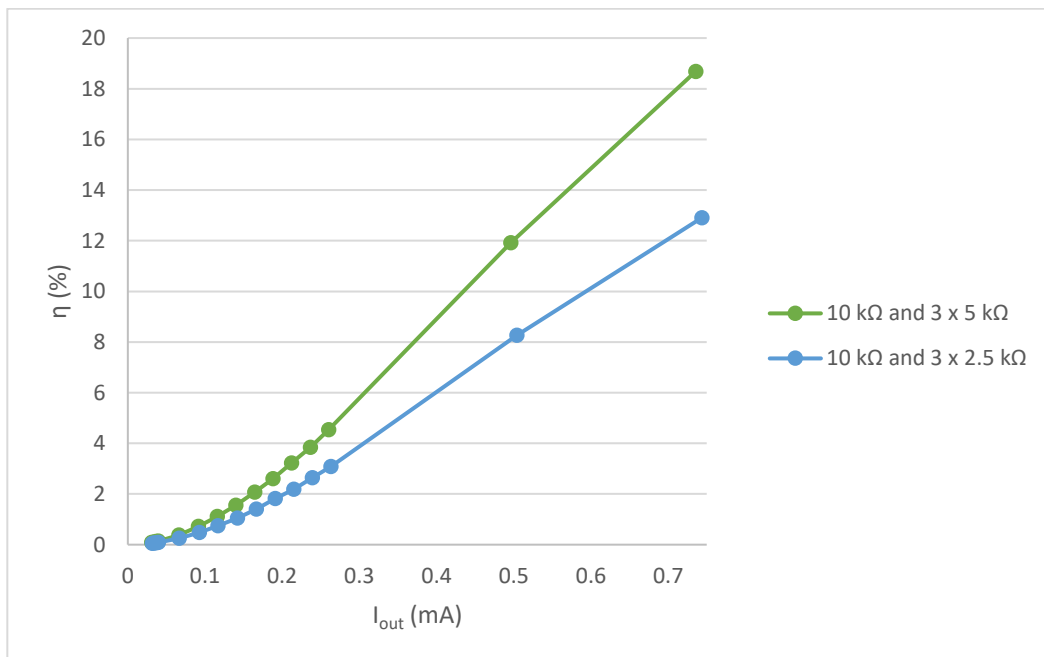


Figure 50: Power efficiency of a four channel system for two different scenarios.

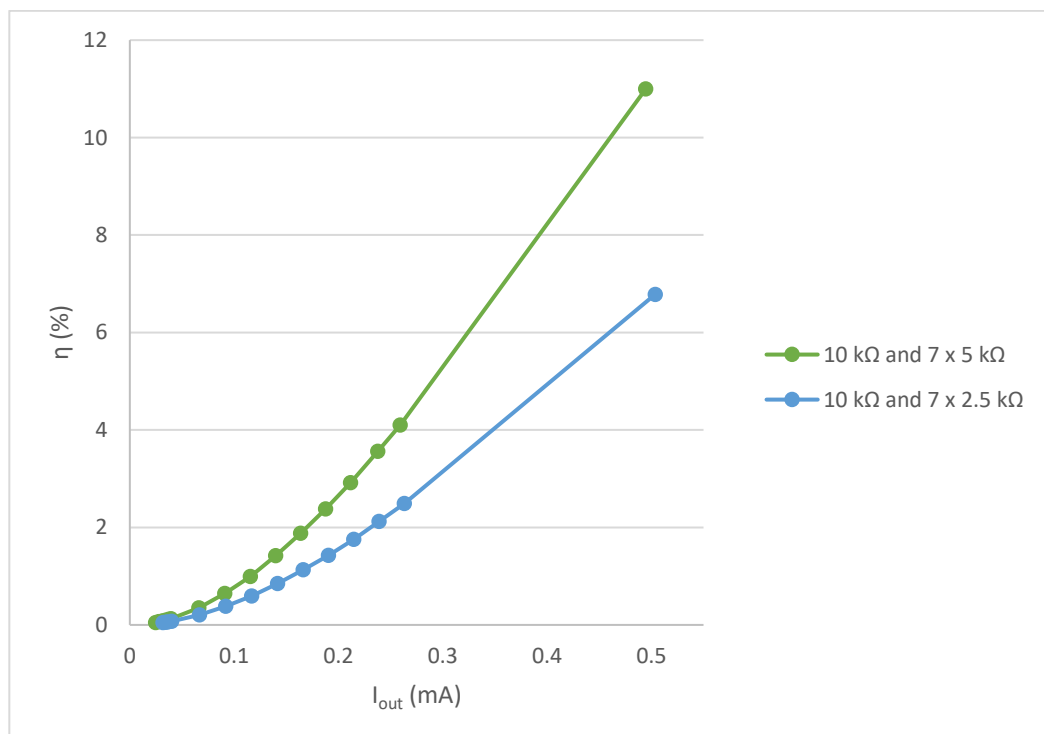


Figure 51: Power efficiency of an eight channel system for two different scenarios.

In order a power efficiency comparison to be made, the third prototype was compared with an ideal fixed voltage current source (CS). For the fixed voltage CS, it is assumed that its

voltage compliance is 22 V, being able to deliver 2 mA to 10 kΩ loads, as well as to provide a 2 V voltage drop, for the proper biasing of the CS. Moreover, the DC/DC converter is assumed to have 80% power efficiency, for creating the compliance voltage from a low voltage power supply, which is a reasonable value. Therefore, the efficiency of the stimulator is calculated as:

$$\eta_{fixed\ voltage\ CS} = 0.8 \frac{V_{compliance} I_{out}}{V_{in} I_{in}} 100 \quad (54)$$

The comparison between the two stimulators is shown in Figure 52. For each stimulator it is assumed that 2 mA total current is delivered to the loads, equivalently distributed between the active channels.

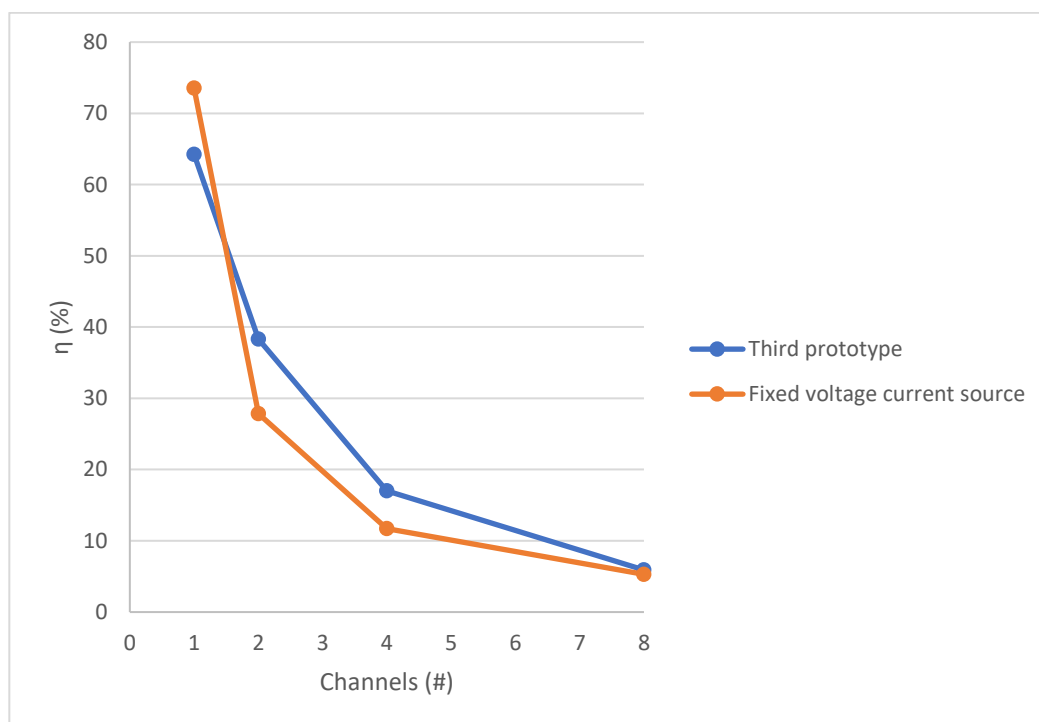


Figure 52: Comparison between the proposed system and a fixed voltage current source stimulator.

As it is shown from Figure 52, the proposed system, even though it has 12.63% less power efficiency than the fixed voltage CS for one active channel, it outperforms the fixed voltage CS by 37.57%, 45.47% and 11.59% for two, four and eight active channels respectively. For only this comparison the I_{sense} and $I_{drivers}$ were assumed to be zero, because they were compared with an ideal system.

One issue that was observed during the measurements was that when the user was changing the output current many times, the high side drivers' capacitors were discharged leading to insufficiency of the system to supply the desired current to the tissue. Furthermore, interference between the loads was observed, when the capacitors were discharged.

Therefore, it is advised, before the start of the stimulation, the high side drivers to be charged at least for 10 seconds.

Except from the power efficiency, it is important to characterize the system regarding its transient response, as well as its steady state current ripple. In Figures 53 and 54, transient responses of load's voltage are displayed without and with overshoot respectively. The overshoot was created because of the closed loop system characteristics. Furthermore, due to the vast range of possible output loads, there is a tradeoff between driving fast loads with big time constant and driving loads with small time constant without overshoot.

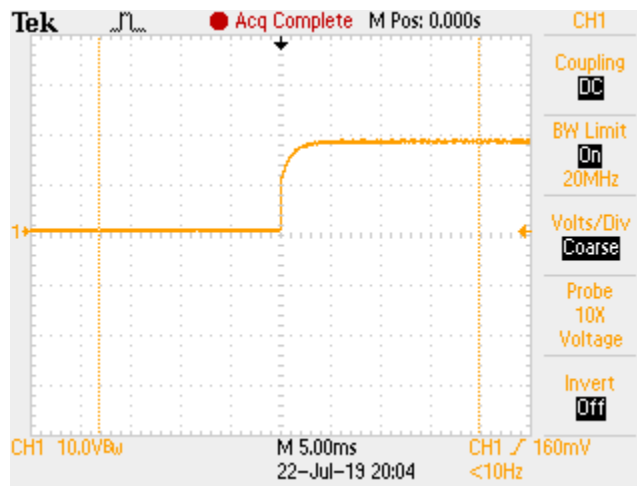


Figure 53: Transient response of the system without overshoot.

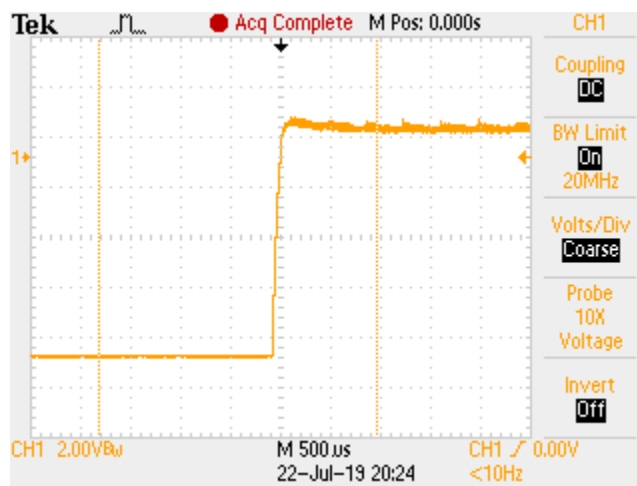


Figure 54: Transient response of the system with overshoot.

From the waveform's transient and ripple analysis, Table 26 was created. The maximum overshoot that was observed is 76%. Even though this seems a high value, all the waveforms settle down to their steady state in less than 2.1 ms. Hence, the transient response is not expected to create problems to the tissue. Furthermore, the biggest voltage ripple that was observed is 800 mV_{pp} for a 2.53kΩ load, creating 316 µA_{pp} current. The first harmonic frequencies of the ripples range from tens of kHz to a little more than 100 kHz. This range of

frequencies is also used for high frequency conduction blocking of the neurons. However, due to the low magnitude of the ripple current, as also because current is not applied directly to the neurons, it is very unlikely for high frequency conduction block to occur [127], [133], [134], [135].

Table 26: Transient and output ripple characteristics for different loads, output currents and converter types.

R_{load} (kΩ)												
10.11												
Converter type												
	Buck-boost						Boost					
I_{out} (mA)	V_{steady state} (V)	f (kHz)	V_{rms} (mV)	V_{pp} (mV)	t_{settling} (ms)	Overshoot (%)	V_{steady state} (V)	f (kHz)	V_{rms} (mV)	V_{pp} (mV)	t_{settling} (ms)	Overshoot (%)
0.25	2.57	20.8	58.5	360	1.27	12.06	2.62	13.9	78.6	600	1.23	9.92
0.5	5.05	49	52.8	320	1.43	6.05	5.10	41	78.4	500	1.59	5.06
1	10.10	178.6	42.1	260	1.54	0.98	10.12	119	52.3	320	1.58	0.84
2	20.21	163.9	51	260	1.99	2.91	20.22	142.9	47	280	2.06	2.87

R_{load} (kΩ)												
5.21												
Converter type												
	Buck-boost						Boost					
I_{out} (mA)	V_{steady state} (V)	f (kHz)	V_{rms} (mV)	V_{pp} (mV)	t_{settling} (μs)	Overshoot (%)	V_{steady state} (V)	f (kHz)	V_{rms} (mV)	V_{pp} (mV)	t_{settling} (μs)	Overshoot (%)
0.25	1.34	20.8	64.7	400	158.9	16.50	1.39	14.7	81.2	520	148.5	27.08
0.5	2.62	48.1	65.8	360	141.3	9.97	2.65	27	84.5	560	81.3	16.27
1	5.22	125	59.1	360	180.6	3.39	5.25	83.3	82.3	520	162	2.11
2	10.45	147.1	66.2	360	426.5	1.46	10.46	125	79.9	420	172	1.36

R_{load} (kΩ)												
2.53												
Converter type												
	Buck-boost						Boost					
I_{out} (mA)	V_{steady state} (V)	f (kHz)	V_{rms} (mV)	V_{pp} (mV)	t_{settling} (μs)	Overshoot (%)	V_{steady state} (V)	f (kHz)	V_{rms} (mV)	V_{pp} (mV)	t_{settling} (μs)	Overshoot (%)
0.25	0.66	20.8	85	480	106.2	76.02	0.68	13.9	102	640	56.5	57.89
0.5	1.29	40	88	560	48.98	67.57	1.31	27	103	680	49	71.12
1	2.55	102	88.9	520	65.79	74.19	2.57	55.6	114	680	44.6	74.18
2	5.10	111.1	86.9	440	126.8	41.23	5.12	75.8	146	800	64.5	45.23

7. Conclusions and recommendations for future work

In this thesis, the world's first discrete components realization of a low power, multichannel stimulation module that uses the UHF technique for tDCS applications was presented. With this approach, the technological benefits of the UHF stimulation technique were derived, combined with a cost effective, low scale production method. Moreover, contrary to previous IC realizations, current controlled feedback was also added to the system.

Three prototypes were designed, fabricated and tested. The first prototype was the first single channel, discrete components, closed loop, implementation that uses the UHF technique. The system uses a 3.5 V low voltage supply for the whole circuitry.

In the second prototype, capacitive coupled high side drivers for the load's H-bridge, as also a novel boosting technique, using the isolation that the H-bridges' mosfets can offer, were used. Furthermore, a pulse skipping modulation algorithm was also used. With these additions, the system was able to provide currents to the loads that require voltages lower than the input voltage supply, using only a boost converter. The system showed increased power efficiency compared to the first prototype reaching the maximum of 42.24%.

In the third prototype, an eight channel neurostimulator was designed, measured and fabricated. The module has a very linear relationship between the selected DAC's codes and the output supply current, and is able to stimulate a wide range of loads (0.148 - 10.11 k Ω) up to 2 mA. Furthermore, the novel boost technique showed 40.57% maximum improvement in the power efficiency compared to the use of a conventional buck-boost converter. Moreover, the feedback system showed significant robustness achieving only 7.6% output current divergence for a 6731% change of the output load. The module can deliver 35 μ A minimum current, with 4 μ A resolution, which is translated into 1.75% and 0.2% of the maximum delivered current respectively. Except from the high resolution, the system also has a fast transient response, which settles in less than 2.1 ms. Additionally, when one channel is active the stimulator showed 43.84% maximum power efficiency, which is 23.49% higher than the maximum efficiency of state of the art adaptive voltage current controlled implementations. Additionally, the multichannel system was tested in real life scenarios and its efficiency was compared to a fixed voltage current controlled module. The system achieved 37.57%, 45.47% and 11.59% power efficiency improvement for two, four and eight channels respectively.

Hence, a novel closed loop multichannel module was created that has high accuracy and improved multichannel power efficiency, offering significant benefits compared to the

existing solutions. Hence, the system has the potential to create a viable solution for future implementations of power efficient multichannel tDCS devices.

Nevertheless, the fabricated module is not perfect and many recommendations can be made for its future improvement. One criticism that can be made about the multichannel prototype regards its size. It is true that the dimensions of the prototype match more to a benchtop stimulator, rather than a portable one. However, some recommendations can be made about minimizing the size of the system. First of all, some components of the system can be used for multiple channels, such as the DACs. Nevertheless, one DAC was implemented for each channel, in order to be sure regarding the signal integrity of the DACs. In future implementations the whole feedback system could be made using the same components for all channels in an interleaved fashion.

Furthermore, the digital part could be made using a field programmable gate array (FPGA) and an SMD MCU. However, due to the time constraints and the focus that was made towards the analog part, the digital part was created at a different PCB and an off the shelf MCU board was used.

Regarding the PCB fabrication, smaller profile SMD components could be used, but because they were placed by hand, there was danger for placement mistakes and misalignments. Moreover, more PCB layers could be used for minimizing the size of the PCB, but the expenses of the PCB order would be very high.

The ultimate minimization approach for the stimulator would be to implement it into an IC, which would have a size of only a few mm². The design towards an IC would be relatively easy, since a lot of blocks of the system were already assigned at transistor level (e.g. the high side gate drivers). Furthermore, the system will have very few passive components outside the chip, making the idea of an IC design significantly space efficient.

Additionally, with the IC implementation, the power efficiency is expected to be improved. Another recommendation for the increase of the system's power efficiency would be the implementation of a better design for the low side drivers, as well as the design of a boost converter using active diodes that are controlled with a zero voltage switching technique.

With the aforementioned recommendations, a smaller form factor and more power efficient system could be created, which it might give the possibility for the addition of more channels without compromising the stimulator's specifications.

Bibliography

- [1] G. Deuschl, C. Schade-Brittinger, P. Krack, J. Volkmann, H. Schäfer, K. Bötzel, C. Daniels, A. Deuschländer, U. Dillmann, W. Eisner, D. Gruber, W. Hamel, J. Herzog, R. Hilker, S. Klebe, M. Kloß, J. Koy, M. Krause, A. Kupsch, D. Lorenz, S. Lorenzl, H. M. Mehdorn, J. R. Moringlane, W. Oertel, M. O. Pinsker, H. Reichmann, A. Reuß, G.-H. Schneider, A. Schnitzler, U. Steude, V. Sturm, L. Timmermann, V. Tronnier, T. Trottenberg, L. Wojtecki, E. Wolf, W. Poewe, and J. Voges, "A Randomized Trial of Deep-Brain Stimulation for Parkinson's Disease," *N. Engl. J. Med.*, vol. 355, no. 9, pp. 896–908, 2006.
- [2] A. Handforth, C. M. DeGiorgio, S. C. Schachter, B. M. Uthman, D. K. Naritoku, E. S. Tecoma, T. R. Henry, S. D. Collins, B. V. Vaughn, R. C. Gilmartin, D. R. Labar, G. L. Morris, M. C. Salinsky, I. Osorio, R. K. Ristanovic, D. M. Labiner, J. C. Jones, J. V. Murphy, G. C. Ney, and J. W. Wheless, "Vagus nerve stimulation therapy for partial-onset seizures," *Neurology*, vol. 51, no. 1, pp. 48–55, 1998.
- [3] T. Cameron, "Safety and efficacy of spinal cord stimulation for the treatment of chronic pain: a 20-year literature review," *J. Neurosurg. Spine*, vol. 100, no. 3, pp. 254–267, 2004.
- [4] B. S. Wilson and M. F. Dorman, "Cochlear implants: A remarkable past and a brilliant future," *Hear. Res.*, vol. 242, no. 1, pp. 3–21, 2008.
- [5] L. N. Ayton, P. J. Blamey, R. H. Guymer, C. D. Luu, D. A. X. Nayagam, N. C. Sinclair, M. N. Shivdasani, J. Yeoh, M. F. McCombe, R. J. Briggs, N. L. Opie, J. Villalobos, P. N. Dimitrov, M. Varsamidis, M. A. Petoe, C. D. McCarthy, J. G. Walker, N. Barnes, A. N. Burkitt, C. E. Williams, R. K. Shepherd, P. J. Allen, and for the Bionic Vision Australia Research Consortium, "First-in-Human Trial of a Novel Suprachoroidal Retinal Prosthesis," *PLoS One*, vol. 9, no. 12, pp. 1–26, 2014.
- [6] S. Harkema, Y. Gerasimenko, J. Hodes, J. Burdick, C. Angeli, Y. Chen, C. Ferreira, A. Willhite, E. Rejc, R. G. Grossman, and V. R. Edgerton, "Effect of epidural stimulation of the lumbosacral spinal cord on voluntary movement, standing, and assisted stepping after motor complete paraplegia: a case study," *Lancet*, vol. 377, no. 9781, pp. 1938–1947, 2011.
- [7] D. R. Merrill, M. Bikson, and J. G. R. Jefferys, "Electrical stimulation of excitable tissue: design of efficacious and safe protocols," *J. Neurosci. Methods*, vol. 141, no. 2, pp. 171–198, 2005.
- [8] D. K. Binder, G. Rau, and P. A. Starr, "Hemorrhagic Complications of Microelectrode-Guided Deep Brain Stimulation," *Stereotact. Funct. Neurosurg.*, vol. 80, no. 1–4, pp. 28–31, 2003.
- [9] I. Williams and T. G. Constandinou, "An Energy-Efficient, Dynamic Voltage Scaling Neural Stimulator for a Proprioceptive Prosthesis," *IEEE Trans. Biomed. Circuits Syst.*, vol. 7, no. 2, pp. 129–139, 2013.
- [10] M. N. van Dongen and W. A. Serdijn, "A Power-Efficient Multichannel Neural Stimulator Using High-Frequency Pulsed Excitation From an Unfiltered Dynamic Supply," *IEEE Trans. Biomed. Circuits Syst.*, vol. 10, no. 1, pp. 61–71, 2016.
- [11] M. N. van Dongen, F. E. Hoebeek, S. K. E. Koekkoek, C. I. De Zeeuw, and W. A. Serdijn, "High frequency switched-mode stimulation can evoke post synaptic responses in cerebellar principal neurons," *Front. Neuroeng.*, vol. 8, p. 2, Mar. 2015.
- [12] H. Thair, A. L. Holloway, R. Newport, and A. D. Smith, "Transcranial Direct Current Stimulation (tDCS): A Beginner's Guide for Design and Implementation," *Front. Neurosci.*, vol. 11, p. 641, 2017.

- [13] F. Fregni, P. S. Boggio, M. Nitsche, F. Berman, A. Antal, E. Feredoes, M. A. Marcolin, S. P. Rigonatti, M. T. A. Silva, W. Paulus, and A. Pascual-Leone, "Anodal transcranial direct current stimulation of prefrontal cortex enhances working memory," *Exp. Brain Res.*, vol. 166, no. 1, pp. 23–30, Sep. 2005.
- [14] M. A. Nitsche, P. S. Boggio, F. Fregni, and A. Pascual-Leone, "Treatment of depression with transcranial direct current stimulation (tDCS): A Review," *Exp. Neurol.*, vol. 219, no. 1, pp. 14–19, 2009.
- [15] F. Hummel, P. Celnik, P. Giroux, A. Floel, W.-H. Wu, C. Gerloff, and L. G. Cohen, "Effects of non-invasive cortical stimulation on skilled motor function in chronic stroke," *Brain*, vol. 128, no. 3, pp. 490–499, 2005.
- [16] M. Bikson, P. Grossman, C. Thomas, A. L. Zannou, J. Jiang, T. Adnan, A. P. Mourdoukoutas, G. Kronberg, D. Truong, P. Boggio, A. R. Brunoni, L. Charvet, F. Fregni, B. Fritsch, B. Gillick, R. H. Hamilton, B. M. Hampstead, R. Jankord, A. Kirton, H. Knotkova, D. Liebetanz, A. Liu, C. Loo, M. A. Nitsche, J. Reis, J. D. Richardson, A. Rotenberg, P. E. Turkeltaub, and A. J. Woods, "Safety of Transcranial Direct Current Stimulation: Evidence Based Update 2016," *Brain Stimul.*, vol. 9, no. 5, pp. 641–661, 2016.
- [17] "Overdose Death Rates | National Institute on Drug Abuse (NIDA)." [Online]. Available: <https://www.drugabuse.gov/related-topics/trends-statistics/overdose-death-rates>. [Accessed: 24-Jun-2019].
- [18] "National Health Expenditures 2017 Highlights." [Online]. Available: <https://www.cms.gov/Research-Statistics-Data-and-Systems/Statistics-Trends-and-Reports/NationalHealthExpendData/Downloads/highlights.pdf>. [Accessed: 14-Aug-2019].
- [19] J. A. DiMasi, H. G. Grabowski, and R. W. Hansen, "Innovation in the pharmaceutical industry: New estimates of R&D costs," *J. Health Econ.*, vol. 47, pp. 20–33, May 2016.
- [20] J. Duke, J. Friedlin, and P. Ryan, "A Quantitative Analysis of Adverse Events and 'Overwarning' in Drug Labeling Analysis of ADEs and Overwarning in Drug Labeling," *JAMA Intern. Med.*, vol. 171, no. 10, pp. 941–954, 2011.
- [21] "Global prescription drug spend seen at \$1.5 trillion in 2021 - report - Reuters." [Online]. Available: <https://de.reuters.com/article/uk-health-pharmaceuticals-spending/global-prescription-drug-spend-seen-at-1-5-trillion-in-2021-report-idUKKBN13V0D3>. [Accessed: 24-Jun-2019].
- [22] "Getting better with 'electroceuticals.'" [Online]. Available: <https://www.tudelft.nl/en/2016/tu-delft/getting-better-with-electroceuticals/>. [Accessed: 24-Jun-2019].
- [23] H. Knotkova, M. A. Nitsche, M. Bikson, and A. J. Woods, Eds., *Practical Guide to Transcranial Direct Current Stimulation*. Cham: Springer International Publishing, 2019.
- [24] L. F. Medeiros, I. C. C. de Souza, L. P. Vidor, A. de Souza, A. Deitos, M. S. Volz, F. Fregni, W. Caumo, and I. L. S. Torres, "Neurobiological effects of transcranial direct current stimulation: a review," *Front. psychiatry*, vol. 3, p. 110, Dec. 2012.
- [25] "Google Scholar." [Online]. Available: https://scholar.google.com/?hl=en&as_sdt=0,5. [Accessed: 14-Aug-2019].
- [26] L. E. Charvet, M. Kasschau, A. Datta, H. Knotkova, M. C. Stevens, A. Alonzo, C. Loo, K. R. Krull, and M. Bikson, "Remotely-supervised transcranial direct current stimulation (tDCS) for clinical trials: guidelines for technology and protocols," *Front. Syst. Neurosci.*, vol. 9, p. 26, Mar. 2015.
- [27] N. Ngernyam, M. P. Jensen, N. Auvichayapat, W. Punjaruk, and P. Auvichayapat, "Transcranial Direct Current Stimulation in Neuropathic Pain," *J. pain Reli.*, vol. Suppl

- 3, p. 1, Apr. 2013.
- [28] D. H. Benninger, M. Lomarev, G. Lopez, E. M. Wassermann, X. Li, E. Consideine, and M. Hallett, "Transcranial direct current stimulation for the treatment of Parkinson's disease," *J. Neurol. Neurosurg. Psychiatry*, vol. 81, no. 10, pp. 1105–1111, Oct. 2010.
- [29] A. Sauvaget, B. Trojak, S. Bulteau, S. Jiménez-Murcia, F. Fernández-Aranda, I. Wolz, J. M. Menchón, S. Achab, J.-M. Vanelle, and M. Grall-Bronnec, "Transcranial direct current stimulation (tDCS) in behavioral and food addiction: a systematic review of efficacy, technical, and methodological issues," *Front. Neurosci.*, vol. 9, p. 349, Oct. 2015.
- [30] A. Pisoni, G. Mattavelli, C. Papagno, M. Rosanova, A. G. Casali, and L. J. Romero Lauro, "Cognitive Enhancement Induced by Anodal tDCS Drives Circuit-Specific Cortical Plasticity," *Cereb. Cortex*, vol. 28, no. 4, pp. 1132–1140, Feb. 2017.
- [31] Y. Lin, Q. Huang, T. Han, Y. Su, D. Gao, W. Chen, H. Ye, T. Liu, X. Tian, Z. Zhen, and Y. Wang, "Evaluating the Effect of Simultaneous Transcranial Direct Current stimulation and Repetitive Transcranial Magnetic Stimulation on Minimally conscious state by Using EEG and Functional MRI," *Brain Stimul. Basic, Transl. Clin. Res. Neuromodulation*, vol. 12, no. 2, pp. 403–404, Mar. 2019.
- [32] S. Das, P. Holland, M. A. Frens, and O. Donchin, "Impact of Transcranial Direct Current Stimulation (tDCS) on Neuronal Functions," *Front. Neurosci.*, vol. 10, p. 550, 2016.
- [33] Q. M. Wang, H. Cui, S. J. Han, R. Black-Schaffer, M. S. Volz, Y.-T. Lee, S. Herman, L. A. Latif, R. Zafonte, and F. Fregni, "Combination of transcranial direct current stimulation and methylphenidate in subacute stroke," *Neurosci. Lett.*, vol. 569, pp. 6–11, 2014.
- [34] N. Gebodh, Z. Esmailpour, D. Adair, P. Schestattsky, F. Fregni, and M. Bikson, "Transcranial Direct Current Stimulation Among Technologies for Low-Intensity Transcranial Electrical Stimulation: Classification, History, and Terminology BT - Practical Guide to Transcranial Direct Current Stimulation: Principles, Procedures and Applica," H. Knotkova, M. A. Nitsche, M. Bikson, and A. J. Woods, Eds. Cham: Springer International Publishing, 2019, pp. 3–43.
- [35] D. Reato, R. Salvador, M. Bikson, A. Opitz, J. Dmochowski, and P. C. Miranda, "Principles of Transcranial Direct Current Stimulation (tDCS): Introduction to the Biophysics of tDCS BT - Practical Guide to Transcranial Direct Current Stimulation: Principles, Procedures and Applications," H. Knotkova, M. A. Nitsche, M. Bikson, and A. J. Woods, Eds. Cham: Springer International Publishing, 2019, pp. 45–80.
- [36] M. Bikson, "Who, where, what, when, and why: Optimizing transcranial Direct Current Stimulation," *Brain Stimul.*, vol. 8, no. 2, p. 432, 2015.
- [37] M. T. Berlim, F. Van den Eynde, and Z. J. Daskalakis, "Clinical utility of transcranial direct current stimulation (tDCS) for treating major depression: A systematic review and meta-analysis of randomized, double-blind and sham-controlled trials," *J. Psychiatr. Res.*, vol. 47, no. 1, pp. 1–7, 2013.
- [38] H. Koo, M. S. Kim, S. W. Han, W. Paulus, M. A. Nitsche, Y.-H. Kim, H.-I. Kim, S.-H. Ko, and Y.-I. Shin, "After-effects of anodal transcranial direct current stimulation on the excitability of the motor cortex in rats," *Restor. Neurol. Neurosci.*, vol. 34, no. 5, pp. 859–868, 2016.
- [39] C. J. Stagg, J. G. Best, M. C. Stephenson, J. O'Keefe, M. Wylezinska, Z. T. Kincses, P. G. Morris, P. M. Matthews, and H. Johansen-Berg, "Polarity-Sensitive Modulation of Cortical Neurotransmitters by Transcranial Stimulation," *J. Neurosci.*, vol. 29, no. 16, pp. 5202–5206, 2009.
- [40] V. P. Clark, B. A. Coffman, M. C. Trumbo, and C. Gasparovic, "Transcranial direct current stimulation (tDCS) produces localized and specific alterations in

- neurochemistry: A 1H magnetic resonance spectroscopy study," *Neurosci. Lett.*, vol. 500, no. 1, pp. 67–71, 2011.
- [41] F. Notturmo, L. Marzetti, V. Pizzella, A. Uncini, and F. Zappasodi, "Local and remote effects of transcranial direct current stimulation on the electrical activity of the motor cortical network," *Hum. Brain Mapp.*, vol. 35, no. 5, pp. 2220–2232, May 2014.
- [42] S. Durand, B. Fromy, P. Bouyé, J. L. Saumet, and P. Abraham, "Vasodilatation in response to repeated anodal current application in the human skin relies on aspirin-sensitive mechanisms," *J. Physiol.*, vol. 540, no. 1, pp. 261–269, Apr. 2002.
- [43] A. J. Woods, A. Antal, M. Bikson, P. S. Boggio, A. R. Brunoni, P. Celnik, L. G. Cohen, F. Fregni, C. S. Herrmann, E. S. Kappenman, H. Knotkova, D. Liebetanz, C. Miniussi, P. C. Miranda, W. Paulus, A. Priori, D. Reato, C. Stagg, N. Wenderoth, and M. A. Nitsche, "A technical guide to tDCS, and related non-invasive brain stimulation tools," *Clin. Neurophysiol.*, vol. 127, no. 2, pp. 1031–1048, 2016.
- [44] A. Rahman, B. Lafon, and M. Bikson, "Chapter 2 - Multilevel computational models for predicting the cellular effects of noninvasive brain stimulation," in *Computational Neurostimulation*, vol. 222, S. B. T.-P. in B. R. Bestmann, Ed. Elsevier, 2015, pp. 25–40.
- [45] Y.-Z. Huang, M. Sommer, G. Thickbroom, M. Hamada, A. Pascual-Leonne, W. Paulus, J. Classen, A. V Peterchev, A. Zangen, and Y. Ugawa, "Consensus: New methodologies for brain stimulation," *Brain Stimul.*, vol. 2, no. 1, pp. 2–13, 2009.
- [46] L. Antunes, "TRANSCRANIAL DIRECT CURRENT STIMULATION AND NEUROPLASTICITY," 2015.
- [47] "Marom Bikson in Twitter: Slides from my talk at 2017 Int Brain Stimulation Meeting tDCS and the Folded Active Plastic Brain." [Online]. Available: <https://twitter.com/marombikson/status/849421593138876416>. [Accessed: 15-Aug-2019].
- [48] V. Rawji, M. Ciocca, A. Zacharia, D. Soares, D. Truong, M. Bikson, J. Rothwell, and S. Bestmann, "tDCS changes in motor excitability are specific to orientation of current flow," *Brain Stimul.*, vol. 11, no. 2, pp. 289–298, 2018.
- [49] A. Shinde, F. Munsch, D. Alsop, and G. Schlaug, "Abstract #18: Establishing a dose response for transcranial direct current stimulation," *Brain Stimul. Basic, Transl. Clin. Res. Neuromodulation*, vol. 12, no. 2, p. e7, Mar. 2019.
- [50] M. Bikson, M. Inoue, H. Akiyama, J. K. Deans, J. E. Fox, H. Miyakawa, and J. G. R. Jefferys, "Effects of uniform extracellular DC electric fields on excitability in rat hippocampal slices in vitro," *J. Physiol.*, vol. 557, no. 1, pp. 175–190, May 2004.
- [51] A. Opitz, W. Paulus, S. Will, A. Antunes, and A. Thielscher, "Determinants of the electric field during transcranial direct current stimulation," *Neuroimage*, vol. 109, pp. 140–150, 2015.
- [52] G. Batsikadze, V. Moliadze, W. Paulus, M.-F. Kuo, and M. A. Nitsche, "Partially non-linear stimulation intensity-dependent effects of direct current stimulation on motor cortex excitability in humans," *J. Physiol.*, vol. 591, no. 7, pp. 1987–2000, Apr. 2013.
- [53] M. Bikson, S. Bestmann, and D. Edwards, "Transcranial devices are not playthings," *Nature*, vol. 501, p. 167, Sep. 2013.
- [54] A. Thibaut, S. Wannez, A.-F. Donneau, C. Chatelle, O. Gosseries, M.-A. Bruno, and S. Laureys, "Controlled clinical trial of repeated prefrontal tDCS in patients with chronic minimally conscious state," *Brain Inj.*, vol. 31, no. 4, pp. 466–474, Mar. 2017.
- [55] A. R. Brunoni, J. Amadera, B. Berbel, M. S. Volz, B. G. Rizzerio, and F. Fregni, "A systematic review on reporting and assessment of adverse effects associated with transcranial direct current stimulation," *Int. J. Neuropsychopharmacol.*, vol. 14, no. 8, pp. 1133–1145, Sep. 2011.
- [56] M. Bikson, A. Datta, and M. Elwassif, "Establishing safety limits for transcranial direct current stimulation," *Clin. Neurophysiol.*, vol. 120, no. 6, pp. 1033–1034, Jun. 2009.

- [57] "Neuroelectrics User Manual-P2. Electrodes." [Online]. Available: https://www.neuroelectrics.com/download/NE_UM_P2_EL_1.4_EN.pdf. [Accessed: 16-Aug-2019].
- [58] C. Poreisz, K. Boros, A. Antal, and W. Paulus, "Safety aspects of transcranial direct current stimulation concerning healthy subjects and patients," *Brain Res. Bull.*, vol. 72, no. 4, pp. 208–214, 2007.
- [59] W. Paulus and A. Priori, "Current Methods and Approaches of Noninvasive Direct Current–Based Neuromodulation Techniques BT - Practical Guide to Transcranial Direct Current Stimulation: Principles, Procedures and Applications," H. Knotkova, M. A. Nitsche, M. Bikson, and A. J. Woods, Eds. Cham: Springer International Publishing, 2019, pp. 115–131.
- [60] M. Bikson, B. Paneri, A. Mourdoukoutas, Z. Esmailpour, B. W. Badran, R. Azzam, D. Adair, A. Datta, X. H. Fang, B. Wingeier, D. Chao, M. Alonso-Alonso, K. Lee, H. Knotkova, A. J. Woods, D. Hagedorn, D. Jeffery, J. Giordano, and W. J. Tyler, "Limited output transcranial electrical stimulation (LOTES-2017): Engineering principles, regulatory statutes, and industry standards for wellness, over-the-counter, or prescription devices with low risk," *Brain Stimul.*, vol. 11, no. 1, pp. 134–157, 2018.
- [61] A. Wexler, "A pragmatic analysis of the regulation of consumer transcranial direct current stimulation (TDCS) devices in the United States," *J. Law Biosci.*, vol. 2, no. 3, pp. 669–696, Oct. 2015.
- [62] F. Fregni, M. A. Nitsche, C. K. Loo, A. R. Brunoni, P. Marangolo, J. Leite, S. Carvalho, N. Bolognini, W. Caumo, N. J. Paik, M. Simis, K. Ueda, H. Ekhitari, P. Luu, D. M. Tucker, W. J. Tyler, J. Brunelin, A. Datta, C. H. Juan, G. Venkatasubramanian, P. S. Boggio, and M. Bikson, "Regulatory Considerations for the Clinical and Research Use of Transcranial Direct Current Stimulation (tDCS): review and recommendations from an expert panel," *Clin. Res. Regul. Aff.*, vol. 32, no. 1, pp. 22–35, Mar. 2015.
- [63] V. Q. Walsh, "Ethics and Social Risks in Brain Stimulation," *Brain Stimul. Basic, Transl. Clin. Res. Neuromodulation*, vol. 6, no. 5, pp. 715–717, Sep. 2013.
- [64] "LM134/LM234/LM334 3-Terminal Adjustable Current Sources," 2000. [Online]. Available: www.ti.com. [Accessed: 16-Aug-2019].
- [65] "Products / STARSTIM / STARSTIM R32 - Neuroelectrics." [Online]. Available: <https://www.neuroelectrics.com/products/starstim/starstim-r32/>. [Accessed: 16-Aug-2019].
- [66] "M×N device – Soterix Medical." [Online]. Available: <https://soterixmedical.com/research/hd/mxn>. [Accessed: 16-Aug-2019].
- [67] A. J. Woods, H. Knotkova, A. Riggs, D. Q. Truong, and M. Bikson, "Stimulation Parameters and Their Reporting BT - Practical Guide to Transcranial Direct Current Stimulation: Principles, Procedures and Applications," H. Knotkova, M. A. Nitsche, M. Bikson, and A. J. Woods, Eds. Cham: Springer International Publishing, 2019, pp. 225–231.
- [68] E. M. Caparelli-Daquer, T. J. Zimmermann, E. Mooshagian, L. C. Parra, J. K. Rice, A. Datta, M. Bikson, and E. M. Wassermann, "A pilot study on effects of 4×1 High-Definition tDCS on motor cortex excitability," in *2012 Annual International Conference of the IEEE Engineering in Medicine and Biology Society*, 2012, pp. 735–738.
- [69] "Halo Sport 1 Owner's Guide – Halo Neuroscience." [Online]. Available: <https://support.haloneuro.com/hc/en-us/articles/115009609407-Halo-Sport-1-Owner-s-Guide>. [Accessed: 16-Aug-2019].
- [70] "neuroConn DC-STIMULATOR MOBILE - neuroCare Group." [Online]. Available: <https://www.neurocaregroup.com/dc-stimulator-mobile.html>. [Accessed: 16-Aug-2019].

- [71] “neuroConn DC-STIMULATOR PLUS - neuroCare Group.” [Online]. Available: https://www.neurocaregroup.com/dc_stimulator_plus.html. [Accessed: 16-Aug-2019].
- [72] “neuroConn DC-STIMULATOR MC - neuroCare Group.” [Online]. Available: https://www.neurocaregroup.com/dc_stimulator_mc.html. [Accessed: 16-Aug-2019].
- [73] “Products / STARSTIM / STARSTIM 8 5G - Neuroelectrics.” [Online]. Available: <https://www.neuroelectrics.com/products/starstim/starstim-8/>. [Accessed: 16-Aug-2019].
- [74] “Products - 1x1 tDCS – Soterix Medical.” [Online]. Available: <https://soterixmedical.com/research/support/products?device=1x1tdcs>. [Accessed: 16-Aug-2019].
- [75] U. Palm, K. B. Feichtner, A. Hasan, G. Gauglitz, B. Langguth, M. A. Nitsche, D. Keeser, and F. Padberg, “The Role of Contact Media at the Skin-electrode Interface During Transcranial Direct Current Stimulation (tDCS),” *Brain Stimul. Basic, Transl. Clin. Res. Neuromodulation*, vol. 7, no. 5, pp. 762–764, Sep. 2014.
- [76] P. Minhas, V. Bansal, J. Patel, J. S. Ho, J. Diaz, A. Datta, and M. Bikson, “Electrodes for high-definition transcutaneous DC stimulation for applications in drug delivery and electrotherapy, including tDCS,” *J. Neurosci. Methods*, vol. 190, no. 2, pp. 188–197, 2010.
- [77] J. Marquez, P. van Vliet, P. McElduff, J. Lagopoulos, and M. Parsons, “Transcranial Direct Current Stimulation (tDCS): Does it Have Merit in Stroke Rehabilitation? A Systematic Review,” *Int. J. Stroke*, vol. 10, no. 3, pp. 306–316, Oct. 2013.
- [78] J. Brunelin, M. Mondino, L. Gassab, F. Haesebaert, L. Gaha, M.-F. Suaud-Chagny, M. Saoud, A. Mechri, and E. Poulet, “Examining Transcranial Direct-Current Stimulation (tDCS) as a Treatment for Hallucinations in Schizophrenia,” *Am. J. Psychiatry*, vol. 169, no. 7, pp. 719–724, Jul. 2012.
- [79] S. André, S. Heinrich, F. Kayser, K. Menzler, J. Kesselring, P. H. Khader, J.-P. Lefaucheur, and V. Mylius, “At-home tDCS of the left dorsolateral prefrontal cortex improves visual short-term memory in mild vascular dementia,” *J. Neurol. Sci.*, vol. 369, pp. 185–190, 2016.
- [80] H. Sunwoo, Y.-H. Kim, W. H. Chang, S. Noh, E.-J. Kim, and M.-H. Ko, “Effects of dual transcranial direct current stimulation on post-stroke unilateral visuospatial neglect,” *Neurosci. Lett.*, vol. 554, pp. 94–98, 2013.
- [81] S. Lefebvre, J.-L. Thonnard, P. Laloux, A. Peeters, J. Jamart, and Y. Vandermeeren, “Single Session of Dual-tDCS Transiently Improves Precision Grip and Dexterity of the Paretic Hand After Stroke,” *Neurorehabil. Neural Repair*, vol. 28, no. 2, pp. 100–110, Mar. 2013.
- [82] A. Monti, F. Cogiamanian, S. Marceglia, R. Ferrucci, F. Mameli, S. Mrakic-Sposta, M. Vergari, S. Zago, and A. Priori, “Improved naming after transcranial direct current stimulation in aphasia,” *J. Neurol. Neurosurg. Psychiatry*, vol. 79, no. 4, pp. 451–453, 2008.
- [83] F. C. Hummel and L. G. Cohen, “Non-invasive brain stimulation: a new strategy to improve neurorehabilitation after stroke?,” *Lancet Neurol.*, vol. 5, no. 8, pp. 708–712, 2006.
- [84] M. A. Nitsche and W. Paulus, “Excitability changes induced in the human motor cortex by weak transcranial direct current stimulation,” *J. Physiol.*, vol. 527, no. 3, pp. 633–639, Sep. 2000.
- [85] V. P. Clark, B. A. Coffman, A. R. Mayer, M. P. Weisend, T. D. R. Lane, V. D. Calhoun, E. M. Raybourn, C. M. Garcia, and E. M. Wassermann, “TDCS guided using fMRI significantly accelerates learning to identify concealed objects,” *Neuroimage*, vol. 59, no. 1, pp. 117–128, 2012.

- [86] L. K. McIntire, R. A. McKinley, C. Goodyear, and J. Nelson, "A Comparison of the Effects of Transcranial Direct Current Stimulation and Caffeine on Vigilance and Cognitive Performance During Extended Wakefulness," *Brain Stimul.*, vol. 7, no. 4, pp. 499–507, 2014.
- [87] M. Meinzer, S. Jähnigen, D. A. Copland, R. Darkow, U. Grittner, K. Avirame, A. D. Rodriguez, R. Lindenberg, and A. Flöel, "Transcranial direct current stimulation over multiple days improves learning and maintenance of a novel vocabulary," *Cortex*, vol. 50, pp. 137–147, 2014.
- [88] D. M. Martin, R. Liu, A. Alonzo, M. Green, M. J. Player, P. Sachdev, and C. K. Loo, "Can transcranial direct current stimulation enhance outcomes from cognitive training? A randomized controlled trial in healthy participants," *Int. J. Neuropsychopharmacol.*, vol. 16, no. 9, pp. 1927–1936, Oct. 2013.
- [89] C. A. Dockery, R. Hueckel-Weng, N. Birbaumer, and C. Plewnia, "Enhancement of Planning Ability by Transcranial Direct Current Stimulation," *J. Neurosci.*, vol. 29, no. 22, pp. 7271–7277, 2009.
- [90] W.-S. Kim, K. Lee, S. Kim, S. Cho, and N.-J. Paik, "Transcranial direct current stimulation for the treatment of motor impairment following traumatic brain injury," *J. Neuroeng. Rehabil.*, vol. 16, no. 1, p. 14, 2019.
- [91] H. Knotkova, A. Clayton, M. Stevens, A. Riggs, L. E. Charvet, and M. Bikson, "Home-Based Patient-Delivered Remotely Supervised Transcranial Direct Current Stimulation BT - Practical Guide to Transcranial Direct Current Stimulation: Principles, Procedures and Applications," H. Knotkova, M. A. Nitsche, M. Bikson, and A. J. Woods, Eds. Cham: Springer International Publishing, 2019, pp. 379–405.
- [92] J. P. Dmochowski, A. Datta, M. Bikson, Y. Su, and L. C. Parra, "Optimized multi-electrode stimulation increases focality and intensity at target," *J. Neural Eng.*, vol. 8, no. 4, p. 046011, Aug. 2011.
- [93] P. AU - Schestatsky, L. AU - Morales-Quezada, and F. AU - Fregni, "Simultaneous EEG Monitoring During Transcranial Direct Current Stimulation," *JoVE*, no. 76, p. e50426, 2013.
- [94] Y. Miao and V. J. Koomson, "A CMOS-Based Bidirectional Brain Machine Interface System With Integrated fdNIRS and tDCS for Closed-Loop Brain Stimulation," *IEEE Trans. Biomed. Circuits Syst.*, vol. 12, no. 3, pp. 554–563, 2018.
- [95] "The largest database of peer-reviewed literature - Scopus | Elsevier Solutions." [Online]. Available: <https://www.elsevier.com/solutions/scopus>. [Accessed: 16-Aug-2019].
- [96] J. Vidal and M. Ghovanloo, "Towards a Switched-Capacitor based Stimulator for efficient deep-brain stimulation," in *2010 Annual International Conference of the IEEE Engineering in Medicine and Biology*, 2010, pp. 2927–2930.
- [97] S. G. Ewing, B. Porr, J. Riddell, C. Winter, and A. A. Grace, "SaBer DBS: a fully programmable, rechargeable, bilateral, charge-balanced preclinical microstimulator for long-term neural stimulation," *J. Neurosci. Methods*, vol. 213, no. 2, pp. 228–235, Mar. 2013.
- [98] M. M. Samani, A. Mahnam, and N. Hosseini, "An Arbitrary Waveform Wearable Neuro-stimulator System for Neurophysiology Research on Freely Behaving Animals," *J. Med. Signals Sens.*, vol. 4, no. 2, pp. 94–102, Apr. 2014.
- [99] A. I. Acosta, M. S. Noor, Z. H. T. Kiss, and K. Murari, "A lightweight discrete biphasic current stimulator for rodent deep brain stimulation," in *2015 IEEE Biomedical Circuits and Systems Conference (BioCAS)*, 2015, pp. 1–4.
- [100] G. E. Olafsdottir, W. A. Serdijn, and V. Giagka, "An Energy-Efficient, Inexpensive, Spinal Cord Stimulator with Adaptive Voltage Compliance for Freely Moving Rats," in *2018 40th Annual International Conference of the IEEE Engineering in Medicine and*

- Biology Society (EMBC)*, 2018, pp. 2937–2940.
- [101] J. Simpson and M. Ghovanloo, “An Experimental Study of Voltage, Current, and Charge Controlled Stimulation Front-End Circuitry,” in *2007 IEEE International Symposium on Circuits and Systems*, 2007, pp. 325–328.
- [102] M. N. van Dongen and W. A. Serdijn, “Design of a versatile voltage based output stage for implantable neural stimulators,” in *2010 First IEEE Latin American Symposium on Circuits and Systems (LASCAS)*, 2010, pp. 132–135.
- [103] S. F. Cogan, “Neural Stimulation and Recording Electrodes,” *Annu. Rev. Biomed. Eng.*, vol. 10, no. 1, pp. 275–309, Jul. 2008.
- [104] M. N. van Dongen and W. A. Serdijn, “System Design of Neural Stimulators,” in *Design of Efficient and Safe Neural Stimulators: A Multidisciplinary Approach*, Cham: Springer International Publishing, 2016, pp. 67–78.
- [105] R. Plonsey and R. C. Barr, *Bioelectricity: A quantitative approach*. 2007.
- [106] S. K. Arfin and R. Sarpeshkar, “An Energy-Efficient, Adiabatic Electrode Stimulator With Inductive Energy Recycling and Feedback Current Regulation,” *IEEE Trans. Biomed. Circuits Syst.*, vol. 6, no. 1, pp. 1–14, 2012.
- [107] C. Lin, W. Chen, and M. Ker, “Implantable Stimulator for Epileptic Seizure Suppression With Loading Impedance Adaptability,” *IEEE Trans. Biomed. Circuits Syst.*, vol. 7, no. 2, pp. 196–203, 2013.
- [108] Z. Luo and M. Ker, “A High-Voltage-Tolerant and Power-Efficient Stimulator With Adaptive Power Supply Realized in Low-Voltage CMOS Process for Implantable Biomedical Applications,” *IEEE J. Emerg. Sel. Top. Circuits Syst.*, vol. 8, no. 2, pp. 178–186, 2018.
- [109] A. Urso, V. Giagka, M. Van Dongen, and W. A. Serdijn, “An Ultra High-Frequency 8-Channel Neurostimulator Circuit with 68% Peak Power Efficiency,” *IEEE Trans. Biomed. Circuits Syst.*, p. 1, 2019.
- [110] P. Luo, W. Deng, H. Li, and S. Zhen, “A high energy efficiency PSM/PWM dual-mode for DC-DC converter in portable applications,” in *2009 International Conference on Communications, Circuits and Systems*, 2009, pp. 702–706.
- [111] Z. Liu and H. Lee, “A 100V gate driver with sub-nanosecond-delay capacitive-coupled level shifting and dynamic timing control for ZVS-based synchronous power converters,” in *Proceedings of the IEEE 2013 Custom Integrated Circuits Conference*, 2013, pp. 1–4.
- [112] S. Carrara and K. Iniewski, “Handbook of bioelectronics : directly interfacing electronics and biological systems.” Cambridge University Press, Cambridge, United Kingdom ;, 2015.
- [113] “Products / ELECTRODES / PISTIM - Neuroelectrics.” [Online]. Available: <https://www.neuroelectrics.com/products/electrodes/pistim/>. [Accessed: 18-Oct-2018].
- [114] L. Yang, M. Dai, C. Xu, G. Zhang, W. Li, F. Fu, X. Shi, and X. Dong, “The Frequency Spectral Properties of Electrode-Skin Contact Impedance on Human Head and Its Frequency-Dependent Effects on Frequency-Difference EIT in Stroke Detection from 10Hz to 1MHz,” *PLoS One*, vol. 12, no. 1, pp. 1–21, 2017.
- [115] X. F. Wei and W. M. Grill, “Impedance characteristics of deep brain stimulation electrodes in vitro and in vivo,” *J. Neural Eng.*, vol. 6, no. 4, p. 46008, 2009.
- [116] Y. L. LIU, D. L. LIN, and Y. DER LIN, “SPICE MODEL FOR COMPUTER AIDED DESIGN OF BIOPOTENTIAL AMPLIFIER,” *Biomed. Eng. Appl. Basis Commun.*, vol. 16, no. 03, pp. 151–156, Jun. 2004.
- [117] J. Rosell, J. Colominas, P. Riu, R. Pallas-Areny, and J. G. Webster, “Skin impedance from 1 Hz to 1 MHz,” *IEEE Trans. Biomed. Eng.*, vol. 35, no. 8, pp. 649–651, 1988.
- [118] Y. M. Chi, T. Jung, and G. Cauwenberghs, “Dry-Contact and Noncontact Biopotential

- Electrodes: Methodological Review," *IEEE Rev. Biomed. Eng.*, vol. 3, pp. 106–119, 2010.
- [119] D. Dobrev and I. Daskalov, "Two-electrode biopotential amplifier with current-driven inputs," *Med. Biol. Eng. Comput.*, vol. 40, no. 1, pp. 122–127, 2002.
- [120] "MATLAB - MathWorks - MATLAB & Simulink." [Online]. Available: <https://nl.mathworks.com/products/matlab.html>. [Accessed: 24-Aug-2019].
- [121] "Solve nonlinear least-squares (nonlinear data-fitting) problems - MATLAB Isqnonlin - MathWorks Benelux." [Online]. Available: <https://nl.mathworks.com/help/optim/ug/Isqnonlin.html>. [Accessed: 18-Oct-2018].
- [122] F. Carvalho, A. P. Brietzke, A. Gasparin, F. P. dos Santos, R. Vercelino, R. F. Ballester, P. R. S. Sanches, D. P. da Silva Jr, I. L. S. Torres, F. Fregni, and W. Caumo, "Home-Based Transcranial Direct Current Stimulation Device Development: An Updated Protocol Used at Home in Healthy Subjects and Fibromyalgia Patients," *JoVE*, no. 137, p. e57614, 2018.
- [123] A. F. DaSilva, M. S. Volz, M. Bikson, and F. Fregni, "Electrode Positioning and Montage in Transcranial Direct Current Stimulation," *JoVE*, no. 51, p. e2744, 2011.
- [124] M. Wens and M. Steyaert, *Design and Implementation of Fully-Integrated Inductive DC-DC Converters in Standard CMOS*. Springer Netherlands, 2013.
- [125] R. W. Erickson and D. Maksimovic, *Fundamentals of Power Electronics*. Springer US, 2001.
- [126] H. Fan, "Design tips for an efficient non-inverting buck-boost converter." [Online]. Available: <http://www.ti.com/lit/an/slyt584/slyt584.pdf>. [Accessed: 18-Oct-2018].
- [127] K. L. Kilgore and N. Bhadra, "Reversible nerve conduction block using kilohertz frequency alternating current," *Neuromodulation*, vol. 17, no. 3, pp. 242–255, Apr. 2014.
- [128] "Natural and Step Responses of RLC Circuits: The Natural Response of a Parallel RLC Circuit." [Online]. Available: http://www.ee.nthu.edu.tw/~sdyang/Courses/Circuits/Ch08_Std.pdf. [Accessed: 18-Oct-2018].
- [129] "Natural and Step Response of Series and Parallel RLC Circuits (Second-order Circuits)." [Online]. Available: https://www.ius.edu.ba/sites/default/files/u772/ch8_rlc.pdf. [Accessed: 02-Sep-2019].
- [130] E. Babaei and H. M. Maheri, "Investigation of Buck-boost DC-DC Converter Operation in Discontinuous Conduction Mode (DCM) and the Effect of Converter Elements on Output Response Using a Mathematical Model Based on Laplace and Z-Transforms," *Electr. Power Components Syst. TA - TT -*, vol. 43, no. 13, pp. 1509–1522, 2015.
- [131] "Arduino Due." [Online]. Available: <https://store.arduino.cc/arduino-due>. [Accessed: 28-Nov-2018].
- [132] ChaseRLewis73003, "Fast PWM Frequency Due." [Online]. Available: <http://forum.arduino.cc/index.php?topic=280241.0>. [Accessed: 26-Nov-2018].
- [133] L. Joseph and R. J. Butera, "High Frequency Stimulation Selectively Blocks Different Types of Fibers in Frog Sciatic Nerve," *Ieee Trans. Neural Syst. Rehabil. Eng.*, vol. 19, no. 5, pp. 550–557, Oct. 2011.
- [134] N. Bhadra and K. L. Kilgore, "Chapter 10 - Fundamentals of Kilohertz Frequency Alternating Current Nerve Conduction Block of the Peripheral Nervous System," in *Neuromodulation (Second Edition)*, Second Edi., E. S. Krames, P. H. Peckham, and A. R. Rezai, Eds. Academic Press, 2018, pp. 111–120.
- [135] K. L. Kilgore and N. Bhadra, "Nerve conduction block utilising high-frequency alternating current," *Med. Biol. Eng. Comput.*, vol. 42, no. 3, pp. 394–406, 2004.

Appendix

A. Matlab code

```
%%%%%%%%%%%%%%%%%%%%%%%%%%%%%%%%%%%%%%%%%%%%%%%%%%%%%%%%%%%%%%%%%%%%%%%%%%  
%  
%%Electrode-tissue impedance model optimization  
%%%%%%%%%%%%%%%%%%%%%%%%%%%%%%%%%%%%%%%%%%%%%%%%%%%%%%%%%%%%%%%%%%%%%%%%%%  
%  
  
%% Frequencies  
ff1=[1.00E+01  
2.00E+01  
5.00E+01  
1.00E+02  
2.50E+02  
5.00E+02  
1.00E+03  
2.80E+03  
5.00E+03  
1.00E+04  
2.00E+04  
5.00E+04  
1.00E+05  
2.00E+05  
5.00E+05  
1.00E+06  
];  
ff=log(ff1);  
%% Real impedances  
Z11=[3.50E+04  
3.00E+04  
2.50E+04  
2.00E+04  
1.00E+04  
4.50E+03  
2.50E+03  
1.00E+03  
5.80E+02  
3.80E+02  
2.60E+02  
2.00E+02  
1.80E+02  
1.70E+02  
1.40E+02  
1.35E+02  
];  
Z1=log(Z11);  
%% Imaginary impedances  
Z22=[5.00E+03  
8.00E+03  
1.20E+04  
1.30E+04  
1.00E+04  
8.00E+03  
5.00E+03
```

```

2.80E+03
1.50E+03
8.00E+02
5.00E+02
2.00E+02
1.10E+02
6.50E+01
3.00E+01
1.30E+01
];
Z2=log(Z22);
%% f contains the equations of the real and imaginary part
f=@(x)nonlin(x,ff,Z1,Z2);
%% initial values of R and C for optimization
RR=logspace(2,5,20);
CC=logspace(-8,-7,20);
%% least squares optimization
k=0;
for i=1:20
    for j=1:20
        opt_x=lsqnonlin(f,[RR(i);CC(j)],[100;10^-8],[100000;10^-7]);
        k=k+1;
        a(k,1)=RR(i);
        a(k,2)=CC(j);
        a(k,3)=opt_x(1,1);
        a(k,4)=opt_x(2,1);
    end
end
%% Comparison between the model and the measurements
for i=1:400
    subplot(1,2,1)
    loglog(ff1,135+abs(a(i,3))./(1+(ff1.*abs(a(i,3)).*abs(a(i,4))).^2))
    hold on
    loglog(ff1,Z11)
    xlabel('Frequency (Hz)')
    ylabel('Real part Impedance (Ohm)')
    subplot(1,2,2)
    loglog(ff1,(ff1.*(abs(a(i,3)).^2)*abs(a(i,4)))./(1+(ff1.*abs(a(i,3)).*abs(a(i,4))).^2))
    hold on
    loglog(ff1,Z22)
    xlabel('Frequency (Hz)')
    ylabel('Imaginary part Impedance (Ohm)')
    waitforbuttonpress
    close all
end
%% solutions' space
scatter(a(:,3),a(:,4))
xlabel('Resistance (Ohm)')
ylabel('Capacitance (F)')
%%%%%%%%%%%%%%%%%%%%%%%%%%%%%%%%%%%%%%%%%%%%%%%%%%%%%%%%%%%%%%%%%%%%%%%%
%

function y = nonlin(x,ff,Z1,Z2)
% This equation calculates the real and imaginary part of the RC model
% x(1)=Rf
% x(2)=Cdl
% Z1= real part measurements
% Z2= imaginary part measurements
y=[Z1-log(135+x(1))./(1+(exp(ff).*x(1).*x(2)).^2));Z2-
log((exp(ff).*x(1).^2)*x(2))./(1+(exp(ff).*x(1).*x(2)).^2))];

```

```

end
%%%%%%%%%%%%%%%%%%%%%%%%%%%%%%%%%%%%%%%%%%%%%%%%%%%%%%%%%%%%%%%%%%%%%%%%
%

%%%%%%%%%%%%%%%%%%%%%%%%%%%%%%%%%%%%%%%%%%%%%%%%%%%%%%%%%%%%%%%%%%%%%%%%
%
%% Plot of the inductor's current
%%%%%%%%%%%%%%%%%%%%%%%%%%%%%%%%%%%%%%%%%%%%%%%%%%%%%%%%%%%%%%%%%%%%%%%%
%

R=10000;
L=175*10^-6;
C=10^-9;
%% Simulation time
t=linspace(0,10*10^-6,10000);
%% Initial inductor's current
I0=-100*10^-3;
%% Neper frequency
a=1/(2*R*C);
%% Natural frequency
w0=1/sqrt(L*C);
%% Damped frequency
wd=sqrt(w0^2-a^2);
%% Inductor's current equation
eq=-(I0./(L.*C.*wd)).*(exp(-a.*t)./(a^2+wd^2)).*(-a*sin(wd.*t)-
wd.*cos(wd.*t));
%% Plot of the inductor's current
plot(t,eq)
%%%%%%%%%%%%%%%%%%%%%%%%%%%%%%%%%%%%%%%%%%%%%%%%%%%%%%%%%%%%%%%%%%%%%%%%
%

%%%%%%%%%%%%%%%%%%%%%%%%%%%%%%%%%%%%%%%%%%%%%%%%%%%%%%%%%%%%%%%%%%%%%%%%
%
%% Find maximum capacitance for maximum discharging time
%%%%%%%%%%%%%%%%%%%%%%%%%%%%%%%%%%%%%%%%%%%%%%%%%%%%%%%%%%%%%%%%%%%%%%%%
%

R=10000;
L=175*10^-6;
syms C
%% Maximum discharging time of the inductor
t=5*10^-6;
%% Initial inductor's current
I0=-100*10^-3;
%% Neper frequency
a=1/(2*R*C);
%% Natural frequency
w0=1/sqrt(L*C);
%% Damped frequency
wd=sqrt(w0^2-a^2);
%% Inductor's current equation
eq=-(I0./(L.*C.*wd)).*(exp(-a.*t)./(a^2+wd^2)).*(-a*sin(wd.*t)-
wd.*cos(wd.*t));
A=solve(eq==0,C);
%% Maximum capacitance
disp(double(real(A)))
%%%%%%%%%%%%%%%%%%%%%%%%%%%%%%%%%%%%%%%%%%%%%%%%%%%%%%%%%%%%%%%%%%%%%%%%
%

```

B. Components' List

Inductors
WURTH ELEKTRONIK - Surface Mount High Frequency Inductor, WE-GFH Series, 180 μ H, 220 mA, 1812 [4532 Metric], Wirewound
SRR1260A-180M - Fixed Inductors 18uH 20% SMD 1260 AEC-Q200
Diodes
BAS70-04-E3-08 - Small Signal Schottky Diode, Dual, 70 V, 150 mA, 1 V, 600 mA, 125 °C
BZX85C20-TAP - Zener Single Diode, 20 V, 1.3 W, DO-41 (DO-204AL), 5 %, 2 Pins, 175 °C
DZ2W24000L - Zener Diodes 24V 5% 1W 10mA FLT LD 1.6mm x 3.5mm
MOSFETs
RUC002N05HZGT116 - MOSFET Transistor, N Channel, 200 mA, 50 V, 1.6 Ω , 4.5 V, 1 V
BSS84AKS - Dual MOSFET, Dual P Channel, -160 mA, -50 V, 4.5 Ω , -10 V, -1.6 V
Drivers
LM5111-1MX/NOPB - MOSFET Driver, Low Side, 3.5 V to 14 V Supply, 5 A Out, 25 ns Delay, SOIC-8
Opamps
AD8616ARZ - Operational Amplifier, Dual, 2 Amplifier, 24 MHz, 12 V/ μ s, 2.7V to 5V, SOIC, 8 Pins
LTC6702ITS8#TRMPBF - Analog Comparators Low Voltage, uPower Dual Comparator
LTC6255CS6#TRMPBF - Precision Amplifiers 6.5MHz, 65 A Pwr Eff R2R I/O Op Amps
DACs
LTC1662IMS8#PBF - Digital to Analog Converters - DAC Ultralow Pwr, 2x 10-B DAC in MS
Voltage references
LT6656BCS6-2.5#TRMPBF - Voltage References 1uA Precision SOT-23 Reference 20ppm, 0.1%
PWM controllers
LTC6992CS6-4#TRMPBF - Switching Controllers PWM with 5% to 100% Pulse Width Control
Charge pumps
LTC1517ES5-5#TRMPBF
Capacitors
10 uF 50 V (SMD)
10 uF 20 V (SMD)
6.8 uF 20 V (SMD)
6.8 uF 50 V (SMD)
3.3 uF 20 V (SMD)
3.3 uF 50 V (SMD)
1 uF 50 V (SMD)
1 uF 16 V (SMD)
0.47 uF 50 V (SMD)
0.1 uF 50 V (SMD)
0.1 uF 16 V (SMD)
10 nF 50 V (SMD)
47 nF 50 V (SMD)
1 uF 20 V (leaded)
0.1 uF 20 V (leaded)

30 nF 50 V (leaded)
35 nF 50 V (leaded)
40 nF 50 V (leaded)
45 nF 50 V (leaded)
50 nF 50 V (leaded)
100 pF 20V (leaded)
Resistors
49.9K OHM 1% Thick Film Resistors (SMD)
7.5K ohm 1% 0.75W AEC-Q200 (SMD)
Thick Film Resistors - CRGP 2512 100R 1% SMD Resistor
Thick Film Resistors - SMD CRGP 2512 1K0 1% SMD Resistor
Thick Film Resistors - SMD 3521 6K2 1% 2W
10 Ω 1% 125 mW (through hole)
1 k Ω 1% 125 mW (through hole)
10 k Ω 1% 125 mW (through hole)
75 k Ω 1% 125 mW (through hole)
1 M Ω 1% 125 mW (through hole)
Thick Film Resistors - SMD 2010 9.1Kohms 5% AEC-Q200
Thick Film Resistors - SMD 2010 6.04Kohms 1% AEC-Q200
Thick Film Resistors - SMD 3/4watt 49.9Kohms 1%
Microcontrollers
A000062 - Development Board, Arduino Due, AT91SAM3X8E MCU, 54 3.3V I/O, 12 Analogue Inputs, With Headers
Connectors
RE899 - IC Adapter, Fiberglass, SOIC/SOP-8, 2.54mm Pitch Spacing, 7.62mm Row Pitch
808-AG11D-ESL-LF - IC & Component Socket, 8 Contacts, DIP Socket, 2.54 mm, 800 Series, 7.62 mm, Copper Alloy
RE910 - IC Adapter, Fiberglass, 6-SOT-23, 2.54mm Pitch Spacing, 7.62mm Row Pitch
2-1571551-1 - IC & Component Socket, 6 Contacts, DIP Socket, 2.54 mm, 7.62 mm, Beryllium Copper
Boards
RE220-LFDS - Labor Card, FR4, Epoxy Glass Composite, 1.5mm, 100mm x 160mm
Headers
SSW-102-01-G-D
TSW-110-05-G-S
TSW-118-05-G-D
TSW-101-07-L-S
SSW-108-01-T-D
TSW-108-05-G-S
TSW-110-05-G-S
SSW-113-01-G-D
TSW-113-14-G-D
SSW-113-01-T-D
TSW-101-14-G-S
TSW-102-14-G-D
TSW-113-14-T-D
Arduino accessories

USB type A to micro USB Type B cable
Logic gates
SN74LVC1G08DBVTG4 - 2 input AND
SN74LVC1G32DBVR - 2 input OR
SN74LVC1G11DCKR - 3 input AND
SN74LVC1G02DCKR - 2 input NOR
SN74LVC1G14QDCKRQ1 - Inverters Sngl Schmitt-Trigger Inverter
SN74LVC1G02DBVR - 2 input NOR
SN74LVC1G132DBVT - 2 input NAND
SN74LVC1G10DCKR - 3 input NAND
CD74AC109M96 - Flip-Flops Dual
DS1100LZ-100+ - Delay Lines/Timing Elements 3V 5-Tap Delay Line
SN74AUP3G34DCUR - Buffers & Line Drivers Low-Power Triple Buffer Gate
SN74LVC1G17DBVRG4 - Buffers & Line Drivers Single Schmitt-Trgr
SN74LVC1G332DCKR - 3 input OR
SN74LV21ADR - 4 input AND

C. MCU Code

Prototype 1

```
#include "Arduino.h"

const int freq1 = 21000000;
const int freq2 = 21000000;
const int pin = 6;
const int minfreq1 = 641;
float DCC=0.50;

//Function that creates PWM waveforms at the selected pins adjusting their frequency and
//their
//duty cycle
void SetPinFrequency(int pin,int frequency,int clock, float DC)
{
    //Configure Pin
    PIO_Configure(g_APinDescription[pin].pPort,
    g_APinDescription[pin].ulPinType,
    g_APinDescription[pin].ulPin,
    g_APinDescription[pin].ulPinConfiguration);
    //Set Pin to count off CLKA set at freq1
    int chan = g_APinDescription[pin].ulPWMChannel;
    int clk = clock == 1 ? PWM_CMR_CPRE_CLKA : PWM_CMR_CPRE_CLKB;
    PWMC_ConfigureChannel(PWM_INTERFACE,chan,clk,0,0);
    int divider = 42000000/frequency;
    PWMC_SetPeriod(PWM_INTERFACE,chan,divider);
    int Duty=round(float(divider)*DC);
    PWMC_SetDutyCycle(PWM_INTERFACE,chan,Duty);
    PWMC_EnableChannel(PWM_INTERFACE,chan);
}

void setup()
```

```

{
  Serial.begin(9600);
  // set pins
  pinMode(6,OUTPUT);
  pinMode(7,OUTPUT);
  pinMode(8,OUTPUT);
  analogWriteResolution(12);
  pmc_enable_periph_clk(PWM_INTERFACE_ID);
  //Configure Clocks
  PWMC_ConfigureClocks(freq1,freq2,2*freq1);
  // pin 6 delivers PWM signal
  SetPinFrequency(6,100000,0,DCC);
  // pin 7 delivers logic low signal
  digitalWrite(7, LOW);
  // pin 8 delivers logic high signal
  digitalWrite(8, HIGH);
}

void loop()
{
  // read the input on analog pin A1
  int sensorValue = analogRead(A1);
  // Convert the analog reading (which goes from 0 - 1023) to a current (0 - 3.3 V/sense
  // resistance/opamp's gain*1000) in mA
  float current = sensorValue * (3.3 / 1023.0/12.0/71*1000);
  // print out the current you read:
  Serial.println(current);
  delay(3000);
  //reads from the user the desired current and it translates it to the duty cycle that must be
  //used
  //for the buck - boost converter.
  float Desired_Current=0; //in mA
  if (Serial.available() >0) {

```

```

if (Serial.peek() == 'c') {
    Serial.read();
    Desired_Current=Serial.parseFloat();
    float DCC_new = DCC *(Desired_Current/current);
    Serial.println(DCC_new);
    pmc_enable_periph_clk(PWM_INTERFACE_ID);
    PWMC_ConfigureClocks(freq1,freq2,2*freq1);
    SetPinFrequency(6,100000,0,DCC_new);
    DCC=DCC_new;
}
}
while (Serial.available() >0) {
    Serial.read();
}
}

```

Prototype 2

```

//sets the code for the DAC
int value=100;

void setup()
{
    //sets if a boost or buck-boost converter will be used
    pinMode(22, OUTPUT);
    // sets if a boost or buck-boost converter will be used
    pinMode(24, OUTPUT);
    // sets if a boost or buck-boost converter will be used
    pinMode(26, OUTPUT);
    // sets the first nmos of the h bridge
    pinMode(28, OUTPUT);
    // sets the second nmos of the h bridge
    pinMode(30, OUTPUT);
    // sets is the high side drivers will be charged
    pinMode(32, OUTPUT);
    // sets the first pmos of the h bridge
    pinMode(34, OUTPUT);
    // sets the second pmos of the h bridge
    pinMode(36, OUTPUT);
    // sets the resolution of the DAC
    analogWriteResolution(12);
}

```

```

    analogWrite(DAC1, value );
// charging phase of the high side drivers
digitalWrite(22, HIGH);
digitalWrite(24, LOW);
digitalWrite(30, LOW);
digitalWrite(34, LOW);
digitalWrite(26, LOW);
digitalWrite(28, LOW);
digitalWrite(32, HIGH);
digitalWrite(36, LOW);
// end of charging phase and polarity select
delayMicroseconds(250);
digitalWrite(28, HIGH);
digitalWrite(32, LOW);
digitalWrite(36, HIGH);
// start of stimulation
delayMicroseconds(3000);
digitalWrite(26, HIGH);
}

void loop()
{

}

```

Prototype 3

```

#define DATA_PIN 11
#define CLOCK_PIN 12
#define LOAD8_PIN 3
#define LOAD7_PIN 4
#define LOAD6_PIN 5
#define LOAD5_PIN 6
#define LOAD4_PIN 7
#define LOAD3_PIN 8
#define LOAD2_PIN 9
#define LOAD1_PIN 10
#define Ch1 13
#define Ch2 22
#define Ch4 23
#define Ch8 24
#define NMOS_Ch1 41
#define NMOS_Ch2 40
#define NMOS_Ch3 39
#define NMOS_Ch4 38
#define NMOS_Ch5 37
#define NMOS_Ch6 36
#define NMOS_Ch7 35
#define NMOS_Ch8 34
#define PMOS_source_Ch1 49
#define PMOS_source_Ch2 48

```

```
#define PMOS_source_Ch3 47
#define PMOS_source_Ch4 46
#define PMOS_source_Ch5 45
#define PMOS_source_Ch6 44
#define PMOS_source_Ch7 43
#define PMOS_source_Ch8 42
#define ENBoost 50
#define EN_channel 51
```

```
int da;
int db;
int dc;
int dd;
int de;
int df;
int dg;
int dh;
int order;
int na;
int nb;
int nc;
int nd;
int ne;
int nf;
int ng;
int nh;
int pa;
int pb;
int pc;
int pd;
int pe;
int pf;
int pg;
int ph;
int ma;
```

```
void setup()
{
  Serial.begin(9600);
  pinMode(DATA_PIN, OUTPUT);
  pinMode(LOAD1_PIN, OUTPUT);
  digitalWrite(LOAD1_PIN, HIGH);
  pinMode(LOAD2_PIN, OUTPUT);
  digitalWrite(LOAD2_PIN, HIGH);
  pinMode(LOAD3_PIN, OUTPUT);
  digitalWrite(LOAD3_PIN, HIGH);
  pinMode(LOAD4_PIN, OUTPUT);
  digitalWrite(LOAD4_PIN, HIGH);
  pinMode(LOAD5_PIN, OUTPUT);
  digitalWrite(LOAD5_PIN, HIGH);
```

```
pinMode(LOAD6_PIN, OUTPUT);
digitalWrite(LOAD6_PIN, HIGH);
pinMode(LOAD7_PIN, OUTPUT);
digitalWrite(LOAD7_PIN, HIGH);
pinMode(LOAD8_PIN, OUTPUT);
digitalWrite(LOAD8_PIN, HIGH);
pinMode(CLOCK_PIN, OUTPUT);
digitalWrite(CLOCK_PIN, LOW);
```

```
pinMode(Ch1, OUTPUT);
pinMode(Ch2, OUTPUT);
pinMode(Ch4, OUTPUT);
pinMode(Ch8, OUTPUT);
pinMode(NMOS_Ch1, OUTPUT);
pinMode(NMOS_Ch2, OUTPUT);
pinMode(NMOS_Ch3, OUTPUT);
pinMode(NMOS_Ch4, OUTPUT);
pinMode(NMOS_Ch5, OUTPUT);
pinMode(NMOS_Ch6, OUTPUT);
pinMode(NMOS_Ch7, OUTPUT);
pinMode(NMOS_Ch8, OUTPUT);
pinMode(PMOS_source_Ch1, OUTPUT);
pinMode(PMOS_source_Ch2, OUTPUT);
pinMode(PMOS_source_Ch3, OUTPUT);
pinMode(PMOS_source_Ch4, OUTPUT);
pinMode(PMOS_source_Ch5, OUTPUT);
pinMode(PMOS_source_Ch6, OUTPUT);
pinMode(PMOS_source_Ch7, OUTPUT);
pinMode(PMOS_source_Ch8, OUTPUT);
pinMode(ENBoost, OUTPUT);
digitalWrite(ENBoost,LOW);
pinMode(EN_channel, OUTPUT);
digitalWrite(EN_channel,LOW);
```

```
digitalWrite(Ch8, LOW);
digitalWrite(Ch4, LOW);
digitalWrite(Ch2, LOW);
digitalWrite(Ch1, LOW);
```

```
digitalWrite(NMOS_Ch1, HIGH);
digitalWrite(NMOS_Ch2, HIGH);
digitalWrite(NMOS_Ch3, HIGH);
digitalWrite(NMOS_Ch4, HIGH);
digitalWrite(NMOS_Ch5, HIGH);
digitalWrite(NMOS_Ch6, HIGH);
digitalWrite(NMOS_Ch7, HIGH);
digitalWrite(NMOS_Ch8, HIGH);
digitalWrite(PMOS_source_Ch1, HIGH);
digitalWrite(PMOS_source_Ch2, HIGH);
```

```

digitalWrite(PMOS_source_Ch3, HIGH);
digitalWrite(PMOS_source_Ch4, HIGH);
digitalWrite(PMOS_source_Ch5, HIGH);
digitalWrite(PMOS_source_Ch6, HIGH);
digitalWrite(PMOS_source_Ch7, HIGH);
digitalWrite(PMOS_source_Ch8, HIGH);

delay(10000);

digitalWrite(PMOS_source_Ch1, LOW);
digitalWrite(PMOS_source_Ch2, LOW);
digitalWrite(PMOS_source_Ch3, LOW);
digitalWrite(PMOS_source_Ch4, LOW);
digitalWrite(PMOS_source_Ch5, LOW);
digitalWrite(PMOS_source_Ch6, LOW);
digitalWrite(PMOS_source_Ch7, LOW);
digitalWrite(PMOS_source_Ch8, LOW);

digitalWrite(Ch1, HIGH);
digitalWrite(EN_channel, HIGH);
//delayMicroseconds(1000000);
//
//digitalWrite(ENBoost, HIGH);

delay(100);
updateDAC1('X',0);
delay(100);
updateDAC2('X',0);
delay(100);
updateDAC3('X',0);
delay(100);
updateDAC4('X',0);
delay(100);
updateDAC5('X',0);
delay(100);
updateDAC6('X',0);
delay(100);
updateDAC7('X',0);
delay(100);
updateDAC8('X',0);
delay(100);

Serial.println("Initial settings");
Serial.println("*****");
Serial.println("*****");
Serial.println("*****");
Serial.println("Number of channels: 1");
Serial.println("DC/DC converter: Buck-boost");
Serial.println("All channels' polarity: Positive");
Serial.println("DAC 'a'-'h' codes: 0");
Serial.println("The capacitors of all the high-side drivers have been charged for 10s.");

```

```

Serial.println("*****
*****
*****");
Serial.println(" ");
Serial.println("*****
*****
*****");
Serial.println("*****
*****
*****");
Serial.println("Dear user,");
Serial.println(" ");
Serial.println("Welcome to the Effipulse stimulator's user interface.");
Serial.println("The channels have been symbolized from 'a' for the first channel to 'h' for the
eighth channel using ascending order.");
Serial.println("The following are the available commands that exist in the static memory of
the MCU.");
Serial.println("'bd': Buck-boost converter is chosen as the used DC/DC converter.");
Serial.println("'be': Boost converter is chosen as the used DC/DC converter.");
Serial.println("'da#-'dh#': Sets the value for the output of each DAC ('a' for the first channel
until 'h' for the 8th channel). Where #, place a number value from 0 to 1023, which is the
code that the DAC reads.");
Serial.println("'ca'-'cd': Selects if one ('ca'), two, four or eight ('cd') channels are used.");
Serial.println("'na#-'nh#': Selects for each channel the polarity that will be used, where # is 1
for the default polarity and 2 for the reverse polarity.");
Serial.println("!!!WARNING!!!");
Serial.println("Please be sure that before using the 'pa#-'ph#' and 'ma#' orders, the buck-
boost converter ('bd')and the 1 channel ('ca') mode must be chosen, as also all the DACs
must have zero value ('da0','db0', ..., 'dh0').");
Serial.println("If the previous line is not followed there might be risk for damaging the
device, as also the load in its outputs.");
Serial.println("!!!WARNING!!!");
Serial.println("'pa#-'ph#': Charges the high-side driver's capacitors for each channel, where
# are the milliseconds that the charging takes place.");
Serial.println("'ma#': Charges the high-side driver's capacitors for all channels, where # are
the milliseconds that the charging takes place.");
Serial.println("'in': Opens the instructions.");
Serial.println("In order to use the aforementioned commands, please open the serial
monitor window.");
Serial.println("Then type the two-digit code for each command you want to execute and the
preferred number, if it is applicable, right after the code without using space.");
Serial.println("Then press enter");
Serial.println("The device works without resetting it.");
Serial.println("!!!WARNING!!!");
Serial.println("In case of resetting the MCU, there might be risk for damaging the device, as
also the load in its outputs.");
Serial.println("!!!WARNING!!!");
Serial.println(" ");
Serial.println("Thank you for your time reading the instructions.");

```

```

Serial.println("*****");
Serial.println("*****");
Serial.println("*****");
Serial.println(" ");
Serial.println("Start");
Serial.println(" ");
}

```

```

void updateDAC1(int XYZ, int val) //val should be 0-1023
{
  byte data1 = 0;
  byte data2 = 0;

  byte first = 0;
  byte mid = 0;

  if(val > 255)
    mid = B00000100;
  if(val > 511)
    mid = B00001000;
  if(val > 767)
    mid = B00001100;

  if(XYZ == 'X' || XYZ == 'x') //Updates Analog Output A
    first = B10010000; //data1= '10010000' First 4 bits are "Command Code"

  if(XYZ == 'Y' || XYZ == 'y') //Updates Analog Output B
    first = B10100000; // sets first four bits to 1010

  if(XYZ == 'Z' || XYZ == 'z') //Updates Analog Output A & B to same value
    first = B11110000; // sets first four bits to 1111

  data1 = first + mid + (byte(val) >> 6);
  data2 = byte(val) << 2;
  digitalWrite(LOAD1_PIN, LOW);
  shiftOut1(DATA_PIN, CLOCK_PIN, MSBFIRST, data1);
  shiftOut1(DATA_PIN, CLOCK_PIN, MSBFIRST, data2);
  digitalWrite(LOAD1_PIN, HIGH);
}

```

```

void updateDAC2(int XYZ, int val) //val should be 0-1023
{
  byte data1 = 0;
  byte data2 = 0;

  byte first = 0;
  byte mid = 0;

```

```

if(val>255)
    mid = B00000100;
if(val>511)
    mid = B00001000;
if(val>767)
    mid = B00001100;

if(XYZ == 'X' || XYZ == 'x') //Updates Analog Output A
    first = B10010000; //data1= '10010000' First 4 bits are "Command Code"

if(XYZ == 'Y' || XYZ == 'y') //Updates Analog Output B
    first = B10100000; // sets first four bits to 1010

if(XYZ == 'Z' || XYZ == 'z') //Updates Analog Output A & B to same value
    first = B11110000; // sets first four bits to 1111

data1 = first + mid + (byte(val)>>6);
data2 = byte(val) << 2;

digitalWrite(Load2_PIN, LOW);
shiftOut1(DATA_PIN, CLOCK_PIN, MSBFIRST, data1);
shiftOut1(DATA_PIN, CLOCK_PIN, MSBFIRST, data2);
digitalWrite(Load2_PIN, HIGH);
}
void updateDAC3(int XYZ, int val) //val should be 0-1023
{
    byte data1 = 0;
    byte data2 = 0;

    byte first = 0;
    byte mid = 0;

    if(val>255)
        mid = B00000100;
    if(val>511)
        mid = B00001000;
    if(val>767)
        mid = B00001100;

    if(XYZ == 'X' || XYZ == 'x') //Updates Analog Output A
        first = B10010000; //data1= '10010000' First 4 bits are "Command Code"

    if(XYZ == 'Y' || XYZ == 'y') //Updates Analog Output B
        first = B10100000; // sets first four bits to 1010

    if(XYZ == 'Z' || XYZ == 'z') //Updates Analog Output A & B to same value
        first = B11110000; // sets first four bits to 1111

    data1 = first + mid + (byte(val)>>6);

```

```

data2 = byte(val) << 2;

digitalWrite(LOAD3_PIN, LOW);
shiftOut1(DATA_PIN, CLOCK_PIN, MSBFIRST, data1);
shiftOut1(DATA_PIN, CLOCK_PIN, MSBFIRST, data2);
digitalWrite(LOAD3_PIN, HIGH);
}
void updateDAC4(int XYZ, int val) //val should be 0-1023
{
  byte data1 = 0;
  byte data2 = 0;

  byte first =0;
  byte mid = 0;

  if(val>255)
    mid = B00000100;
  if(val>511)
    mid = B00001000;
  if(val>767)
    mid = B00001100;

  if(XYZ == 'X' || XYZ == 'x') //Updates Analog Output A
    first = B10010000; //data1= '10010000' First 4 bits are "Command Code"

  if(XYZ == 'Y' || XYZ == 'y') //Updates Analog Output B
    first = B10100000; // sets first four bits to 1010

  if(XYZ == 'Z' || XYZ == 'z') //Updates Analog Output A & B to same value
    first = B11110000; // sets first four bits to 1111

  data1 = first + mid + (byte(val)>>6);
  data2 = byte(val) << 2;

  digitalWrite(LOAD4_PIN, LOW);
  shiftOut1(DATA_PIN, CLOCK_PIN, MSBFIRST, data1);
  shiftOut1(DATA_PIN, CLOCK_PIN, MSBFIRST, data2);
  digitalWrite(LOAD4_PIN, HIGH);
}
void updateDAC5(int XYZ, int val) //val should be 0-1023
{
  byte data1 = 0;
  byte data2 = 0;

  byte first =0;
  byte mid = 0;

  if(val>255)
    mid = B00000100;
  if(val>511)

```

```

    mid = B00001000;
if(val>767)
    mid = B00001100;

if(XYZ == 'X' || XYZ == 'x') //Updates Analog Output A
    first = B10010000; //data1= '10010000' First 4 bits are "Command Code"

if(XYZ == 'Y' || XYZ == 'y') //Updates Analog Output B
    first = B10100000; // sets first four bits to 1010

if(XYZ == 'Z' || XYZ == 'z') //Updates Analog Output A & B to same value
    first = B11110000; // sets first four bits to 1111

data1 = first + mid + (byte(val)>>6);
data2 = byte(val) << 2;

digitalWrite(Load5_PIN, LOW);
shiftOut1(DATA_PIN, CLOCK_PIN, MSBFIRST, data1);
shiftOut1(DATA_PIN, CLOCK_PIN, MSBFIRST, data2);
digitalWrite(Load5_PIN, HIGH);
}
void updateDAC6(int XYZ, int val) //val should be 0-1023
{
    byte data1 = 0;
    byte data2 = 0;

    byte first = 0;
    byte mid = 0;

    if(val>255)
        mid = B00000100;
    if(val>511)
        mid = B00001000;
    if(val>767)
        mid = B00001100;

    if(XYZ == 'X' || XYZ == 'x') //Updates Analog Output A
        first = B10010000; //data1= '10010000' First 4 bits are "Command Code"

    if(XYZ == 'Y' || XYZ == 'y') //Updates Analog Output B
        first = B10100000; // sets first four bits to 1010

    if(XYZ == 'Z' || XYZ == 'z') //Updates Analog Output A & B to same value
        first = B11110000; // sets first four bits to 1111

    data1 = first + mid + (byte(val)>>6);
    data2 = byte(val) << 2;

    digitalWrite(Load6_PIN, LOW);

```

```

    shiftOut1(DATA_PIN, CLOCK_PIN, MSBFIRST, data1);
    shiftOut1(DATA_PIN, CLOCK_PIN, MSBFIRST, data2);
    digitalWrite(LOAD6_PIN, HIGH);
}
void updateDAC7(int XYZ, int val) //val should be 0-1023
{
    byte data1 = 0;
    byte data2 = 0;

    byte first = 0;
    byte mid = 0;

    if(val > 255)
        mid = B00000100;
    if(val > 511)
        mid = B00001000;
    if(val > 767)
        mid = B00001100;

    if(XYZ == 'X' || XYZ == 'x') //Updates Analog Output A
        first = B10010000; //data1= '10010000' First 4 bits are "Command Code"

    if(XYZ == 'Y' || XYZ == 'y') //Updates Analog Output B
        first = B10100000; // sets first four bits to 1010

    if(XYZ == 'Z' || XYZ == 'z') //Updates Analog Output A & B to same value
        first = B11110000; // sets first four bits to 1111

    data1 = first + mid + (byte(val) >> 6);
    data2 = byte(val) << 2;

    digitalWrite(LOAD7_PIN, LOW);
    shiftOut1(DATA_PIN, CLOCK_PIN, MSBFIRST, data1);
    shiftOut1(DATA_PIN, CLOCK_PIN, MSBFIRST, data2);
    digitalWrite(LOAD7_PIN, HIGH);
}
void updateDAC8(int XYZ, int val) //val should be 0-1023
{
    byte data1 = 0;
    byte data2 = 0;

    byte first = 0;
    byte mid = 0;

    if(val > 255)
        mid = B00000100;
    if(val > 511)
        mid = B00001000;
    if(val > 767)
        mid = B00001100;

```

```

if(XYZ == 'X' || XYZ == 'x') //Updates Analog Output A
    first = B10010000; //data1= '10010000' First 4 bits are "Command Code"

if(XYZ == 'Y' || XYZ == 'y') //Updates Analog Output B
    first = B10100000; // sets first four bits to 1010

if(XYZ == 'Z' || XYZ == 'z') //Updates Analog Output A & B to same value
    first = B11110000; // sets first four bits to 1111

data1 = first + mid + (byte(val)>>6);
data2 = byte(val) << 2;

digitalWrite(Load8_PIN, LOW);
shiftOut1(DATA_PIN, CLOCK_PIN, MSBFIRST, data1);
shiftOut1(DATA_PIN, CLOCK_PIN, MSBFIRST, data2);
digitalWrite(Load8_PIN, HIGH);
}
void shiftOut1(uint8_t dataPin, uint8_t clockPin, uint8_t bitOrder, uint8_t val)
{
    uint8_t i;

    for (i = 0; i < 8; i++) {
        if (bitOrder == LSBFIRST)
            digitalWrite(dataPin, !(val & (1 << i)));
        else
            digitalWrite(dataPin, !(val & (1 << (7 - i))));

        delayMicroseconds(10000);
        digitalWrite(clockPin, HIGH);
        delayMicroseconds(10000);
        digitalWrite(clockPin, LOW);

    }
}

void loop()
{
    char buff[2];
    if (Serial.readBytes(buff, 2) == 2){

        order = buff[0] << 8;
        order |= buff[1];
        if (order == 'da') {
            da=Serial.parseInt();
            Serial.print("DAC 'a' code: ");
            Serial.println(da);
            updateDAC1('X',da);
            order =0;
        }
    }
}

```

```

if (order == 'db') {
    db=Serial.parseInt();
    Serial.print("DAC 'b' code: ");
    Serial.println(db);
    updateDAC2('X',db);
    order =0;
}
if (order == 'dc') {
    dc=Serial.parseInt();
    Serial.print("DAC 'c' code: ");
    Serial.println(dc);
    updateDAC3('X',dc);
    order =0;
}
if (order == 'dd') {
    dd=Serial.parseInt();
    Serial.print("DAC 'd' code: ");
    Serial.println(dd);
    updateDAC4('X',dd);
    order =0;
}
if (order == 'de') {
    de=Serial.parseInt();
    Serial.print("DAC 'e' code: ");
    Serial.println(de);
    updateDAC5('X',de);
    order =0;
}
if (order == 'df') {
    df=Serial.parseInt();
    Serial.print("DAC 'f' code: ");
    Serial.println(df);
    updateDAC6('X',df);
    order =0;
}
if (order == 'dg') {
    dg=Serial.parseInt();
    Serial.print("DAC 'g' code: ");
    Serial.println(dg);
    updateDAC7('X',dg);
    order =0;
}
if (order == 'dh') {
    dh=Serial.parseInt();
    Serial.print("DAC 'h' code: ");
    Serial.println(dh);
    updateDAC8('X',dh);
    order =0;
}
if (order == 'ca') {
    Serial.println("Number of channels: 1");
}

```

```

digitalWrite(Ch8, LOW);
digitalWrite(Ch4, LOW);
digitalWrite(Ch2, LOW);
digitalWrite(Ch1, HIGH);
delay(100);
updateDAC1('X',0);
delay(100);
updateDAC2('X',0);
delay(100);
updateDAC3('X',0);
delay(100);
updateDAC4('X',0);
delay(100);
updateDAC5('X',0);
delay(100);
updateDAC6('X',0);
delay(100);
updateDAC7('X',0);
delay(100);
updateDAC8('X',0);
delay(100);
order =0;
}
if (order == 'cb') {
  Serial.println("Number of channels: 2");
  digitalWrite(Ch8, LOW);
  digitalWrite(Ch4, LOW);
  digitalWrite(Ch1, LOW);
  digitalWrite(Ch2, HIGH);
  delay(100);
  updateDAC1('X',0);
  delay(100);
  updateDAC2('X',0);
  delay(100);
  updateDAC3('X',0);
  delay(100);
  updateDAC4('X',0);
  delay(100);
  updateDAC5('X',0);
  delay(100);
  updateDAC6('X',0);
  delay(100);
  updateDAC7('X',0);
  delay(100);
  updateDAC8('X',0);
  delay(100);
  order =0;
}
if (order == 'cc') {
  Serial.println("Number of channels: 4");
  digitalWrite(Ch8, LOW);

```

```

digitalWrite(Ch1, LOW);
digitalWrite(Ch2, LOW);
digitalWrite(Ch4, HIGH);
delay(100);
updateDAC1('X',0);
delay(100);
updateDAC2('X',0);
delay(100);
updateDAC3('X',0);
delay(100);
updateDAC4('X',0);
delay(100);
updateDAC5('X',0);
delay(100);
updateDAC6('X',0);
delay(100);
updateDAC7('X',0);
delay(100);
updateDAC8('X',0);
delay(100);
order =0;
}
if (order == 'cd') {
  Serial.println("Number of channels: 8");
  digitalWrite(Ch1, LOW);
  digitalWrite(Ch2, LOW);
  digitalWrite(Ch4, LOW);
  digitalWrite(Ch8, HIGH);
  delay(100);
  updateDAC1('X',0);
  delay(100);
  updateDAC2('X',0);
  delay(100);
  updateDAC3('X',0);
  delay(100);
  updateDAC4('X',0);
  delay(100);
  updateDAC5('X',0);
  delay(100);
  updateDAC6('X',0);
  delay(100);
  updateDAC7('X',0);
  delay(100);
  updateDAC8('X',0);
  delay(100);
  order =0;
}
if (order == 'be') {
  Serial.println("DC/DC converter: Boost");
  digitalWrite(ENBoost, HIGH);
  order =0;
}

```

```

}
if (order == 'bd') {
    Serial.println("DC/DC converter: Buck-boost");
    digitalWrite(ENBoost, LOW);
    order =0;
}
if (order == 'na') {
    na=Serial.parseInt();
    if (na==1){
        digitalWrite(NMOS_Ch1, HIGH);
        Serial.println("1st channel's polarity: Positive");
    }
    if (na==2){
        digitalWrite(NMOS_Ch1, LOW);
        Serial.println("1st channel's polarity: Negative");
    }
    order =0;
}
if (order == 'nb') {
    nb=Serial.parseInt();
    if (nb==1){
        digitalWrite(NMOS_Ch2, HIGH);
        Serial.println("2nd channel's polarity: Positive");
    }
    if (nb==2){
        digitalWrite(NMOS_Ch2, LOW);
        Serial.println("2nd channel's polarity: Negative");
    }
    order =0;
}
if (order == 'nc') {
    nc=Serial.parseInt();
    if (nc==1){
        digitalWrite(NMOS_Ch3, HIGH);
        Serial.println("3rd channel's polarity: Positive");
    }
    if (nc==2){
        digitalWrite(NMOS_Ch3, LOW);
        Serial.println("3rd channel's polarity: Negative");
    }
    order =0;
}
if (order == 'nd') {
    nd=Serial.parseInt();
    if (nd==1){
        digitalWrite(NMOS_Ch4, HIGH);
        Serial.println("4th channel's polarity: Positive");
    }
    if (nd==2){
        digitalWrite(NMOS_Ch4, LOW);
        Serial.println("4th channel's polarity: Negative");
    }
}

```

```

}
order =0;
}
if (order == 'ne') {
ne=Serial.parseInt();
if (ne==1){
digitalWrite(NMOS_Ch5, HIGH);
Serial.println("5th channel's polarity: Positive");
}
if (ne==2){
digitalWrite(NMOS_Ch5, LOW);
Serial.println("5th channel's polarity: Negative");
}
order =0;
}
if (order == 'nf') {
nf=Serial.parseInt();
if (nf==1){
digitalWrite(NMOS_Ch6, HIGH);
Serial.println("6th channel's polarity: Positive");
}
if (nf==2){
digitalWrite(NMOS_Ch6, LOW);
Serial.println("6th channel's polarity: Negative");
}
}
order =0;
}
if (order == 'ng') {
ng=Serial.parseInt();
if (ng==1){
digitalWrite(NMOS_Ch7, HIGH);
Serial.println("7th channel's polarity: Positive");
}
if (ng==2){
digitalWrite(NMOS_Ch7, LOW);
Serial.println("7th channel's polarity: Negative");
}
}
order =0;
}
if (order == 'nh') {
nh=Serial.parseInt();
if (nh==1){
digitalWrite(NMOS_Ch8, HIGH);
Serial.println("8th channel's polarity: Positive");
}
if (nh==2){
digitalWrite(NMOS_Ch8, LOW);
Serial.println("8th channel's polarity: Negative");
}
}
order =0;
}

```

```

if (order == 'pa') {
pa=Serial.parseInt();
delay(100);
updateDAC1('X',0);
delay(100);
updateDAC2('X',0);
delay(100);
updateDAC3('X',0);
delay(100);
updateDAC4('X',0);
delay(100);
updateDAC5('X',0);
delay(100);
updateDAC6('X',0);
delay(100);
updateDAC7('X',0);
delay(100);
updateDAC8('X',0);
delay(100);
digitalWrite(PMOS_source_Ch1, HIGH);
delay(pa);
digitalWrite(PMOS_source_Ch1, LOW);
Serial.print("The capacitors of the 1st channel's high-side drivers have been charged for
");
Serial.print(pa);
Serial.println(" ms.");
order =0;
}
if (order == 'pb') {
pb=Serial.parseInt();
delay(100);
updateDAC1('X',0);
delay(100);
updateDAC2('X',0);
delay(100);
updateDAC3('X',0);
delay(100);
updateDAC4('X',0);
delay(100);
updateDAC5('X',0);
delay(100);
updateDAC6('X',0);
delay(100);
updateDAC7('X',0);
delay(100);
updateDAC8('X',0);
delay(100);
digitalWrite(PMOS_source_Ch2, HIGH);
delay(pb);
digitalWrite(PMOS_source_Ch2, LOW);

```

```

Serial.print("The capacitors of the 2nd channel's high-side drivers have been charged for
");
Serial.print(pb);
Serial.println(" ms.");
order =0;
}
if (order == 'pc') {
pc=Serial.parseInt();
delay(100);
updateDAC1('X',0);
delay(100);
updateDAC2('X',0);
delay(100);
updateDAC3('X',0);
delay(100);
updateDAC4('X',0);
delay(100);
updateDAC5('X',0);
delay(100);
updateDAC6('X',0);
delay(100);
updateDAC7('X',0);
delay(100);
updateDAC8('X',0);
delay(100);
digitalWrite(PMOS_source_Ch3, HIGH);
delay(pc);
digitalWrite(PMOS_source_Ch3, LOW);
Serial.print("The capacitors of the 3rd channel's high-side drivers have been charged for
");
Serial.print(pc);
Serial.println(" ms.");
order =0;
}
if (order == 'pd') {
pd=Serial.parseInt();
delay(100);
updateDAC1('X',0);
delay(100);
updateDAC2('X',0);
delay(100);
updateDAC3('X',0);
delay(100);
updateDAC4('X',0);
delay(100);
updateDAC5('X',0);
delay(100);
updateDAC6('X',0);
delay(100);
updateDAC7('X',0);
delay(100);

```

```

updateDAC8('X',0);
delay(100);
digitalWrite(PMOS_source_Ch4, HIGH);
delay(pd);
digitalWrite(PMOS_source_Ch4, LOW);
Serial.print("The capacitors of the 4th channel's high-side drivers have been charged for
");
Serial.print(pd);
Serial.println(" ms.");
order =0;
}
if (order == 'pe') {
pe=Serial.parseInt();
delay(100);
updateDAC1('X',0);
delay(100);
updateDAC2('X',0);
delay(100);
updateDAC3('X',0);
delay(100);
updateDAC4('X',0);
delay(100);
updateDAC5('X',0);
delay(100);
updateDAC6('X',0);
delay(100);
updateDAC7('X',0);
delay(100);
updateDAC8('X',0);
delay(100);
digitalWrite(PMOS_source_Ch5, HIGH);
delay(pe);
digitalWrite(PMOS_source_Ch5, LOW);
Serial.print("The capacitors of the 5th channel's high-side drivers have been charged for
");
Serial.print(pe);
Serial.println(" ms.");
order =0;
}
if (order == 'pf') {
pf=Serial.parseInt();
delay(100);
updateDAC1('X',0);
delay(100);
updateDAC2('X',0);
delay(100);
updateDAC3('X',0);
delay(100);
updateDAC4('X',0);
delay(100);
updateDAC5('X',0);

```

```

delay(100);
updateDAC6('X',0);
delay(100);
updateDAC7('X',0);
delay(100);
updateDAC8('X',0);
delay(100);
digitalWrite(PMOS_source_Ch6, HIGH);
delay(pf);
digitalWrite(PMOS_source_Ch6, LOW);
Serial.print("The capacitors of the 6th channel's high-side drivers have been charged for
");
Serial.print(pf);
Serial.println(" ms.");
order =0;
}
if (order == 'pg') {
pg=Serial.parseInt();
delay(100);
updateDAC1('X',0);
delay(100);
updateDAC2('X',0);
delay(100);
updateDAC3('X',0);
delay(100);
updateDAC4('X',0);
delay(100);
updateDAC5('X',0);
delay(100);
updateDAC6('X',0);
delay(100);
updateDAC7('X',0);
delay(100);
updateDAC8('X',0);
delay(100);
digitalWrite(PMOS_source_Ch7, HIGH);
delay(pg);
digitalWrite(PMOS_source_Ch7, LOW);
Serial.print("The capacitors of the 7th channel's high-side drivers have been charged for
");
Serial.print(pg);
Serial.println(" ms.");
order =0;
}
if (order == 'ph') {
ph=Serial.parseInt();
delay(100);
updateDAC1('X',0);
delay(100);
updateDAC2('X',0);
delay(100);

```

```

    updateDAC3('X',0);
    delay(100);
    updateDAC4('X',0);
    delay(100);
    updateDAC5('X',0);
    delay(100);
    updateDAC6('X',0);
    delay(100);
    updateDAC7('X',0);
    delay(100);
    updateDAC8('X',0);
    delay(100);
    digitalWrite(PMOS_source_Ch8, HIGH);
    delay(ph);
    digitalWrite(PMOS_source_Ch8, LOW);
    Serial.print("The capacitors of the 8th channel's high-side drivers have been charged for
");
    Serial.print(ph);
    Serial.println(" ms.");
    order =0;
}
// if (order == 'ee') {
//   digitalWrite(EN_channel, HIGH);
//   Serial.println("Enable");
//   order =0;
// }
// if (order == 'ed') {
//   digitalWrite(EN_channel, LOW);
//   Serial.println("Disable");
//   order =0;
// }
if (order == 'ma') {
    ma=Serial.parseInt();
    delay(100);
    updateDAC1('X',0);
    delay(100);
    updateDAC2('X',0);
    delay(100);
    updateDAC3('X',0);
    delay(100);
    updateDAC4('X',0);
    delay(100);
    updateDAC5('X',0);
    delay(100);
    updateDAC6('X',0);
    delay(100);
    updateDAC7('X',0);
    delay(100);
    updateDAC8('X',0);
    delay(100);
    digitalWrite(PMOS_source_Ch1, HIGH);

```

```

digitalWrite(PMOS_source_Ch2, HIGH);
digitalWrite(PMOS_source_Ch3, HIGH);
digitalWrite(PMOS_source_Ch4, HIGH);
digitalWrite(PMOS_source_Ch5, HIGH);
digitalWrite(PMOS_source_Ch6, HIGH);
digitalWrite(PMOS_source_Ch7, HIGH);
digitalWrite(PMOS_source_Ch8, HIGH);
delay(ma);
digitalWrite(PMOS_source_Ch1, LOW);
digitalWrite(PMOS_source_Ch2, LOW);
digitalWrite(PMOS_source_Ch3, LOW);
digitalWrite(PMOS_source_Ch4, LOW);
digitalWrite(PMOS_source_Ch5, LOW);
digitalWrite(PMOS_source_Ch6, LOW);
digitalWrite(PMOS_source_Ch7, LOW);
digitalWrite(PMOS_source_Ch8, LOW);
Serial.print("The capacitors of all the high-side drivers have been charged for ");
Serial.print(ma);
Serial.println(" ms.");
order =0;
}
if (order == 'in') {
  Serial.println(" ");

Serial.println("*****
*****
*****");

Serial.println("*****
*****
*****");

  Serial.println("Dear user,");
  Serial.println(" ");
  Serial.println("Welcome to the Effipulse stimulator's user interface.");
  Serial.println("The channels have been symbolized from 'a' for the first channel to 'h' for
the eighth channel using ascending order.");
  Serial.println("The following are the available commands that exist in the static memory
of the MCU.");
  Serial.println("'bd': Buck-boost converter is chosen as the used DC/DC converter.");
  Serial.println("'be': Boost converter is chosen as the used DC/DC converter.");
  Serial.println("'da#-'dh#': Sets the value for the output of each DAC ('a' for the first
channel until 'h' for the 8th channel). Where #, place a number value from 0 to 1023, which
is the code that the DAC reads.");
  Serial.println("'ca-'cd': Selects if one ('ca'), two, four or eight ('cd') channels are used.");
  Serial.println("'na#-'nh#': Selects for each channel the polarity that will be used, where
# is 1 for the default polarity and 2 for the reverse polarity.");
  Serial.println("!!!WARNING!!!");
  Serial.println("Please be sure that before using the 'pa#-'ph#' and 'ma#' orders, the
buck-boost converter ('bd')and the 1 channel ('ca') mode must be chosen, as also all the
DACs must have zero value ('da0','db0', ..., 'dh0').");

```

```

Serial.println("If the previous line is not followed there might be risk for damaging the
device, as also the load in its outputs.");
Serial.println("!!!WARNING!!!");
Serial.println("pa#'-ph#': Charges the high-side driver's capacitors for each channel,
where # are the milliseconds that the charging takes place.");
Serial.println("ma#': Charges the high-side driver's capacitors for all channels, where #
are the milliseconds that the charging takes place.");
Serial.println("in': Opens the instructions.");
Serial.println("In order to use the aforementioned commands, please open the serial
monitor window.");
Serial.println("Then type the two-digit code for each command you want to execute and
the preferred number, if it is applicable, right after the code without using space.");
Serial.println("Then press enter");
Serial.println("The device works without resetting it.");
Serial.println("!!!WARNING!!!");
Serial.println("In case of resetting the MCU, there might be risk for damaging the
device, as also the load in its outputs.");
Serial.println("!!!WARNING!!!");
Serial.println(" ");
Serial.println("Thank you for your time reading the instructions.");

```

```

Serial.println("*****
*****
*****");

```

```

Serial.println("*****
*****
*****");

```

```

Serial.println(" ");
order =0;
}
}
}

```